A CONTRIBUTION TO THE STUDY OF SINGLE NUCLEON TRANSFER REACTIONS ON SOME 2s-1d SHELL NUCLEI

by

John C. Kroon

Submitted in partial fulfillment
of the requirements for the degree of
Doctor of Philosophy

Department of Physics
Faculty of Science and Engineering
University of Ottawa
Ottawa, Canada

1971.

ERRATA

Compound Nuclear Contribution

The compound nuclear contribution to the total cross-section leading to final states which are weakly observed in the reactions is probably significant. These weak transitions are shown in figures 4-4, 5-6 and 7-3.

Hamada-Johnston Potential

The Hamada-Johnston energy independent nucleon-nucleon scattering potential represents two-nucleon data below 315 MeV more accurately than any other potential model known to date. Both p-p and n-p data have been consistently represented by this potential model. The model appears applicable in the calculation of nuclear systems containing more than two nucleons. The central task involved in this approach is to overcome certain difficulties in the calculations due to the presence of hard cores, such as the Hamada-Johnston potential. A solution is achieved by considering the method of the reaction matrix theory.

Abstract

Angular distributions of deuterons from the $^{26}Mg(p, d)^{25}Mg$, $^{27}Al(p, d)^{26}Al$ at a proton energy of 20 MeV and $^{37}Cl(p, d)^{36}Cl$, $^{23}Na(p, d)^{22}Na$ at 19 MeV incident energy have been measured.

Angular distributions in ^{25}Mg up to 3.903 MeV excitation were compared with distorted wave predictions. A spectroscopic factor analysis was carried out based on the Nilsson Model where ^{25}Mg was assumed to consist of a deformed core with the odd neutron in a mixture of all possible N ± 2 Nilsson states. The theory was further extended to include Coriolis band mixing among all the (2s-1d) shells, which improved the comparison between theoretical spectroscopic factors and measured factors. The observed $7/2^+$ and $9/2^+$ levels were populated much more strongly than predicted by single step direct neutron pick-up theory.

Altogether 30 levels were resolved in the $^{27}Al(p, d)^{26}Al$ reaction. The strongest transitions were compared with distorted wave predictions. The data was further analyzed using the Nilsson model and shell model. The level at 4.699 MeV has been identified as the isobaric analog to the 4.331 MeV state in ^{26}Mg.

Angular distributions in ^{36}Cl up to 4.292 MeV excitation were analyzed using distorted wave predictions. A detailed comparison is made between experimentally extracted spectroscopic factors and theoretical spectroscopic factors derived from "$2s_{1/2} - 1d_{3/2}$" and "$1d_{5/2} - 2s_{1/2} - 1d_{3/2}$" shell model wave functions.

Transitions to states in ^{22}Na were compared with distorted wave predictions. The data was analyzed using the Nilsson model. The analysis confirms a previously unreported level at 4.294 MeV.

Acknowledgements

Four and a half years of academic life as a graduate student can only be evaluated, if the contributions of many individuals are considered.

First of all, the opportunity afforded to me by Dr. B. Hird to participate in the Chalk River experiments is gratefully acknowledged. His personal involvement throughout the course of this project has been a rewarding experience and is sincerely appreciated.

I wish to express my thanks to Dr. G. C. Ball of the Chalk River Nuclear Laboratories for the numerous stimulating discussions that contributed greatly in the understanding of the physics of this project.

In addition, the assistance of the following members of the staff at CRNL is acknowledged; R. L. Brown for the help with the electronic set up, A. S. Hyde and J. Hill for the aid with the experimental set up, J. L. Gallant for the target preparation, Mrs. Jenny Sprake for drawing the figures and the operations staff of the tandem accelerator.

Thanks are extended to Dr. W. G. Davies and Dr. R. Hodgson for the use of the shell model program and band mixing program, respectively.

A special thanks goes out to Dr. J. Robson for suggesting a certain course of action at two crucial stages of my graduate student career.

Special mention is appropriate to Dr. R. Smith and Dr. B. Logan who over the years were always available for helpful discussions.

A most deserving thanks is due to my wife, Marian, for her encouragement and understanding and being able to put up often with a part-time husband.

I also wish to thank Miss L. Sawyer for her cooperation in typing this thesis.

Finally the financial support of the N.R.C. in the form of a Graduate Fellowship was much appreciated.

Table of Contents

List of Figures

page

page

List of Tables

page

page

CHAPTER 1

INTRODUCTION

1.1 Objectives

For many years the s-d shell has been used as a testing ground for many nuclear models. This study attempts to correlate these models and their extensions to the experimental data. The main features of the investigation follow,

(a) a high resolution study of the single nucleon transfer reaction on a even-even nucleus (^{26}Mg) in the deformed region of the 2s-1d shell.

(b) a high resolution study of the single nucleon transfer reaction on two odd-Z nuclei (^{27}Al, ^{23}Na) in the deformed region of the 2s-1d shell.

(c) a high resolution study of the single nucleon transfer reaction on an odd-Z nucleus (^{37}Cl) near a closed shell.

(d) a test of the applicability of the Nilsson Model and the Shell Model to describe the nuclear structure of these nuclei.

(e) an assessment of the conventional spectroscopic factor analysis of single nucleon transfer reactions.

1.2 General Background

During the last decade, the single nucleon transfer reaction has been extensively studied as a basic experimental technique for the investigation of the wavefunctions of the ground and excited states of nuclei. By a transfer reaction a rearrangement collision is meant in which a nucleon, or cluster of nucleons, is transferred to the target nucleus in the case of a stripping reaction or removed in the case of a pick-up reaction. These transitions are of most interest when direct and minimally perturb the nuclear cores.

Since its original observation by Standing in 1954 (S1), the (p, d) reaction has in particular contributed greatly to unfold the wealth of information contained in transfer reactions. The shapes of the angular distributions and the magnitudes of the cross sections of this reaction can be analyzed with the distorted-wave Born approximation (DWBA) to extract the values of the transferred orbital angular momenta. Making use of angular momentum selection rules, information can then be obtained about spins and parities of the states involved.

From the strength of particular transitions, an assessment can be made to what extent the initial nucleus may be considered as the final nucleus plus a neutron in a single particle shell model level. In oversimplified language, pick-up reactions select single hole states. This information is usually extracted in terms of the spectroscopic factor and if data are obtained for an adequate sampling of residual levels, the sums of the spectroscopic factors yield the nucleon occupation number for the accessible shell model orbits in the target nucleus ground state. Configuration admixtures in the target nucleus are thus detectable by this reaction.

Investigations until recently have been restricted to targets which are easily available and, since the Q-value of the (p, d) reaction in most instances is in the range -5 to -15 MeV, only the first few excited states have been measured. With higher incident proton energies and with semiconductor detector resolution and particle identification techniques, it is now possible to separate and measure more excited states.

This report presents results of an experimental study of single nucleon transfer reactions on some nuclei within the 2s-1d shell. The reactions considered are the $^{26}Mg(p, d)^{25}Mg$, $^{27}Al(p, d)^{26}Al$, $^{37}Cl(p, d)^{36}Cl$ and $^{23}Na(p, d)^{22}Na$. Many charged particle reactions

have been performed in the region between ^{16}O and ^{40}Ca and the results of several of these reactions are utilized for inter-comparison.

In particular, the study examined the application of several theoretical models (N1, M1, K1, H6) which have been proposed for the deformed nuclei in the 2s-1d shell. These models were extended to include major shell mixing of all Nilsson states and a Coriolis band mixing calculation for all 2s-1d orbits. Their respective degree of validity were evaluated by a comparison of experimentally determined spectroscopic factors for neutron pick-up to the various predicted values.

In addition, the applicability of shell-model calculations to nuclei in the s-d shell are tested primarily using the $^{37}Cl(p, d)^{36}Cl$ reaction.

CHAPTER 2

EXPERIMENTAL ARRANGEMENT AND PROCEDURES

2.1 Machine and External Beam Facilities

The experiments under investigation were carried out using a 20 MeV proton beam, from the Chalk River 10 MV van de Graaff MP Tandem Accelerator. The negative-ion beam was injected into the accelerator from a Duoplasmatron negative-ion source. Figure 2-1 shows the accelerator with beam transport and target area layout. Positive ions emerging from the high energy base of the accelerator were focussed using a magnetic quadrupole lens. A set of electrostatic steerers after the quadrupole lens, enabled the beam position and direction to be adjusted prior to entering the 90^{o} energy analysing magnet. The analysed beam of the correct energy was then deflected through 10^{o} by the switching magnet and further beam alignment was attained with the aid of the precision apertures. Two additional sets of quadrupole lenses were used to focus the beam finally to the centre of the Ortec 17" scattering chamber*. The entrance to the scattering chamber included a tantalum collimator arrangement. The purpose of this arrangement was to define the axis of

* ORTEC, Model 600.

Figure 2-1: Drawing of accelerator and target area layout.

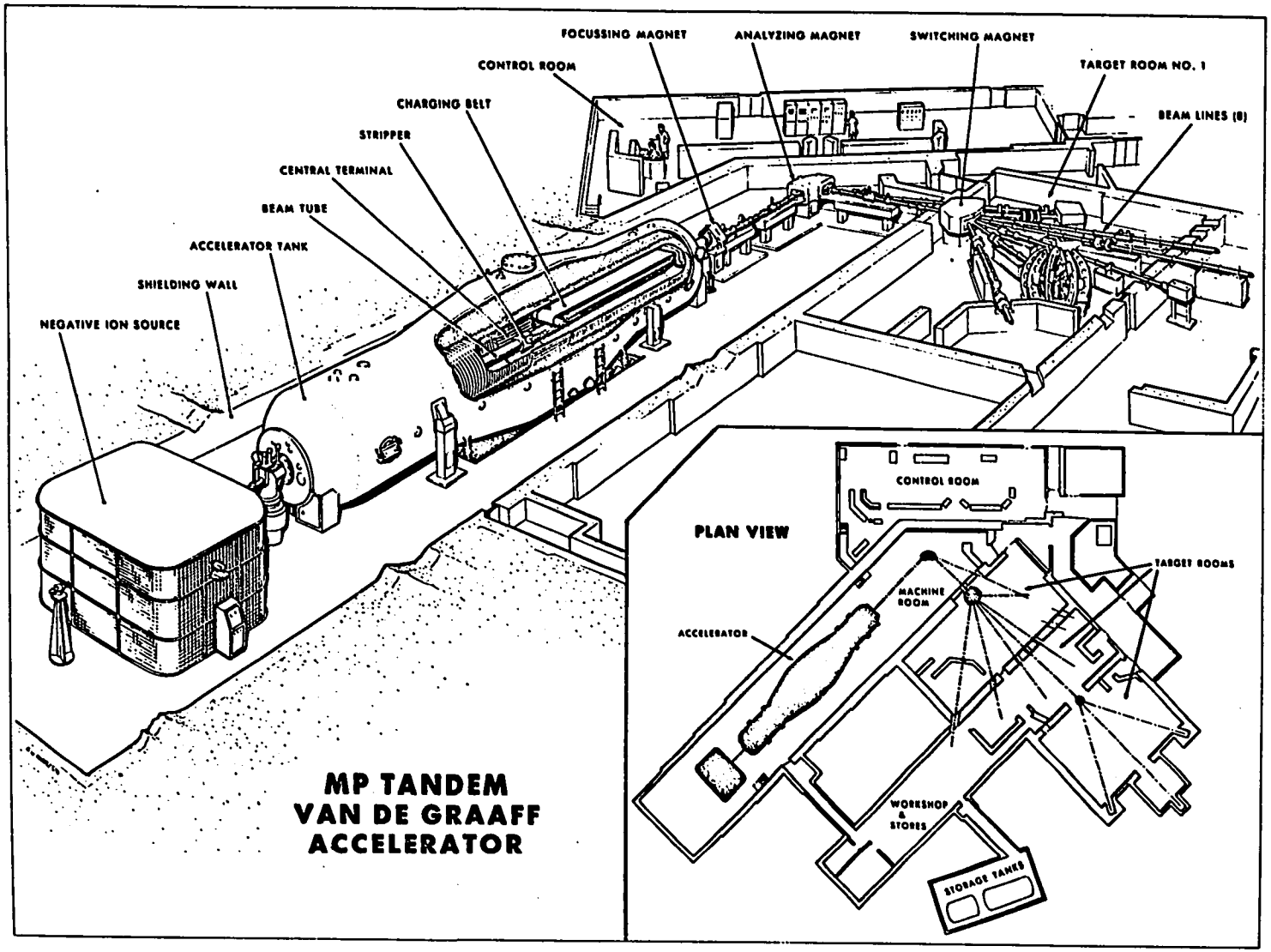
FOCUSSING MAGNET
ANALYZING MAGNET
SWITCHING MAGNET
CONTROL ROOM
TARGET ROOM NO. 1
CHARGING BELT
BEAM LINES (8)
STRIPPER
CENTRAL TERMINAL
BEAM TUBE
ACCELERATOR TANK
SHIELDING WALL
NEGATIVE ION SOURCE
PLAN VIEW
CONTROL ROOM
TARGET ROOMS
MACHINE ROOM
ACCELERATOR
WORKSHOP & STORES
STORAGE TANKS
MP TANDEM
VAN DE GRAAFF
ACCELERATOR

the beam through the scattering chamber and to eliminate any scattering from the target frame. Typical beam spots on targets were between 1 and 2 mm in diameter. Beam currents were measured using a Faraday-cup with an air-cooled tantalum beam stop biased at 1500 V, which was connected to a Keithly integrating electrometer. Variable beam intensities up to 1 μA were obtained with a beam energy resolution of 0.01%.

Particles were detected in a counter telescope which was permanently mounted onto the lower turntable of the scattering chamber. Figure 2-2 shows a photograph of the scattering chamber and accessories. In this photograph, the detector-housing or telescope is located along the forward direction of the beam at 60^{o} laboratory angle. A view is also shown of the beam entrance-scraper which prevented, through anti-scattering slits, particles scattered from the beam defining apertures in the collimator to reach the counters. The target as shown in the centre of the scattering chamber was part of the target handling system, which was capable of accommodating several targets at the same time.

The detectors were completely enclosed in a brass detector-housing as shown in Figure 2-3. This was done in order to minimize the effects of scattered particles on the detectors. The entrance collimator of the detector-housing was designed to include a magnetic electron deflector and defining entrance aperture.

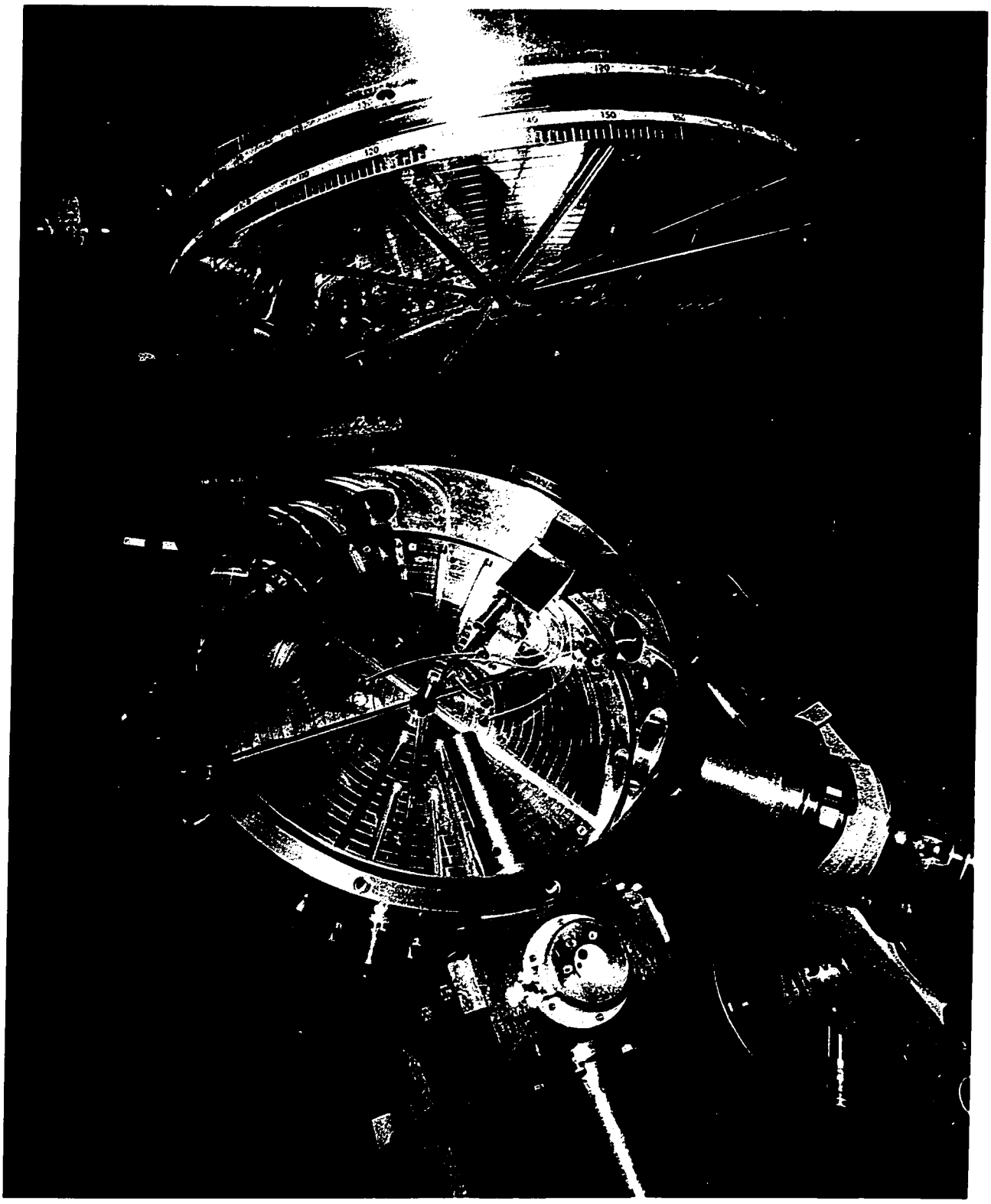

Fig. II-2. Scattering chamber and accessories

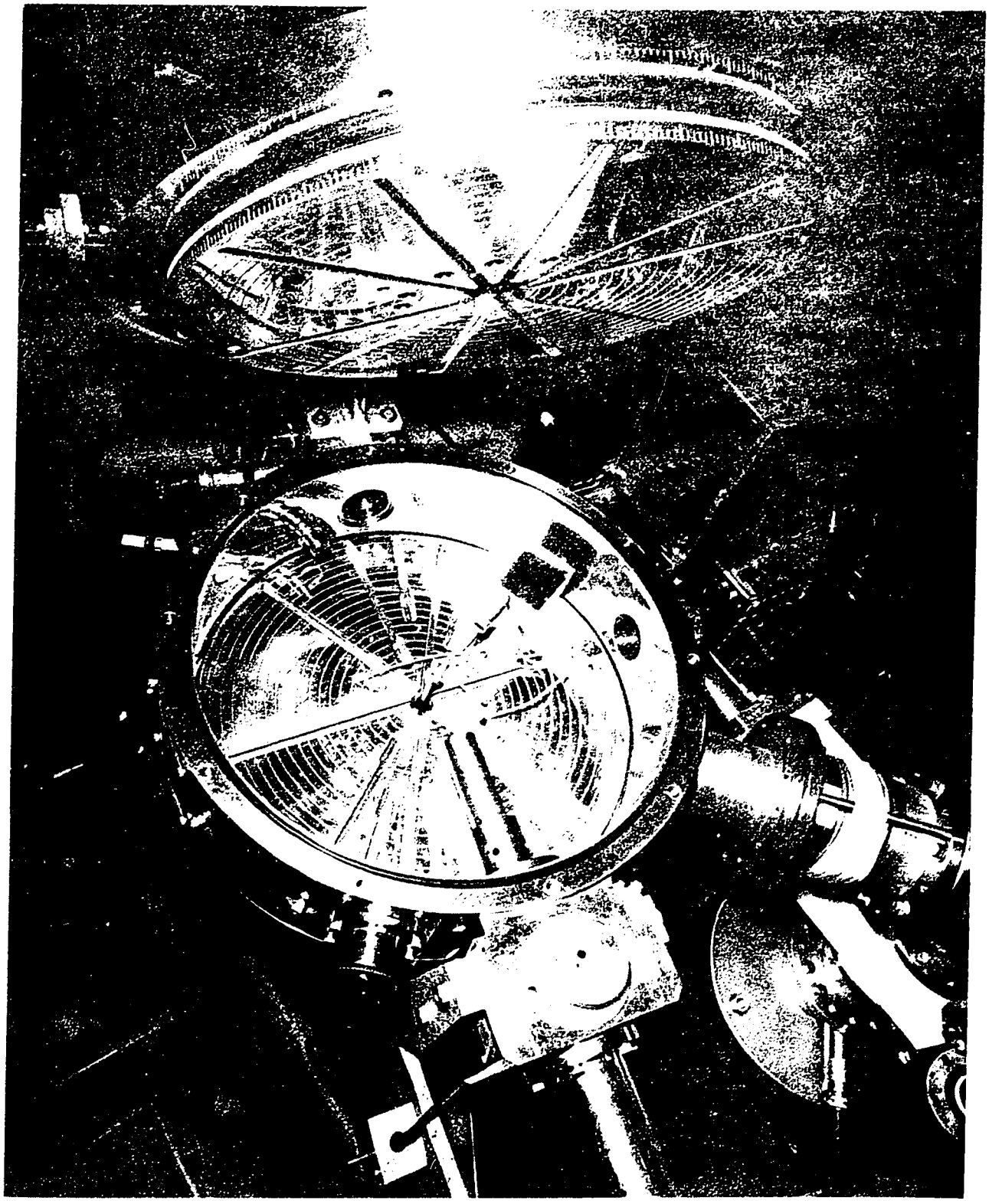

Fig. II-2. Scattering chamber and accessories

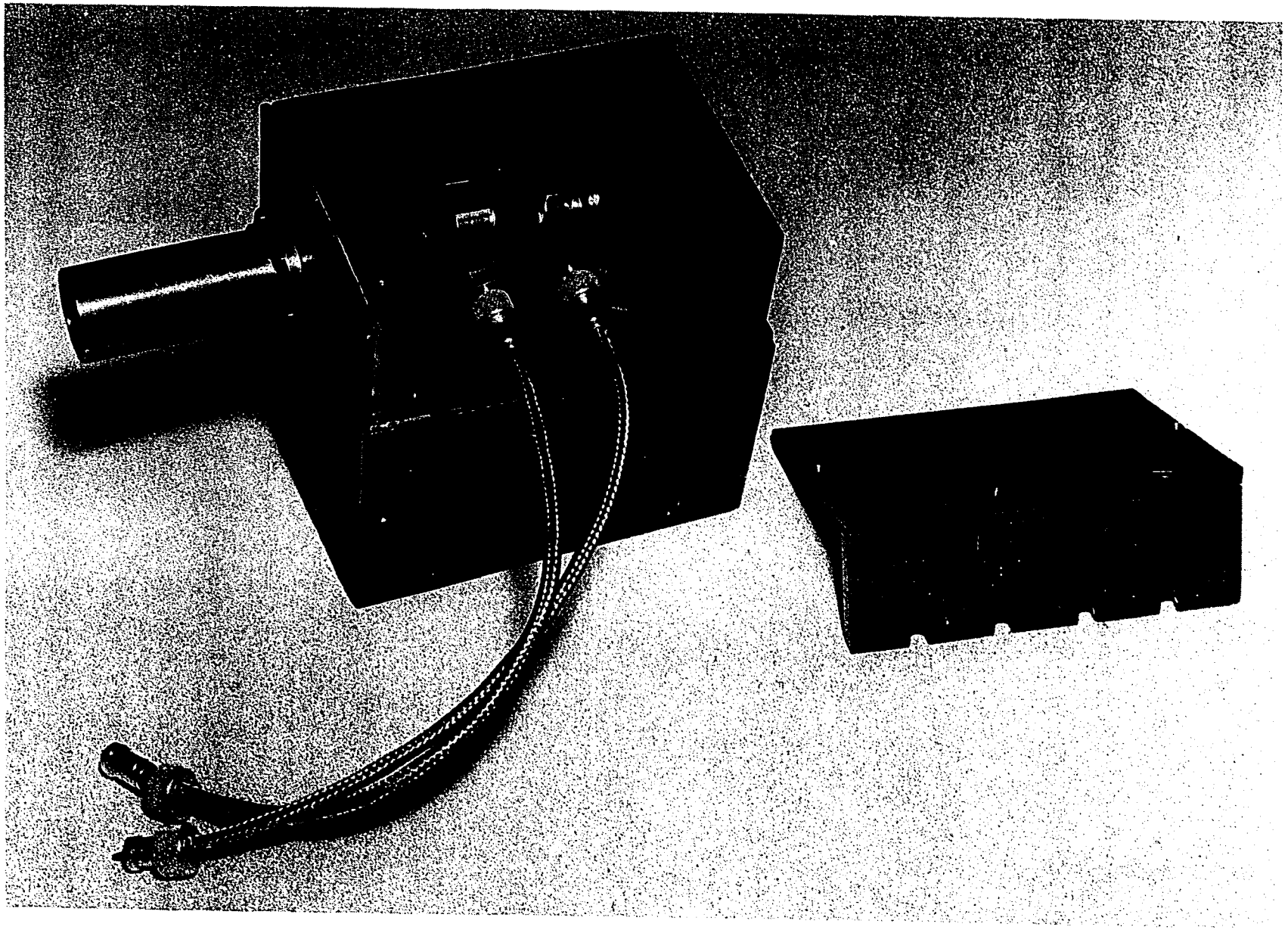

Fig. II-3. Detector-Housing.

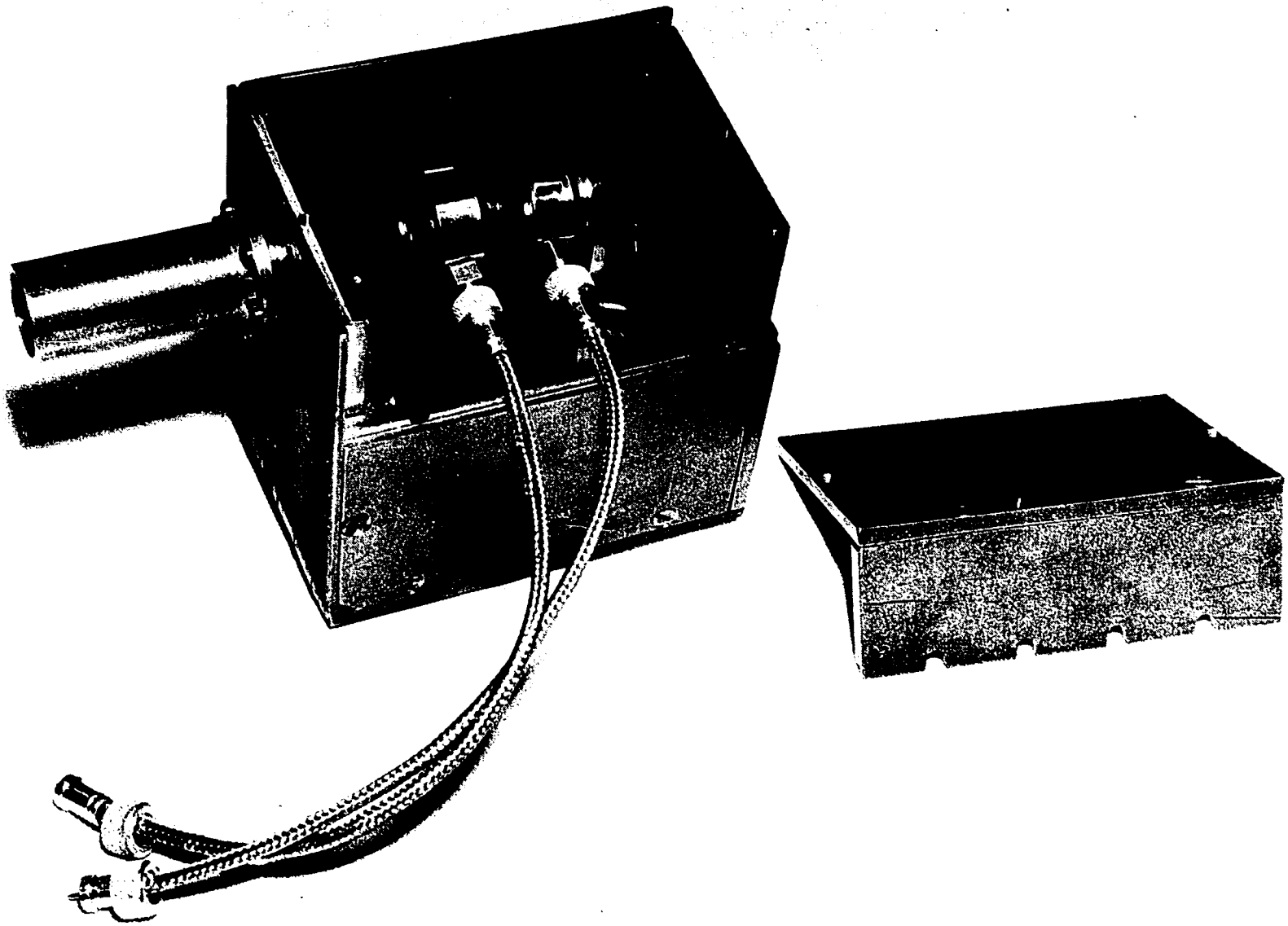

Fig. II-3. Detector-Housing.

A convenient technique was devised, to remove or insert the detectors into the detector enclosure. Figure 2-4 shows a detailed view of the detector mounts which were fitted into recessed slots of the detector enclosure. Capacitances were minimized by using short cables between detector and preamplifier.

The smallest scattering angle attainable with this arrangement was 10^{o}.

The scattering chamber and supporting beam pipe were kept under vacuum by several Triode ion pumps.

2.2 Detectors and Electronics

The aforementioned counter telescope consisted of three semiconductor detectors mounted in line: a 50 μ transmission detector (ΔE), a 200 μ transmission detector (E), and a standard 500 μ surface barrier detector ($\overline{E}$). In particular, the detection system is designed to select deuterons and tritons in the presence of a high background of high energy protons. The low energy deuterons and tritons were stopped in the E counter, whereas the high energy protons will pass into the back counter ($\overline{E}$); which will be operated in anticoincidence to reject proton events immediately.

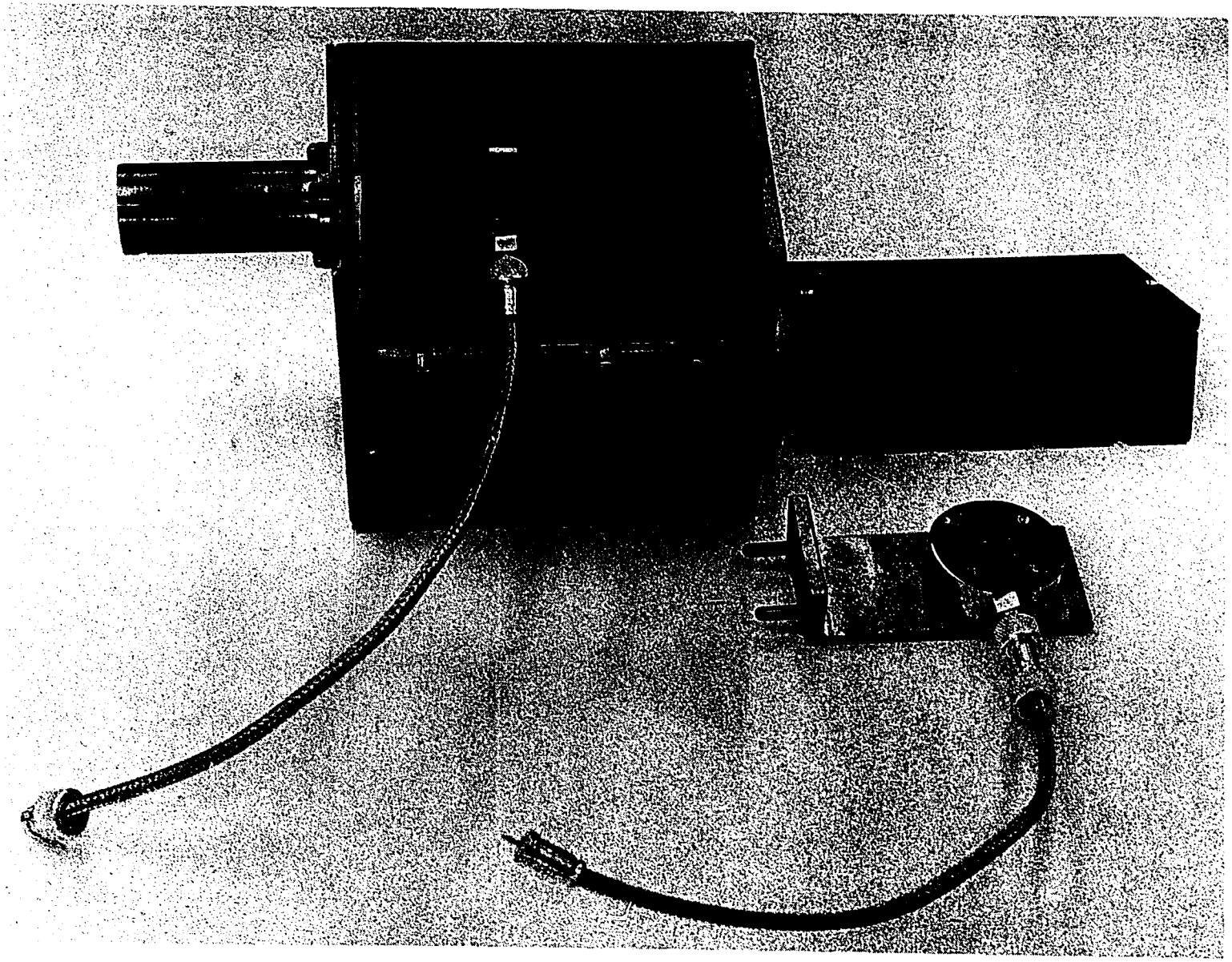

Fig. II-4. Detector-Housing with removable mount.

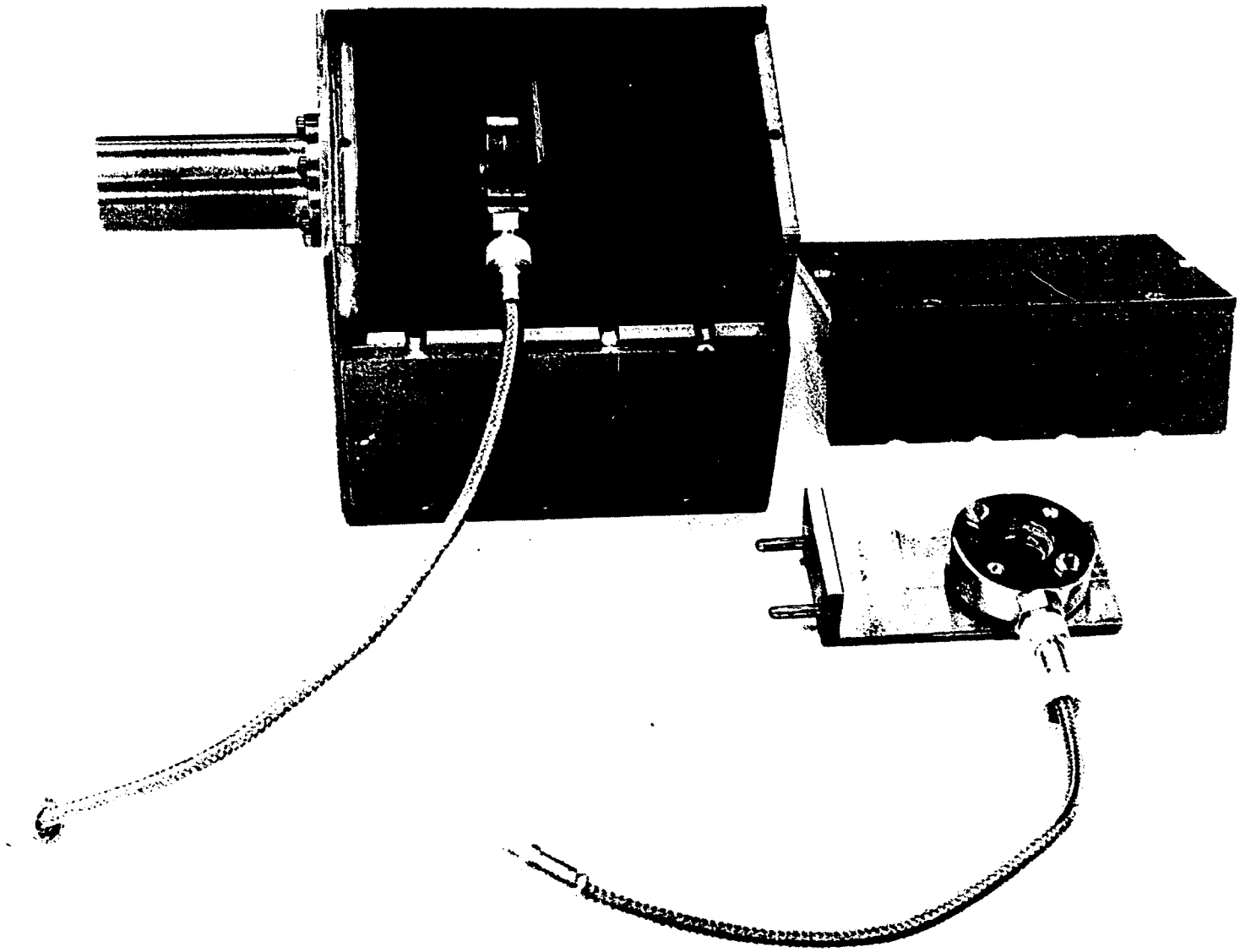

Fig. II-4. Detector-Housing with removable mount.

The first counter telescope systems used for particle identification (S2) relied on the property of the Bethe rate-of-energy loss formula, that the product $E.\frac{dE}{dx}$ is approximately independent of the incident particle energy, but varies with the mass and charge of the particle as MZ^2. This method is restricted since the energy lost in the front counter, ΔE, must be a small proportion of the total incident energy.

The Goulding-Landis particle identifier (G1) eliminated the need to have a thin front counter by utilizing the emperical range-energy relationship $R = \underline{a}E^{\underline{b}}$ where $\underline{a}$ is characteristic of the type of particle and $\underline{b}$ is nearly the same for all light particles above 10 MeV. The numerical value used for $\underline{b}$ was 1.73.

The particle reactions investigated in this report only deal with single nucleon transfer reactions, although the two nucleon transfer reactions formed an integral part of the overall study using a particle identifier. Both (p,d) and (p,t) are highly endothermic reactions and the energy range of the tritons and deuterons was between 3 MeV to 11 MeV. In this energy-range the exponential law on which the Goulding-method relies is a poor approximation. The alternative method employed for these experiments used the experimental range-energy table directly and is applicable over the full range of energies and for any particle type produced in the reactions (H1). Data for the range-energy table was obtained from Williamson, Boujot and Picard (W1).

In making the particle selection, it is necessary to calculate a certain parameter which is independent of particle energy, but which gives a unique value for the desired particle type. A suitable parameter is the front counter thickness (T), which is given by the relation

$$T = R(E + \Delta E) - R(E)$$

where R(E) is the range of the selected particle type having energy E and ΔE and E are the energies deposited in the first two counters respectively of the telescope. These particle energies were converted into ranges in silicon by referring to the experimental range-energy table which is permanently stored in the computer memory, and T is obtained as the difference between two tabulated values. Only particles of the type whose range-energy relation is stored in the computer memory will give a calculated value which is the true front counter thickness, and can therefore be selected on this basis. In this experiment the triton range-energy in silicon was permanently stored in computer memory.

Other particle types which are detected have specific energy losses, which are sufficiently different that the calculated front counter "thickness" never has the same value as the true thickness. In Figure 2 -5 is shown the computed front counter "thickness" as a function of incident energy for each of the Z = 1 particles when the triton range-energy table is used. Although the proton and deuteron "thickness"

Figure 2-5: Front counter "thickness" as a function of particle energy.

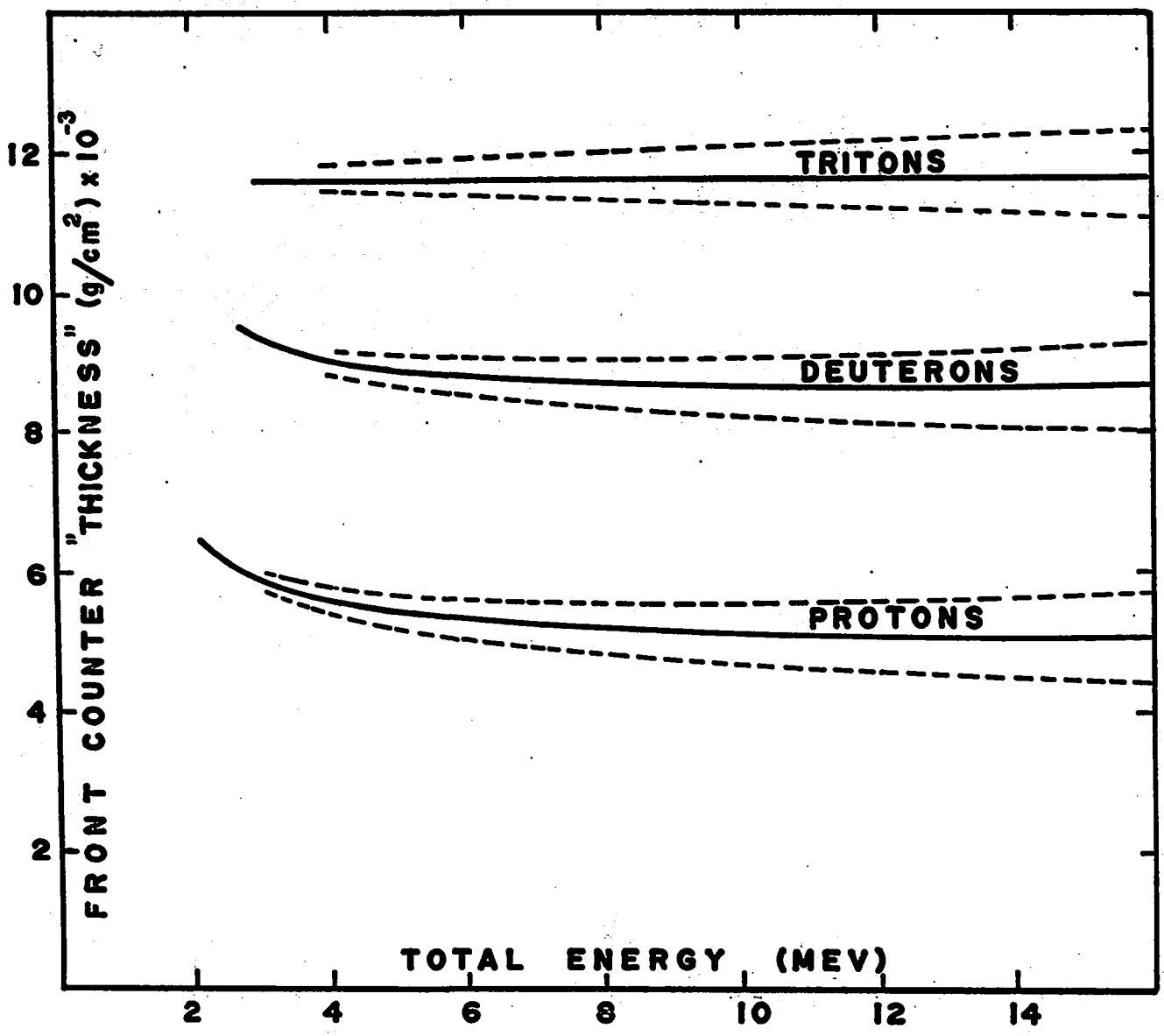
TRITONS
DEUTERONS
PROTONS
FRONT COUNTER "THICKNESS" (g/cm²) x 10⁻³
TOTAL ENERGY (MEV)
2
4
6
8
10
12
14

varies with energy it is nevertheless different from the triton thickness at all energies. Separation of the three particles is therefore accomplished. A typical particle identifier spectrum observed in these experiments is shown in Figure 2-6, with well resolved proton, deuteron and triton peaks. Energy spectra for protons, deuterons and tritons were subsequently obtained by setting digital windows on the corresponding peaks in the particle identifier spectrum.

A block diagram of the electronics is shown in Figure 2 -7. Signals from the three detectors were first sent to charge sensitive preamplifiers which then fed to the main amplifiers in the circuit. A slow coincidence (2τ = 1 μsec) was demanded between the ΔE and E signals and pulses which satisfied this requirement entered the ΔE and E analogue to digital converter which were both operating in the 2048 channel mode. The PDP-1 on-line computer incorporated soft-ware based on the principle of reaction product detection as outlined previously. All energy calibrations of the Si-detectors were achieved using a ^{241}Am α-source. Typical energy resolution (FWHM) for deuterons obtained from the energy spectra were 35 keV to 40 keV.

A continuous monitoring system was part of the electronic circuitry. Elastically scattered protons from the target were stopped in a 3 mm lithium-drifted Si detector. This counter as shown in Figure 2 -2 is situated at a fixed angle of 20^{o} with respect to the beam direction.

Figure 2-6: Particle identifier spectrum.

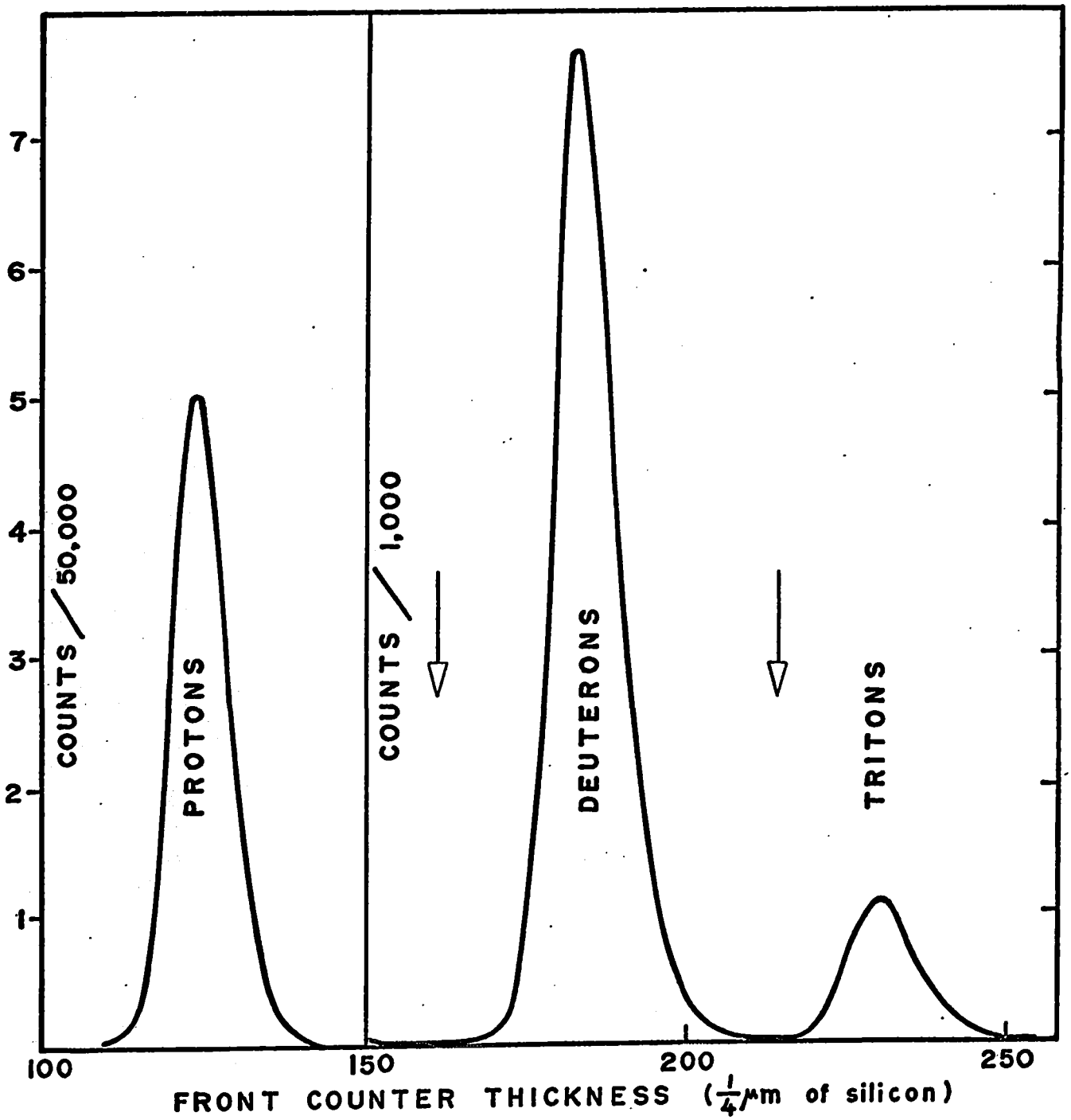
7
6
5
4
3
2
1
COUNTS / 50,000
PROTONS
COUNTS / 1,000
DEUTERONS
TRITONS
100
150
200
250
FRONT COUNTER THICKNESS (1/4 μm of silicon)

Figure 2-7: Block diagram of the electronics.

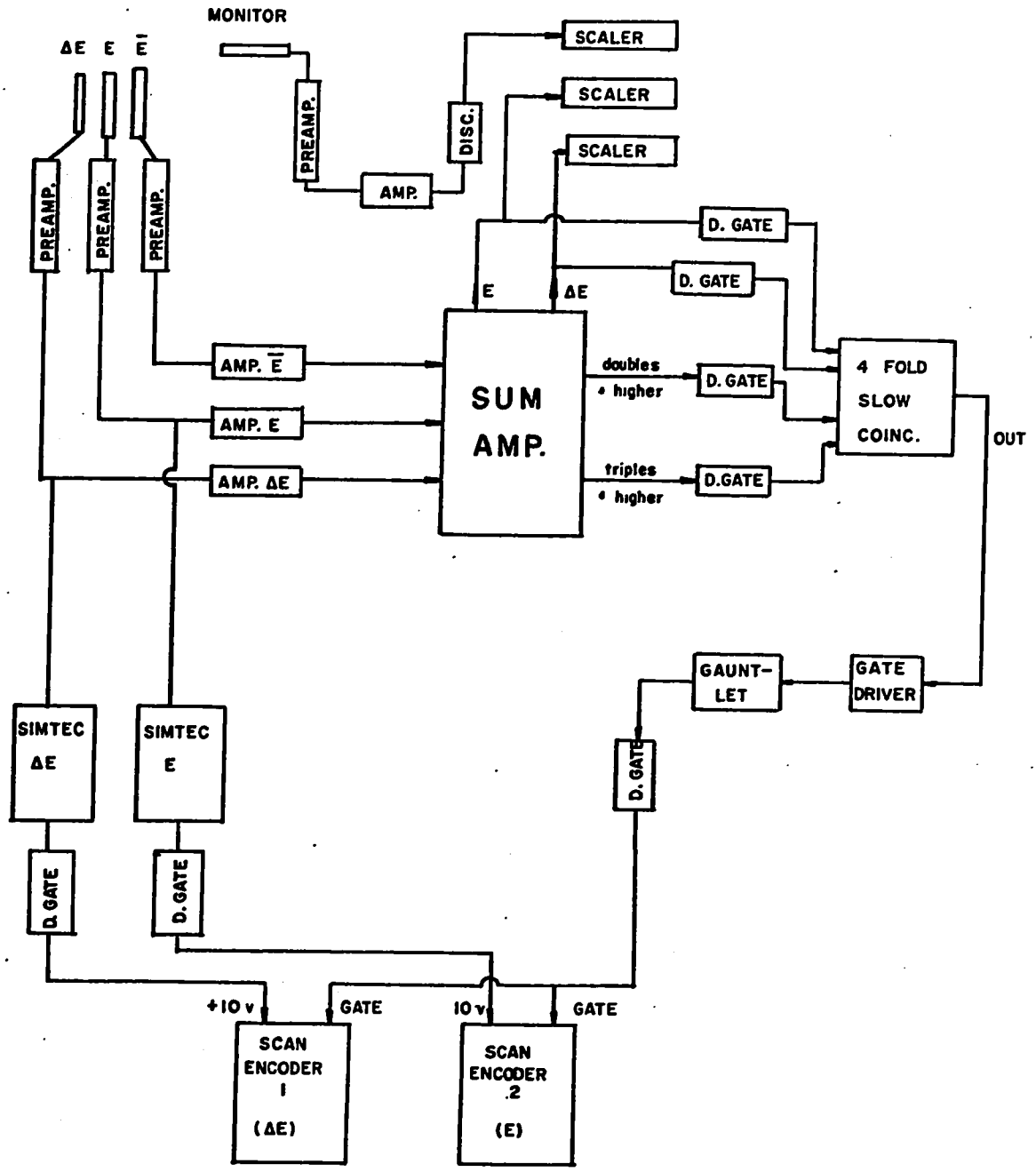
MONITOR
ΔE
E
Ē
PREAMP.
PREAMP.
PREAMP.
PREAMP.
AMP.
DISC.
SCALER
SCALER
SCALER
D. GATE
D. GATE
E
ΔE
AMP. Ē
AMP. E
AMP. ΔE
SUM AMP.
doubles + higher
triples + higher
D. GATE
D.GATE
4 FOLD SLOW COINC.
OUT
GAUNT-LET
GATE DRIVER
D. GATE
SIMTEC ΔE
SIMTEC E
D. GATE
D. GATE
+10 v
GATE
10 v
GATE
SCAN ENCODER 1 (ΔE)
SCAN ENCODER 2 (E)

The energy spectrum was recorded and a gate was set on the elastic peak. A scaler measured the number of counts from this peak. This technique allowed for an additional overall normalization of the data supplementing the beam current integrator. It was found that the ratio of beam-charge to monitor counts for each run was constant to within statistics.

2.3 Data Analysis

The stored data from the PDP-1 on-line computer was written on DECTAPE for further analysis. Part of the computer hardware was a CALCOMP-plotter which after each run plotted a histogram of the energy spectra.

The first step in the analysis of the energy spectra was the determination of the energies of the various final states populated in the reactions. With the aid of the computer program LORNA (L1), known final state peak positions were used to determine the energy scale, from which the excitations of all other levels in the spectrum could be determined. This method was used to obtain unknown levels in ^{26}Al, ^{36}Cl and ^{22}Na and proved highly successful in separating the overlapping states in the sodium-chloride target.

Peak areas and positions were obtained with the computer program "Anneliese" from J. W. Tepel (T1). The program fitted a standard peak shape determined from one of the spectra to the various peaks in a spectrum. The program is superior to a gaussian fitting procedure in that the actual peak shape rather than an assumed one is used. After appropriate background correction, the total number of counts in each peak for all the levels of interest was obtained and subsequently an angular distribution was determined.

2.4 Targets

The targets used in these experiments were solid targets, mounted on square stainless steel frames which contained a circular aperture of 7.9 mm in diameter. All targets were prepared by evaporation. The isotopically enriched magnesium and sodium-chloride targets were deposited onto a 10$\mu g/cm^2$ carbon foil, whereas the aluminum target was self-supporting.

The range of target thickness to be measured varied from about 25 $\mu gm/cm^2$ to 50 $\mu gm/cm^2$ and one of the more reliable methods which has proven to give satisfactory results in this target thickness range is Rutherford scattering of heavy ions. This method also identifies at the same time different target constituents and an accurate assessment of

target impurities is obtained. The heavy ions used for this target thickness determination were 6 MeV α-particles. Further details about Rutherford scattering are contained in Appendix 1.

Most of the contaminant peaks observed in the energy spectra were oxygen, carbon and nitrogen.

None of the targets showed any appreciable deterioration under bombardment.

2.5 Absolute Normalization of Cross Sections

The absolute differential cross-section was calculated using the formula,

$$\left(\frac{d\sigma}{d\Omega}\right)_{cm} = \left(\frac{C}{B}\right)_{\theta_L} * J_{\theta_L} * \frac{Z\ MR^2}{NAT} * (2.66 * 10^{-7})\ \text{mb/sr.}$$

where

C/B = the total number of counts per μc of incident beam of charge Z

θ_L = the laboratory scattering angle

J_{θ_L} = the factor for conversion from laboratory to centre-of-mass coordinates.

M = molecular weight of target

N = the number of nuclei per mole

T = target thickness in mg/cm^2

Geometrical parameters, all measured in inches.

R = the distance from the centre of the target to the front face of the entrance aperture of detector housing

A = area of entrance aperture.

All absolute cross-sections are accurate to ±9%.

CHAPTER 3

THEORETICAL CONSIDERATIONS

3.1 Selection rules

In all direct reactions, the total angular momentum transferred (j_n) in the reaction is related to the angular momentum of the initial state (J_i) and the angular momentum of the final state (J_f). The conservation of total angular momentum requires that (G7),

$$\vec{J}_i = \vec{J}_f + \vec{j}_n$$
$$= \vec{J}_f + \vec{\ell}_n + \vec{s}_n$$

where $\vec{\ell}_n$ and $\vec{s}_n$ refer to the transferred particle's orbital and spin angular momentum.

This in turn gives,

$$|J_i - J_f| - \frac{1}{2} < \ell_n < (J_i + J_f + \frac{1}{2})$$

The change in parity between the initial and final nuclear state is,

$$\Delta\pi = (-1)^{\ell_n}$$

3.2 Distorted Wave Born Approximation (DWBA) Method.

A great number of reactions have been studied where one nucleon is added or removed from the target (including (p, d), (d, t), (^{3}He, α), (d, n), etc.). It has been observed that in many of these reactions, a selected group of final states are populated with appreciable probability and the angular distributions of the exiting particle exhibit pronounced maxima and minima especially in the forward direction. These are characteristics of the direct transfer which occurs between the incident particle and a specific orbit in the residual nucleus without significantly exciting the internal degrees of freedom of the target.

Consider, then, the single-nucleon transfer reaction (p,d),

$$A + a \rightleftarrows B + b \qquad \text{where}$$

$b = a + x$

$A = B + x$

and x is the transferred nucleon. Forward arrows refer to pick-up and backward arrows to stripping.

The theoretical description of this process involves three basic physical assumptions:

a) Nucleon transfer occurs directly between the two active channels (A,a) and (B, b).

b) Optical model wavefunctions for A + a and B + b are correct in all relevant regions of configuration space.

c) Transfer process is weak enough to permit a first order treatment.

The differential cross section for a direct reaction of the form A(a, b)B, in the distorted wave Born Approximation can be written as (S10, B6):

$$\frac{d\sigma}{d\Omega}\ (p,\ d) = \frac{\mu_a \mu_b}{(2\pi\hbar^2)^2}\ \frac{k_a}{k_b}\ \frac{\Sigma\ |T_{AB}|^2}{(2J_B + 1)(2s_b + 1)} \qquad \text{where}$$

μ_a and μ_b are the reduced masses of the pairs (a,A) and (b, B);

k_a and k_b are the wave vectors for particles a and b;

J_A, J_B, s_a and s_b are the spins of particles A, B, a and b, respectively with z components M_A, M_B, m_a and m_b;

T_{AB} is the transition amplitude and takes the form

$$T_{AB} = \int d\vec{r}_a \int d\vec{r}_b\ \chi_b^{(-)*}(\vec{k}_b, \vec{r}_b) \langle B, b\ |V|\ A, a\rangle\ \chi_a^{(+)}(\vec{k}_a, \vec{r}_a)$$

Here $\vec{r}_a$ is the vector between the center of mass of the projectile and the center of mass of the target, similarly for $\vec{r}_b$. The functions χ_a and χ_b are distorted waves which describe the elastic scattering (weak coupling) in the entrance and exit channels and are solutions of a radial Schrodinger equation. The remaining factor in the amplitude represents the matrix element of the effective interaction taken between the internal states of the colliding pairs.

This transformation has been formulated (S6) and results in the following expression for the differential cross section,

$$\frac{d\sigma}{d\Omega} \quad (p, d) \quad = \quad \frac{3}{2} \; C^2 S(\ell, j) \; \sigma_{\ell j}(\theta)$$

The quantity C is the isotopic spin Clebsch-Gordon coefficient and $S(\ell, j)$ is the usual spectroscopic factor. In the present work, the single nucleon cross sections $\sigma_{\ell j}(\theta)$ are calculated using the Smith-Code (S6). The finite range corrections were accomplished using the method of Buttle and Goldfarb (B7).

The entrance and exit channel elastic scattered wave functions were calculated using the following form of the optical potential

$$U(r) = U_c(r) - V_s f(r, r_{os}, a_s) - i[\, W_s f(r, r_{oI}, a_I) +$$

$$+ \; 4a_I \, W_D \; \frac{d}{dr} f \, (r, r_{oI}, a_I)]$$

where the function $f(r, r_o, a)$ is the Saxon-Wood form factor

$$f(r, r_o, a) = \{1 + \exp [(r - r_o A^{1/3}) / a]\}^{-1}$$

and U_c is the Coulomb potential between a light particle of point-charge and a uniformly charged sphere.

CHAPTER 4

THE ^{26}Mg (p, d) ^{25}Mg REACTION

4.1 Introduction

The properties of low-lying states of ^{25}Mg up to an excitation energy of 4 MeV have been successfully represented by the Nilsson model which describes them as reasonably pure single particle states, based on Nilsson orbits 5($K^{\pi} = 5/2^{+}$), 9($K^{\pi} = 1/2^{+}$) and 11($K^{\pi} = 1/2^{+}$), coupled to a prolate spheroidal core (L2, N1, M1, H2, S3, E1).

In deformed light nuclei, the single-particle energies and rotational energies are of the same order of magnitude, so that coupling between the rotation and the particle motion has to be taken into account (K1). As a consequence, the mixing between states with the same spin and parity belonging to different bands will affect both absolute and relative spectroscopic factors.

In ^{25}Mg the lowest two bands above the $K^{\pi} = 5/2^{+}$ ground state band have $K^{\pi} = 1/2^{+}$. The $\Delta K = \pm 1$ selection rule therefore prevents rotation-particle coupling of these bands to the ground state band.

The $K^{\pi} = 3/2^{+}$ band which is based on Nilsson orbit 8 should start at an excitation of about 4 MeV, although it has not yet been identified. Also states at about the same excitation should occur which correspond to a hole in orbit number 7 ($K^{\pi} = 3/2^{+}$). Therefore, the simple picture of three pure rotational bands should be extended at energies near 4 MeV and above, in order to allow for the Coriolis interaction of these bands with the bands corresponding to Nilsson orbits 5, 9 and 11.

Single nucleon pick-up reactions are rather sensitive to hole state configurations in the core and the theoretical spectroscopic factors are found to be significantly changed by small proportions of orbits numbers 6 and 7 in the wave functions (D2). The three band description may therefore be inadequate in this type of analysis even for the low lying levels of ^{25}Mg. When $K^{\pi} = 3/2^{+}$ states are taken into account, the RPC effects are comparable in magnitude and a full six band mixing calculation is indicated.

A collective interpretation of the lower levels of ^{26}Mg is less well established. The energy which is required in order to break a neutron pair in ^{26}Mg is believed to be considerably less than in ^{24}Mg (D3),

so that the same purity of Nilsson configurations should not be expected. Considerable mixing of several Nilsson orbits in the ground state of ^{26}Mg has been required to fit single nucleon transfer spectroscopic factors in previous investigations. Hamburger and Blair (H3) estimated the mixing of orbits 5, 9 and 11 from the $^{26}Mg(d,t)^{25}Mg$ reaction. Cujec (C1) considered the lowest 0^+ levels of ^{26}Mg to be formed from a neutron pair in mixed orbits 5 and 9 when she analyzed the $^{25}Mg(d,p)^{26}Mg$ reaction. Dehnhard and Yntema (D2) considered mixing of orbits 5, 6, 7, 9, 11 and 8 in their analysis of the $^{26}Mg(d,t)^{25}Mg$ reaction.

This study reports an analysis of the $^{26}Mg(p,d)^{25}Mg$ reaction at a proton energy of 20 MeV, in which we assume that the ^{25}Mg levels below 4 MeV are described by mixed single particle states outside a spheroidal core. Band mixing among all the orbits in the (1d-2s) shell is taken into account. The spectroscopic factor information is used to estimate the probability V_α^2 that a particular Nilsson orbit α is filled by a neutron in the ^{26}Mg target.

4.2 Experimental Results

The reaction was studied at an incident proton beam energy of 20 MeV. A ^{26}Mg target enriched to >99% was obtained from AWRE Aldermaston; it was prepared by evaporating MgO onto a carbon foil. The target

thickness was measured to be 27 $\mu g/cm^2$ using Rutherford scattering. A spectrum of the deuterons at 18^o in the laboratory system is shown in Figure 4-1. Energy resolutions of approximately 40 keV were achieved using the previously described counter telescope system.

The principal feature of the deuteron spectrum appears to be that all states under investigation are strongly excited. The only impurity in the spectrum is the ground state transition of the $^{16}O(p,d)^{15}O$ reaction. In addition the spectrum shows the j-forbidden transitions to the $J^\pi = 7/2^+$ and $J^\pi = 9/2^+$ states at 1.611 MeV and 3.399 MeV respectively (D5). These transitions are relatively strongly excited although the $9/2^+$ level at 3.399 MeV could not be resolved from the $3/2^-$ level at 3.408 MeV. Angular distributions of the deuteron groups for most states were recorded over the range from 20^o to 125^o.

The experimental angular distributions together with the calculated curves are shown in Figures 4-2 to 4-4. The error bars refer to the statistical uncertainties of the data points, and there is an additional uncertainty of 9 % in the absolute differential cross sections. A discussion on absolute differential cross sections has been previously described in section 2.5.

Figure 4-1: Energy spectrum of the $^{26}Mg(p, d)^{25}Mg$ reaction.

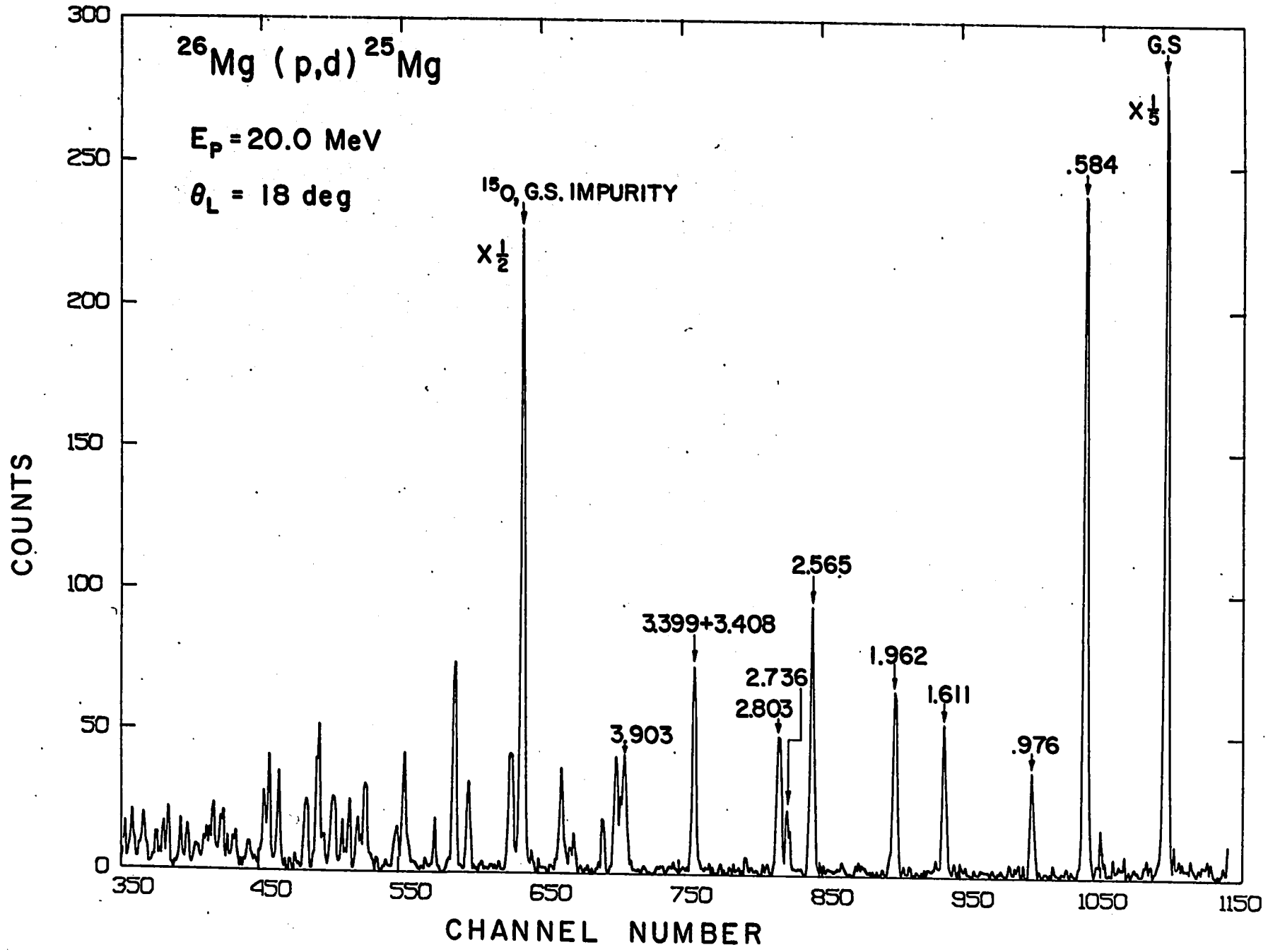
$^{26}Mg\ (p,d)\ ^{25}Mg$
$E_p = 20.0$ MeV
$\theta_L = 18$ deg
^{15}O, G.S. IMPURITY
X 1/2
G.S
X 1/5
.584
2.565
3.399+3.408
1.962
2.736
2.803
1.611
3.903
.976
COUNTS
CHANNEL NUMBER
0
50
100
150
200
250
300
350
450
550
650
750
850
950
1050
1150

Figure 4-2: The $\ell_n = 2$ angular distributions for the reaction $^{26}Mg(p, d)^{25}Mg$.

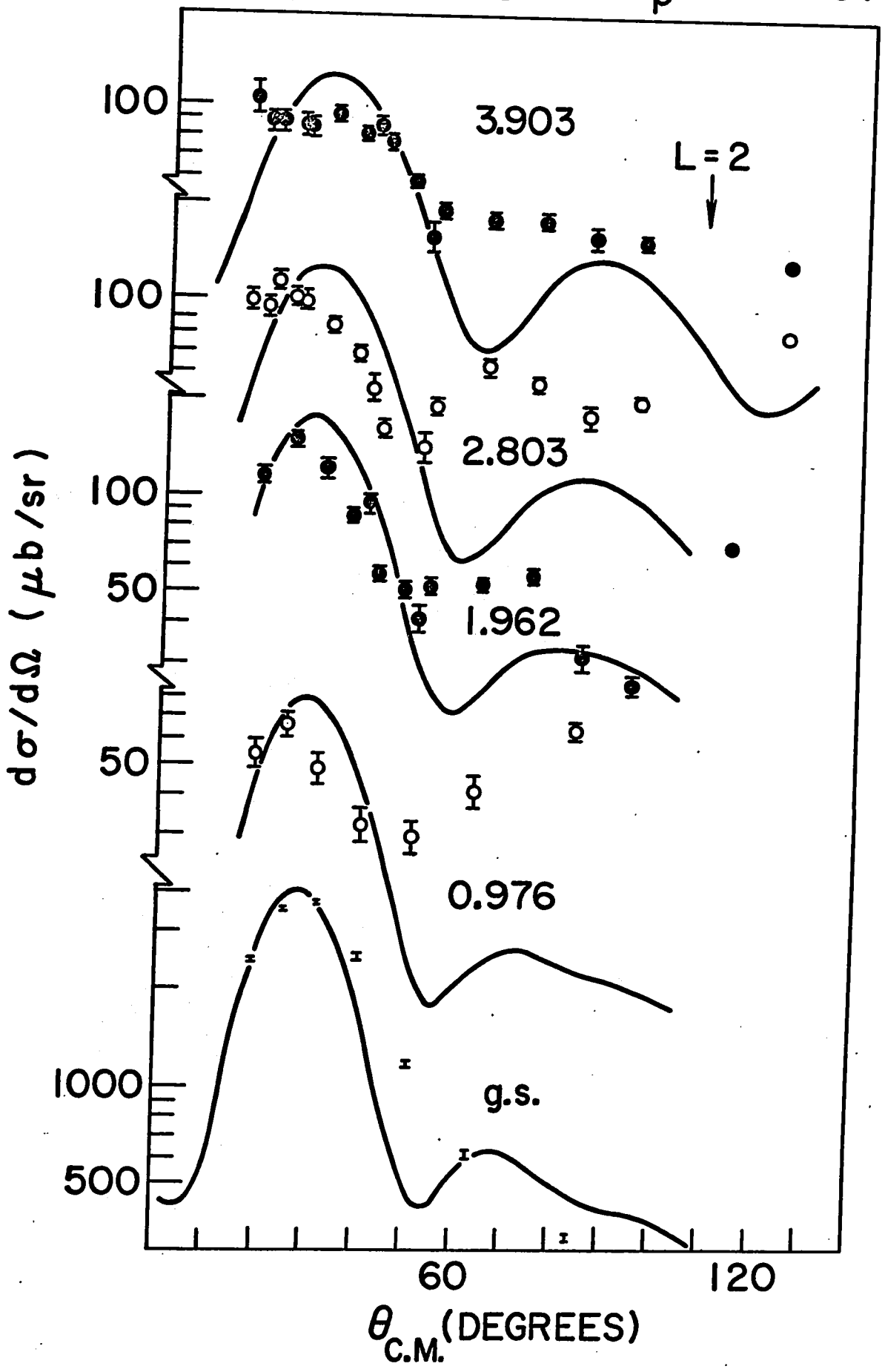
^{26}Mg (p,d) ^{25}Mg, E_p = 20 MeV
100
3.903
L = 2
100
2.803
100
50
1.962
50
0.976
1000
g.s.
500
dσ/dΩ (μb/sr)
60
120
θ C.M. (DEGREES)

Figure 4-3: The $\ell_n = 0$ angular distributions for the reaction $^{26}Mg(p, d)^{25}Mg$.

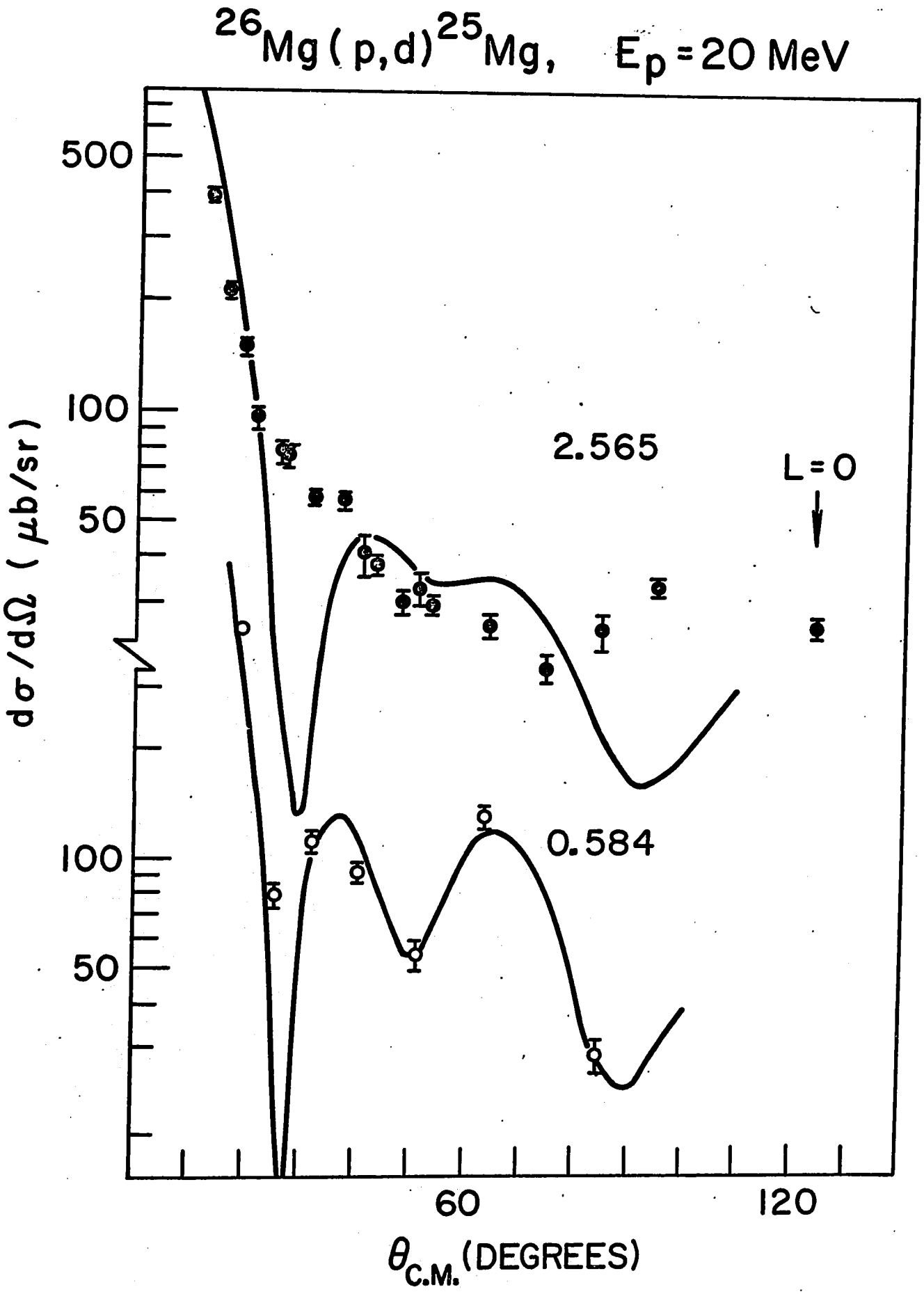
$^{26}Mg(p,d)^{25}Mg$, $E_p = 20$ MeV
500
100
50
100
50
2.565
L=0
0.584
60
120
$d\sigma/d\Omega$ (μb/sr)
$\theta_{C.M.}$ (DEGREES)

Figure 4-4: The $\ell_n = 4$ angular distributions for the reaction $^{26}Mg(p, d)^{25}Mg$.

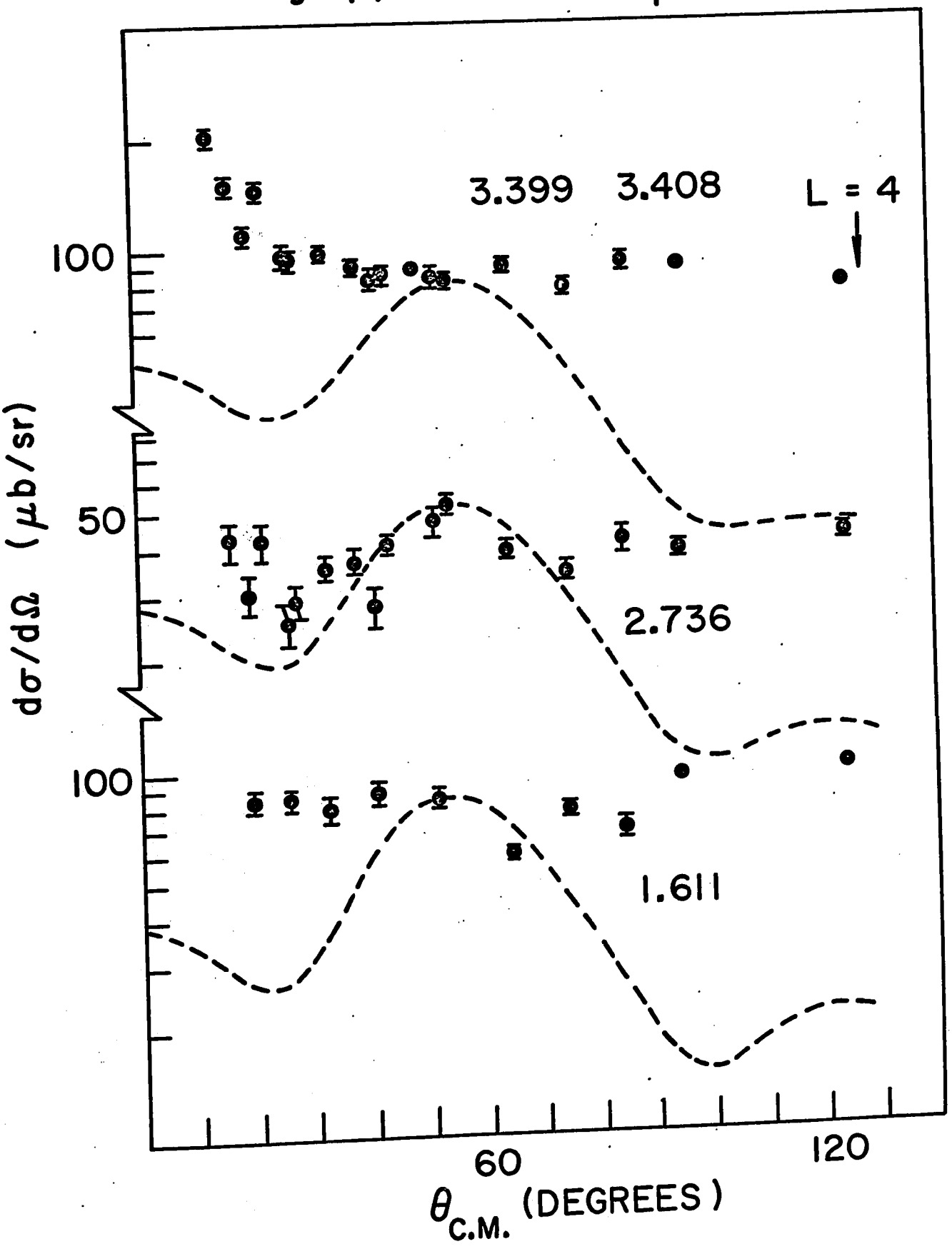
$^{26}Mg(p,d)^{25}Mg$, E_p=20 MeV
3.399
3.408
L = 4
100
50
100
2.736
1.611
$d\sigma/d\Omega$ (μb/sr)
60
120
$\theta_{c.m.}$ (DEGREES)

4.3 Theoretical spectroscopic factor calculation for single nucleon pick-up reaction.

The wave function $|N\Omega\alpha\rangle$ of a single particle in Nilsson orbit α can be expanded into spherical wave functions as follows:

$$|N\Omega\alpha\rangle = \sum_j C_{Nj\Omega} |Nj\Omega\rangle ,$$

The square of the Nilsson coefficient $C_{Nj\Omega}$ measures the probability that a particle in orbit α has angular momentum ℓ and total spin j. The symbol Ω is the projection of the total spin of the odd nucleon onto the symmetry axis. Nilsson neglected the interaction between different shells and accordingly the summation is restricted to a single oscillator shell. For the 1d-2s shell, N is 2. The expansion coefficients $C_{Nj\Omega\alpha}$ are tabulated by Davidson (D4) and are related to the $A_{\ell\Lambda}$ which are tabulated for D = 0 by Nilsson (N1) and, for a range of D values, by Bishop (B1). The transformation between the coefficients is given by

$$C_{Nj\Omega} = \{ \sum_\Lambda (\ell \tfrac{1}{2}\Lambda\Sigma|j\Omega) A_{\ell\Lambda}\}/(\sum_\Lambda A^2_{\ell\Lambda})^{\frac{1}{2}} ,$$

where Λ and Σ are the projections of the orbital angular momentum and the particle's spin respectively. The condition for axial symmetry requires that

$$\Omega = \Lambda + \Sigma$$

The expression derived by Satchler (S4) for the spectroscopic factor, for pick-up of a nucleon leading to a nucleus described as an odd-nucleon strongly coupled to an axially symmetric deformed core is:

$$S_{\ell j} = \rho^2 \frac{2J_o + 1}{2J + 1} (J_o j\ K_o \Omega | JK)^2 C^2_{Nj\Omega\alpha} ,$$

where J_o and K_o are the spin and its projection along the nuclear symmetry axis respectively, for the residual nucleus A. J and K are the corresponding values for the (A + 1) target. Ω is the spin projection on the symmetry axis of the transferred particle. ρ^2 takes the value 2 where either $K_o = 0$ or $K = 0$, otherwise $\rho^2 = 1$. For a spin zero target, $J = K = 0$, and the spectroscopic factor simplifies to $S_{\ell j} = 2C^2_{Nj\Omega\alpha}$. The sum rule for pick-up is then $\sum_{\ell J} S_{\ell j} = 2$, which corresponds to the sum rule given by Macfarlane and French (M2) for stripping.

We extend the theory to include the off diagonal N ± 2 elements which take into account the coupling between the major shells. Major shell mixing has a small effect on the magnitude of the $C_{2j\Omega\alpha}$ coefficients and can usually be ignored. However, the j-forbidden transitions to excited states of spin greater than 5/2 are enhanced in this reaction and the theoretical spectroscopic factor can only be evaluated for these transitions if the $C_{4j\Omega\alpha}$ coefficients are included.

The resulting $|N\Omega\alpha>$ wave function becomes

$$|N\Omega\alpha> = \sum_{Nj} C_{Nj\Omega} |Nj\Omega>$$

Figure 4-5 shows the $C_{Nj\Omega\alpha}$ coefficients as a function of deformation when major shell mixing is taken into account. As expected the coefficients of those states with N = 4 from the g-shell are small and can be neglected in comparison with the more dominant N = 2 components, when both contribute to the evaluation of the theoretical spectroscopic factor.

Also it is noted the close similarity between the coefficients calculated here (Table 4-1) for a deformed harmonic oscillator potential and those calculated by Rost and reported by Dehnhard and Yntema (D2) for a deformed Saxon-Woods potential. The Nilsson energy level diagram in this region was found to be qualitatively unchanged when the N = 0 and N = 4 terms are included, though the energies on the whole shift downwards for positive deformation.

The effects of pairing (Y1, C2) are considered in this calculation. In a simple approximation, the ground state of ^{26}Mg may be considered to consist of two neutrons in Nilsson orbit number 5 ($K^{\pi} = 5/2^{+}$) coupled to a deformed ^{24}Mg core. An extension to this

Figure 4-5: The Nilsson model expansion coefficients $C^2_{Nj\Omega}$, including major shell mixing, plotted as a function of the deformation parameter β.

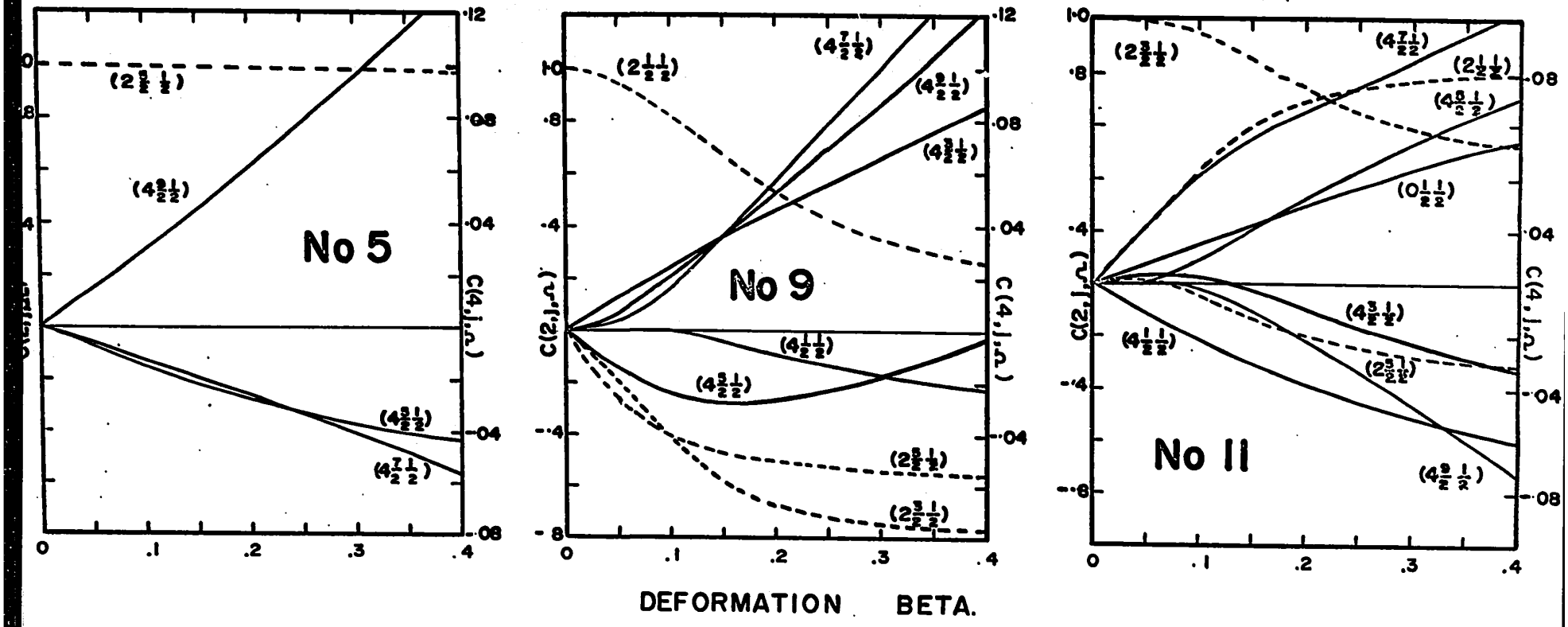
No 5
No 9
No 11
DEFORMATION BETA.

Table 4-1

Values of the Nilsson coefficients $C_{Nj\,\Omega}$, as obtained from the major shell-mixing calculation

$\alpha(\Omega)$			$6(\frac{1}{2}^+)$	$7(\frac{3}{2}^+)$	$5(\frac{5}{2}^+)$	$9(\frac{1}{2}^+)$	$11(\frac{1}{2}^+)$	$8(\frac{3}{2}^+)$
N	j	ℓ						
0	$\frac{1}{2}$	0	-0.0588	0.0	0.0	0.0032	0.0335	0.0
2	$\frac{1}{2}$	0	-0.4966	0.0	0.0	0.4766	-0.7172	0.0
2	$\frac{3}{2}$	2	-0.2518	-0.2135	0.0	0.7035	0.6475	0.9710
2	$\frac{5}{2}$	2	0.8109	0.9662	0.9944	0.5094	-0.2297	0.2155
4	$\frac{1}{2}$	0	0.0441	0.0	0.0	-0.0113	-0.0207	0.0
4	$\frac{3}{2}$	2	0.0499	0.0190	0.0	-0.0566	0.0144	0.0223
4	$\frac{5}{2}$	2	-0.0867	-0.0288	0.0308	0.0252	-0.0441	0.0251
4	$\frac{7}{2}$	4	-0.0411	-0.0494	-0.0381	0.0881	0.0912	0.0927
4	$\frac{9}{2}$	4	0.1236	0.1306	0.0939	0.0816	-0.0387	0.0310

Nilsson parameters: $\eta = 4.31$, $\mu = 0.0$ and $\kappa = 0.05$

model would include admixtures due to pairing interaction of higher Nilsson orbits. In this analysis the assumption is made that the 1s-1p shells and Nilsson orbits 6 and 7 are completely filled and that the remaining two neutrons partly fill Nilsson orbits 5, 9, 8 and 11. $V^2_{\Omega\alpha}$ represents the probability that a particular Nilsson orbit α is occupied by a nucleon pair.

In addition rotation-particle coupling has to be taken into account. The symbol $W_{\Omega\alpha}$ represents the band mixing coefficients which will be described in section 4.4.

The resulting spectroscopic factor for a pick-up reaction on a spin-zero target becomes

$$S_{Nj} = 2 \left\{ \sum_{\Omega\alpha} V_{\Omega\alpha} \; W_{\Omega\alpha} \; C_{Nj\Omega} \right\}^2$$

4.4 Calculation of Coriolis band mixing coefficients.

The complete Hamiltonian that describes the motion of the odd particle in the deformed-field of the nucleus, the rotation of the nucleus and the rotation-particle coupling can be written as:

$$H = H_{intr.} + H_{rot.} + H_{R.P.C.}$$

$H_{intr.}$ is the part of the Hamiltonian describing the intrinsic states and has been solved by Nilsson. Nilsson assumed a single-particle Hamiltonian of the following form:

$$H = H_o + C\,\ell.s + D\,\ell.\ell$$

where H_o is the oscillator potential, to which is added a spin orbit potential $C\ell.s$ and the term $D\ell.\ell$. Nilsson then studied the effect of a deformation of the nuclear potential with cylindrical symmetry. H_o is further split into a spherically symmetric term $\mathring{H}_o$ and a term H_δ representing the coupling of the particle to the axis of the deformation. Neglecting the RPC, the basic set of wavefunctions is a product of the single particle wavefunctions $|K\alpha>$ with a core wavefunction D^I_{MK},

$$|IMK> = \left[\frac{2I+1}{16\pi^2}\right]^{\frac{1}{2}} \{ D^I_{MK}|K\alpha> + (-1)^{I-j} D^I_{M-K} |-K\alpha>\}$$

where I is the total angular momentum of the nucleus and M its projection on the space fixed axis. The symbol K (or Ω since we assume axial symmetry) is its projection on the nuclear symmetry axis.

The $H_{R.P.C.}$ term is responsible for coupling states with the same value of I with $\Delta K = \pm 1$ or $\Delta K = 0$ if, and only if, $K = K' = \frac{1}{2}$.

The Coriolis band mixing coefficients $W_{\Omega\alpha}$ were calculated by carrying out a perturbation treatment of the R.P.C. Hamiltonian,

$$H_{R.P.C.} = \frac{-\hbar^2}{2J} \quad (I^+ j^- + I^- j^+)$$

where the operators $I^{\pm}$ and $j^{\pm}$ connect only states as previously postulated and J is the moment of inertia. The unmixed energies represent the diagonal matrix elements of the Hamiltonian and are given by,

$$E_K(I) = E_K^{(o)} + E_K^{(1)} \quad \{I(I+1) + \delta_{K,\frac{1}{2}} \quad a(-)^{I+\frac{1}{2}} \quad (I+\tfrac{1}{2})\}$$

$$- \quad E_K^{(2)} \quad \{I(I+1) + \delta_{K,\frac{1}{2}} \quad a(-)^{I+\frac{1}{2}} \quad (I+\tfrac{1}{2})\}^2$$

where $E_K^{(1)} = h^2/2J$, and $E_K^{(2)}$ is the strength of the rotation-vibration term.

The decoupling parameter a is

$$a = - \sum_j \quad (-)^{j+\frac{1}{2}} \quad (j+\tfrac{1}{2}) \quad c^2_{j,\frac{1}{2}}$$

In the band-mixing calculation, all Nilsson bands number 5 - 9 and 11 were allowed to mix. The off-diagonal elements of the Hamiltonian are

$$\langle IMK'\alpha' | H(RPC) | IMK\alpha \rangle$$

$$= - \frac{\hbar^2}{2J} \quad A_{K,K'} \quad [(I + K_>) \quad (I - K_> + 1)]^{\frac{1}{2}}$$

with

$$A_{K,K'} = \sum_j C_{NjK'} C_{NjK} \left[(j + K_>)(j - K_> + 1)\right]^{\frac{1}{2}}$$

where $K_>$ is the greater of K' and K.

The energy matrix was diagonalized to give the energy of each mixed state $|IM>$ and the expansion coefficient $W_{\Omega\alpha}$ of its wave function

$$|IM> = \sum_{\Omega\alpha} W_{\Omega\alpha} |IMK>$$

A computer code performed the calculations as described below. Nilsson wavefunctions were generated with $\eta = 4.3$, $\kappa = 0.05$, $\mu = 0$ and $\beta = 0.22$. The values of the $C_{Nj\Omega}$ coefficients were computed from the major shell mixing as outlined previously. The remaining parameters to be fixed are the values of $E_K^{(0)}$, $E_K^{(1)}$ and $E_K^{(2)}$ for each band.

The experimental energies of the band heads fix the $E_K^{(0)}$ to a large extent, however the band heads of orbits number 6, 7, and 8 have not been identified in ^{25}Mg and for these the estimates used by Dehnhard and Yntema (D2) of 6.0 MeV, 4.2 MeV and 4.0 MeV respectively were taken for the calculation. Values of $E_K^{(1)}$ were also estimated from the foregoing reference, although some variation was allowed in trying to achieve the best least-squares fit to the experimental energies. This fit was primarily achieved however, through a variation of $E_K^{(2)}$. The results are shown in Figure 4-6 where the experimental energy spectrum of ^{25}Mg

Figure 4-6: The band structure of ^{25}Mg as given by Sharpey-Schafer et al., compared to the predictions of a Coriolis band mixed Nilsson single particle calculation.

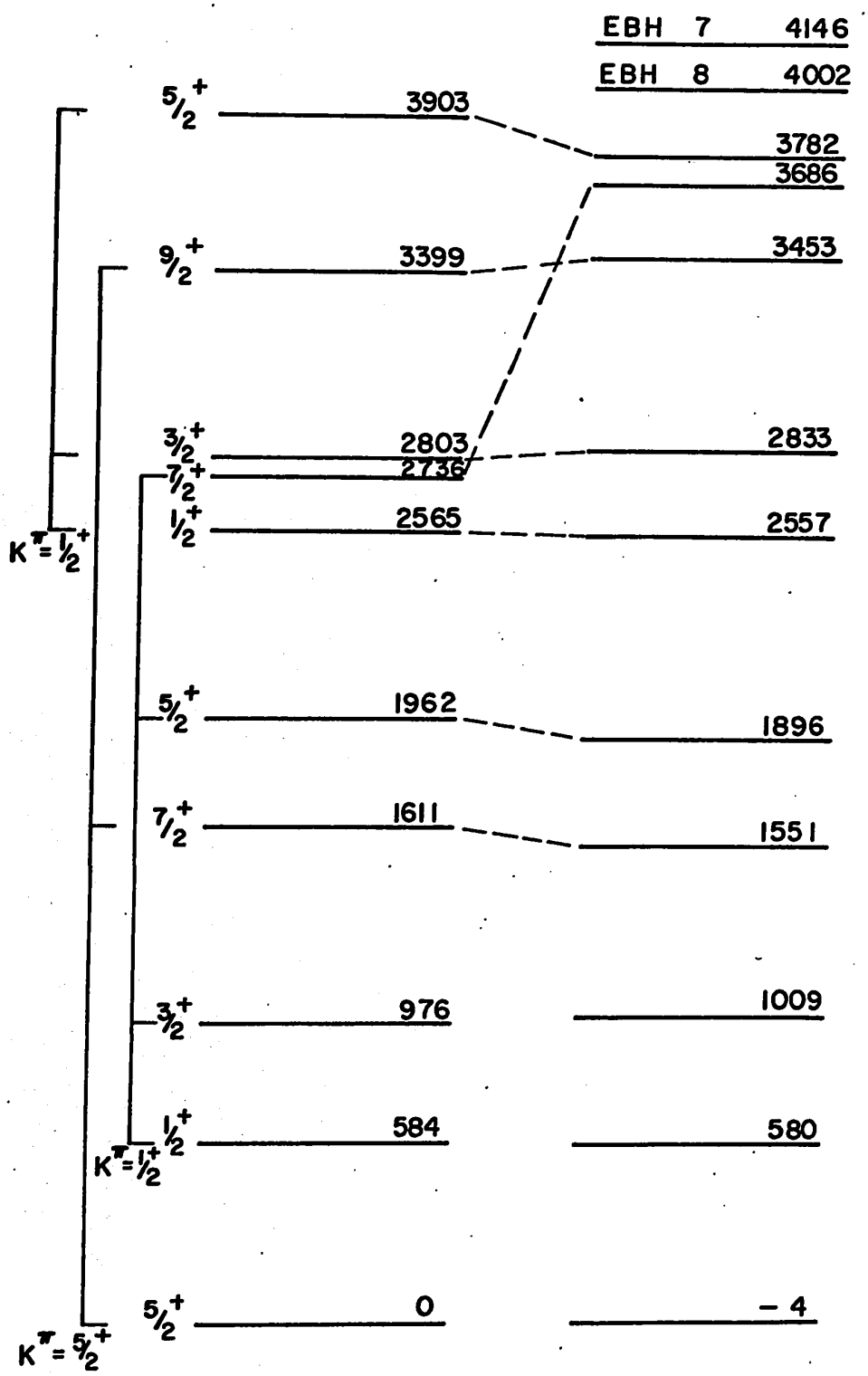
EBH 7 4146
EBH 8 4002
5/2+
3903
3782
3686
9/2+
3399
3453
3/2+
2803
2833
7/2+
2736
1/2+
2565
2557
K^π = 1/2+
5/2+
1962
1896
7/2+
1611
1551
3/2+
976
1009
1/2+
584
580
K^π = 1/2+
5/2+
0
-4
K^π = 5/2+
EXP.
25Mg
CALC.

as proposed by Sharpey-Schafer et. al. (S5) is illustrated in comparison with the Coriolis coupling results. The agreement can be considered adequate in view of the uncertainties in the band head energies and in the theory (B2). The values of the mixing coefficients $W_{\Omega\alpha}$ which are pertinent to the spectroscopic factors for the $^{26}Mg(p,d)^{25}Mg$ reaction are listed in Table 4-2.

4.5 Core-excited states

In considering the $T = \frac{1}{2}$ excited states in ^{25}Mg, we are assuming that one nucleon can be excited from the Nilsson orbits 6 and 7. This excited nucleon may be either a proton or a neutron, which is then coupled to the extra neutron to form a $T = \frac{1}{2}$ state. These states in ^{25}Mg in (T, T_z) space have the form,

$$\psi(\tfrac{1}{2},\tfrac{1}{2}) = \sqrt{\tfrac{2}{3}}\,\psi_{core}\ (\tfrac{1}{2}, -\tfrac{1}{2})\psi_{pair}\ (1,1) - \sqrt{\tfrac{1}{3}}\,\psi_{core}\ (\tfrac{1}{2},\tfrac{1}{2})\psi_{pair}(1,0).$$

In the $^{26}Mg(p,d)^{25}Mg$ reaction a neutron is picked up from ^{26}Mg which has a neutron pair outside a ^{24}Mg core. Since strong pairing exists between like nucleons and if only one particle is excited from the core then that particle will be a neutron to pair off with the one already there.

Table 4-2.

Values of the Coriolis band mixing coefficients $W_{\Omega\alpha}$ for $\eta = 4.3$, $\kappa = .05$ and $\mu = 0$

Level (MeV)	Spin I	$W_{\Omega\alpha}$					
		$\alpha = 5$	6	7	8	9	11
0.0	$\frac{5}{2}$	.944	.088	.280	.064	.130	-.037
.584	$\frac{1}{2}$	-	.028	-	-	.999	-.002
.976	$\frac{3}{2}$	-	.066	.169	.146	.972	-.018
1.611	$\frac{7}{2}$	.881	.100	.388	.117	.213	-.058
1.962	$\frac{5}{2}$	-.213	.156	.191	.215	.920	-.028
2.565	$\frac{1}{2}$	-	-.036	-	-	.003	.999
2.736	$\frac{7}{2}$	-.311	.083	.105	.359	.869	.034
2.803	$\frac{3}{2}$	-	-.096	-.306	.250	.038	.913
3.399	$\frac{9}{2}$	.794	.270	.495	.177	.278	-.07
3.903	$\frac{5}{2}$	.131	-.293	-.393	.446	.08	.734

Therefore, in a band mixing calculation, if W_6 is the amplitude of the number 6 band component in the wave function of an excited $T = \frac{1}{2}$ level, then that part which will be observed in a pick-up reaction is $\sqrt{\frac{2}{3}} \times W_6$. The equivalent is true for W_7.

4.6 Experimental results and distorted wave analysis.

A DWBA fitting of the levels up to 3.903 MeV excitation was attempted using a programme written by W. R. Smith (S6) which was outlined in Chapter 3. This programme assumes a Saxon-Woods potential for the neutron bound state, where the well depth is adjusted to produce an eigenstate of the separation energy. No non-local corrections were made, but finite range effects were included by means of the local energy approximation.

A search was made among available proton (P1) and deuteron (P2, H4) optical model parameters which are known to fit the elastic scattering data at energies near to the channel energies of our measurements. The six proton potentials and the five deuteron potentials listed in Table 4-3 were chosen, and a search made with all combinations for the best simultaneous fits to all the levels. The shape of the angular distributions was found to vary between the different potentials, but those combinations which gave reasonable fits all gave closely similar spectroscopic factors. A typical set corresponding to solution number 2

Table 4-3

Optical model parameters which were used in the search for the best overall fit to the $^{26}Mg(p,d)^{25}$ angular distributions for the levels listed in Table 4-3. The rotation is from Perey (P1).

Solution Number		V_s MeV	r_{os} fm	a_s fm	W_s MeV	W_D MeV	r_{oI} fm	a_I fm	Ref.
Proton	1	46.9	1.25	0.65	0	8.2	1.25	0.47	P1
	2	51.8	1.29	0.48	8.6	0	1.29	0.48	H5
	3	42.7	1.30	0.62	0	10.6	1.30	0.44	C3
	4	47.3	1.20	0.64	0	5.7	1.20	0.50	C4
	5	46.9	1.25	0.65	0	11.0	1.25	0.47	C4
	6	43.4	1.25	0.65	0	9.0	1.25	0.47	P1
Deuteron	1	73.1	1.187	0.805	0	27.7	1.398	0.605	P3
	2	92.83	1.20	0.75	12.62	0	1.91	0.38	J1
	3	91.08	1.20	0.78	0	27.4	1.51	0.48	J1
	4	90.99	1.20	0.79	0	21.92	1.55	0.46	J1
	5	96.0	1.40	0.70	12.3	0	1.40	0.70	S8

for the proton, and solution number 3 for the deuteron potential, was therefore chosen. The $\ell = 2$ transitions are shown in figure 4-2 and the $\ell = 0$ transitions in figure 4-3. It is clear that no combination of the potential would provide a satisfactory fit to all the levels. In particular the wave number changes between the ground state and the 976 keV level were insufficient to account for their quite different angular distribution shapes. The shift of the peak with excitation energy between the $\ell = 2$ transitions is in an opposite sense to that predicted by the DWBA theory.

It has been suggested (L3, L4) that the deviation between the shape of the theoretical curve for the reaction leading to the ground state and the experimental angular distribution can be attributed to a j-dependent effect, where the $j = \frac{3}{2}$ transition exhibits a sharp drop-off at about 55^{o} and the $j = \frac{5}{2}$ does not. In general the agreement between theoretical prediction and experimental data for the $\ell = 0$ and $\ell = 2$ is fairly good except for the 0.976 MeV state, where the sharp rise in the angular distribution beyond 60^{o} was impossible to fit.

The transitions to the $J^{\pi} = \frac{7+}{2}$ levels at 1.611 MeV and 2.736 MeV, which appear quite strongly, are forbidden by the shell model assuming pick-up of a (1d-2s) neutron from the target. Major shell mixing of the Nilsson orbits introduces (1g) components into the orbit wave functions and $\ell_n = 4$ pick-up is then possible. However

figure 4-4† shows that the angular distributions to these levels are not well fitted by the $\ell_n = 4$ DWBA theory.

An alternative reaction process seems likely to be important in populating the $\frac{7^+}{2}$ and $\frac{9^+}{2}$ levels. In the DWBA theory the transition is assumed to take place directly from the entrance channel to the exit channel. That is, the transition is assumed to be a one-step process. Usually the one-step process will dominate if the state of the daughter nucleus has good overlap with the ground state of the target nucleus and the entrance or exit channel is not very strongly coupled to some other channel. However, there are cases when slightly less direct transitions play an important role. For instance, the entrance channel may be strongly coupled to a low-lying state corresponding to the excitation of a collective mode of the target nucleus. The two-step process (I1, A1), excitation of the target nucleus followed by pick-up to the exit channel, will play a role comparable to that of the one-step process. In particular, the two-step process is likely to be important in magnesium where the proton inelastic scattering cross section to the first $J^\pi = 2^+$ excited state has a large cross section (K2). Moreover, an analogous two-step process, involving the excitation of a collective mode in the daughter nucleus, can also be expected to make a significant contribution to the stripping cross section.

† see Errata.

4.7 Absolute spectroscopic factor analysis

In order to minimize the effects of processes other than single step neutron pick-up, the initial analysis was confined to the ground state, the 0.584 MeV level, and the 2.565 MeV level. These are the band-head levels so that their main components have non-rotating cores. The three experimental spectroscopic factors which were obtained from the DWBA fits were used to solve for the three filling coefficients V_9, V_{11} and V_5. The mixing of the number 8 Nilsson orbit was quite small in these ^{25}Mg levels so that any reasonable value of V_8 would have a negligible effect. Values of $V_5 = .78$, $V_9 = .57$ and $V_{11} = .30$ were obtained.

The experimental spectroscopic factors deduced by DWBA analysis are presented in column number 5 of Table 4-4. The theoretical spectroscopic factors leading to states which are members of the number 5, 9 and 11 bands are shown in column 6. The calculations are based on the filling coefficients derived previously. The role which RPC and N mixing play is reflected in the results of column 6 particularly when these results are compared to columns 7 and 8.

Column 9 of Table 4-4 shows the theoretical spectroscopic factors which were calculated by Dehnard and Yntema (D2) with the same assumptions as in column 6, but using the Nilsson coefficients corresponding to a

Table 4-4: Values of the spectroscopic factor for transitions in the reaction $^{26}Mg(p,d)^{25}Mg$.

level (MeV)	Main Component j	Ω	α	S_{exp}	S_{theory} N mixed R.P.C.	N mixed no R.P.C.	N = 2 only no R.P.C.	a)	S_{exp} (40 MeV)b
0.0	$\frac{5}{2}$	$\frac{5}{2}$	5	2.28	2.28	1.3	1.2	2.3	2.28
0.584	$\frac{1}{2}$	$\frac{1}{2}$	9	0.13	0.13	0.14	0.16	0.13	0.15
0.976	$\frac{3}{2}$	$\frac{1}{2}$	9	.06	0.20	0.27	.31	0.27	0.10
1.611	$\frac{7}{2}$	$\frac{5}{2}$	5	.29	0.003	0.002	0	0.004	-
1.962	$\frac{5}{2}$	$\frac{1}{2}$	9	.15	0.24	0.19	0.17	0.22	0.14
2.565	$\frac{1}{2}$	$\frac{1}{2}$	11	.077	.077	0.09	0.09	0.06	0.03
2.736	$\frac{7}{2}$	$\frac{1}{2}$	9	.19	.004	.005	0	-	-
2.803	$\frac{3}{2}$	$\frac{1}{2}$	11	.17	0.14	0.08	0.08	0.04	0.22
3.399	$\frac{9}{2}$	$\frac{1}{2}$	5	<.3[c]	0.04	0.01	0	0.058	-
3.903	$\frac{5}{2}$	$\frac{1}{2}$	11	.22	0.33	0.04	0.01	0.002	-

a) Dehnhard, D. and Yntema, J. L., Phys. Rev. 160, 964(1967). Calculated for a Saxon-Woods deformed well.
b) Reynolds, G. M., Ph.D. Thesis, University of Minnesota 1966 (unpublished). Normalized to S = 2.28 for the ground state.
c) unresolved doublet.

particle in a deformed Saxon-Woods potential. Finally column 10 shows the experimental spectroscopic factors which where calculated by Reynolds (R1) for the ^{26}Mg (p,d) ^{25}Mg reaction at the higher bombarding energy of 40 MeV. It is seen that general agreement is obtained.

4.8 Discussion

The $\ell_n = 4$ angular distributions of the $J^\pi = \frac{7+}{2}$ levels in ^{25}Mg bear no resemblance to the calculated curves. Also the theoretical spectroscopic factors under-estimate the experimentally extracted factors, indicating that the direct nucleon pick-up theory is inadequate for transitions to these levels. This conclusion is further substantiated by the fact that recent calculations which included the two step process through the generalized DWBA model, have obtained much better agreement for these levels (S7).

Little can be said of the $\frac{9+}{2}$ level at 3.399 MeV since it was not resolved from the $\ell_n = 1$ transition to the level at 3.404 MeV. Neither of these levels should be populated strongly in the Nilsson single particle model.

The over-estimate of the 0.967 MeV level spectroscopic factor is hard to understand without a large contribution to the reaction

mechanism from a predominantly backward peaking mechanism. Both the 0.967 MeV and the 0.548 MeV levels are predicted to be reasonably pure orbit number 9 states from the band mixing calculations, and the predicted spectroscopic factor ratio is close to the ratio $C^2_{N\ 3/2\ 1/2}:C^2_{N\ 1/2\ 1/2} = 0.495:0.227 = 2.2$ for this orbit. However the experimental ratio is 0.44.

The large differences between columns 6 and 7 in Table 4-4 show that rotation particle coupling is important for the lower levels of ^{25}Mg. This is particularly true of the 3.903 MeV state where the proximity of the orbit number 7 has a considerable effect. An increase in the orbit number 7 band energy from the assumed value of 4.2 MeV to about 6.3 MeV reduces the spectroscopic factor to the experimental value without significantly changing the fit to the experimental energy levels of Figure 4-6.

The differences between columns 7 and 8, on the other hand, are much smaller. Therefore, as originally pointed out by Nilsson, the effect of major shell mixing is small and is certainly insufficient to account for the experimental spectroscopic factors to the $\frac{7^+}{2}$ and $\frac{9^+}{2}$ levels which are otherwise forbidden in direct pick-up.

The results of this analysis to obtain the Nilsson orbit filling coefficients V_α in ^{26}Mg were found to be reasonably insensitive to the

optical potentials which were used in the DWBA analysis, so long as the same set was used for all the levels. However there was considerable variation in the results when a different value for the deformation was assumed.

The values of the V_α are in good agreement with previous calculations based on other single nucleon transfer reaction measurements. This is somewhat surprising considering the doubtful assumptions of the one-step, direct DWBA theory which has been used to analyze these experiments, and the differing contributions which would be expected to the different reactions of the two-step and higher order processes.

CHAPTER 5

THE $^{27}Al(p, d)^{26}Al$ REACTION

5.1 Introduction

The study of the (1d - 2s) shell has been extended in this chapter to the nucleus ^{26}Al. ^{26}Al is an odd-odd nucleus and has one more proton than ^{25}Mg. The previous chapter indicated that the low lying states of ^{25}Mg have been successfully described in terms of rotational bands built on the various Nilsson states occupied by the last nucleon. Far less understood is the situation in the neighbouring ^{26}Al nucleus, where several model calculations applied to ^{26}Al have not succeeded in describing the low lying states adequately. It seemed natural however to apply the Nilsson model. Horvat et al. (H6) extended the rotational model to ^{26}Al by describing the eight lowest levels as states obtained by the coupling of two nucleons moving in the Nilsson orbits from the A = 25 nuclei. This model description has been improved upon by Wasielewski et al.(W2). They included the rotation-particle coupling term in the Hamiltonian and a residual interaction between the last odd proton and neutron. The agreement obtained between the experimental levels and the calculated results is not

satisfactory. This discrepancy can be attributed to the restrictions of the axially symmetric model.

The intermediate coupling model by Bouten et al. (B3) reproduced the lowest six levels of ^{26}Al satisfactorily, but the high density of states above 2 MeV is beyond the scope of this calculation. Recent shell model calculations (W3) for A = 20 - 28 nuclei did not succeed in the case of the ^{26}Al nucleus. The deviations between calculated and experimental energies were of the order of 1 to 2 MeV.

Experimentally, the energy levels of ^{26}Al are well established. The charged particle reactions ^{24}Mg(^{3}He, p)^{26}Al, ^{27}Al(^{3}He, α)^{26}Al and ^{28}Si(d, α)^{26}Al determined the existence of more than 20 levels below 4 MeV excitation (E2). The single-nucleon transfer reactions ^{25}Mg(^{3}He, d)^{26}Al (W4) and ^{25}Mg(d, n)^{26}Al (F1) have established levels up to 6 MeV excitation energy. The reaction ^{24}Mg(^{3}He, pγ)^{26}Al (B4, H7) has been used to measure particle-gamma correlations which gave gamma-ray branching ratios and spins.

Results from spectroscopic factor analysis have only become available recently. The reaction ^{27}Al(^{3}He, α)^{26}Al has been studied at 10 MeV bombarding energy (N2). The ^{27}Al(p, d)^{26}Al reaction at 16 MeV (A2) appears to be the most recent data and spectroscopic factors were extracted up to 2.55 MeV excitation.

The present investigation extends the spectroscopic factor analysis for the eleven strongest transitions leading to final states in ^{26}Al up to an excitation energy of 4.699 MeV, using an incident proton bombarding energy of 20 MeV. It was of particular interest to study the properties of T = 1 states at 0.229, 2.07, 3.159 and 4.699 MeV which correspond to the analog states in ^{26}Mg at 0, 1.81, 2.94 and 4.33 MeV respectively. The spectroscopic factors extracted from the present data for these levels are in agreement with values predicted from shell model calculations (W5) for the ^{26}Mg nucleus. This agreement provides a test of the validity of the shell model for ^{26}Mg and indicates that the respective levels in ^{26}Al belong to the same shell model configuration. A spin of 4^+ is proposed for the 4.699 MeV level, based on the aforementioned analysis.

5.2 Experimental Results

The measurements were carried out at an incident proton beam energy of 20 MeV. Spectra were obtained by bombarding a self-supporting ^{27}Al target (99.99% purity), which was 38 $\mu g/cm^2$ thick. The counter telescope and experimental arrangement, as described in chapter 2, remained unchanged for the analysis of this reaction.

The spectrum of deuterons leading to states in ^{26}Al is shown in figure 5-1. Altogether 30 levels were observed with an energy resolution of approximately 35 keV. These levels represent all known excited states of ^{26}Al below 5 MeV. The triplet at 2.07 MeV (H8) and doublets at 3.72 MeV, 4.20 MeV and 4.60 MeV have not been resolved. The previously unresolved level at 3.918 MeV (E2) is clearly separated from the 3.962 MeV state. This level was also resolved in the ^{25}Mg(^{3}He, d)^{26}Al reaction (W4). The only contaminant in the spectrum is the ^{16}O(p, d)^{15}O reaction. The 2.740 MeV excited state is masked by this impurity in the energy spectrum shown.

One of the more interesting features shown in the energy spectrum, is the strong population of the 4.699 MeV level. This state appears at an energy at which the isobaric analog of the 4.34 MeV ($J^{\pi} = 4^{+}$) in ^{26}Mg is expected from the Coulomb energy differences. This contention will be supported in the subsequent analysis of the experimental results.

The angular distributions for the various final states are shown in figures 5-2 to 5-5. The cross sections quoted are absolute with an accuracy of ± 9%, due mainly to uncertainty in the target thickness. The solid curves are DWBA predictions, which will be discussed below. It is unfortunate that many of the resolved levels in the energy spectra were not populated strongly enough (<.05 mb/sr)

Figure 5-1: Energy spectrum of the $^{27}Al(p, d)^{26}Al$ reaction.

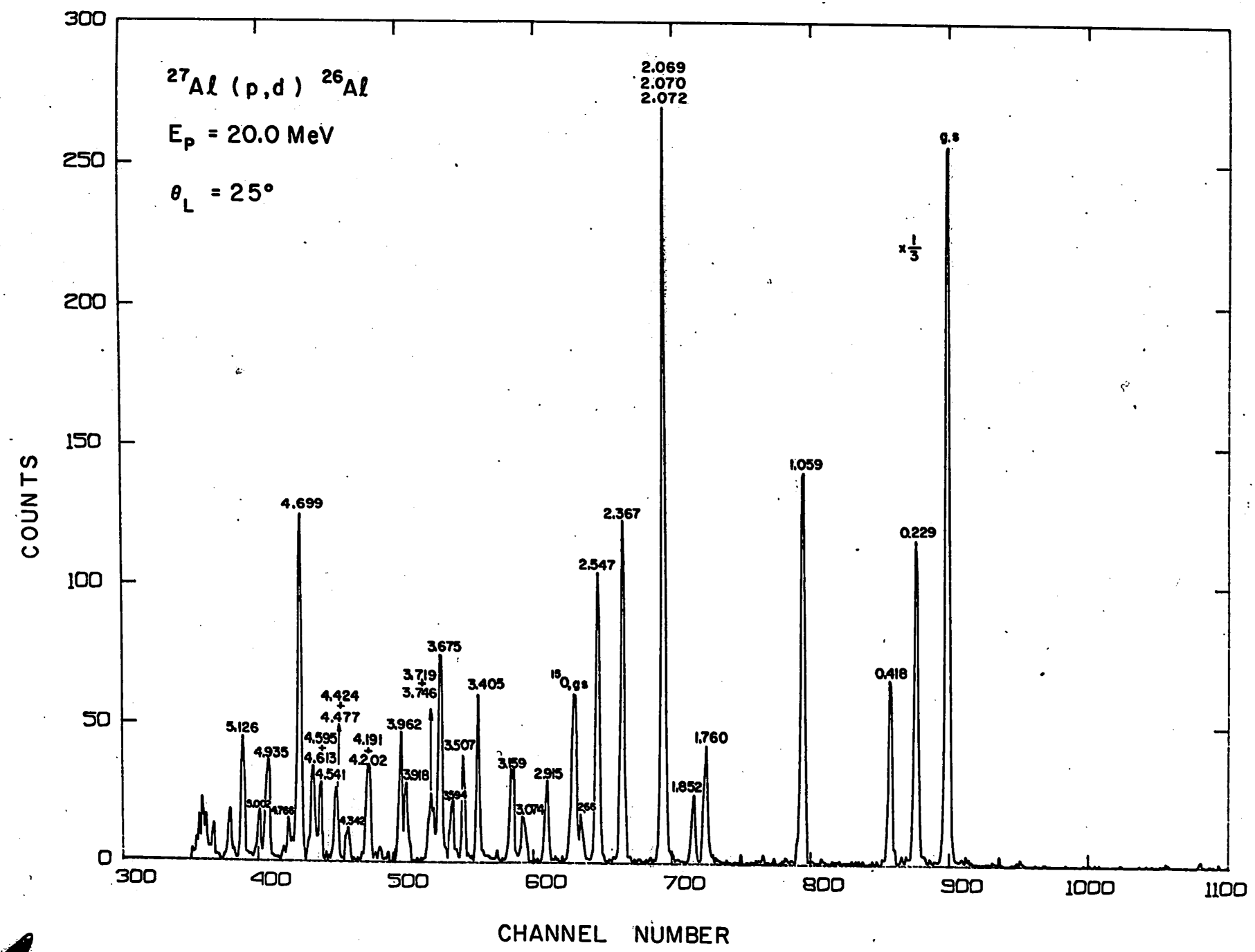

Figure 5-2: Optical model fits of the $^{27}Al(d, d)^{27}Al$ and $^{27}Al(p, p)^{27}Al$ at 9 MeV and 20 MeV respectively.

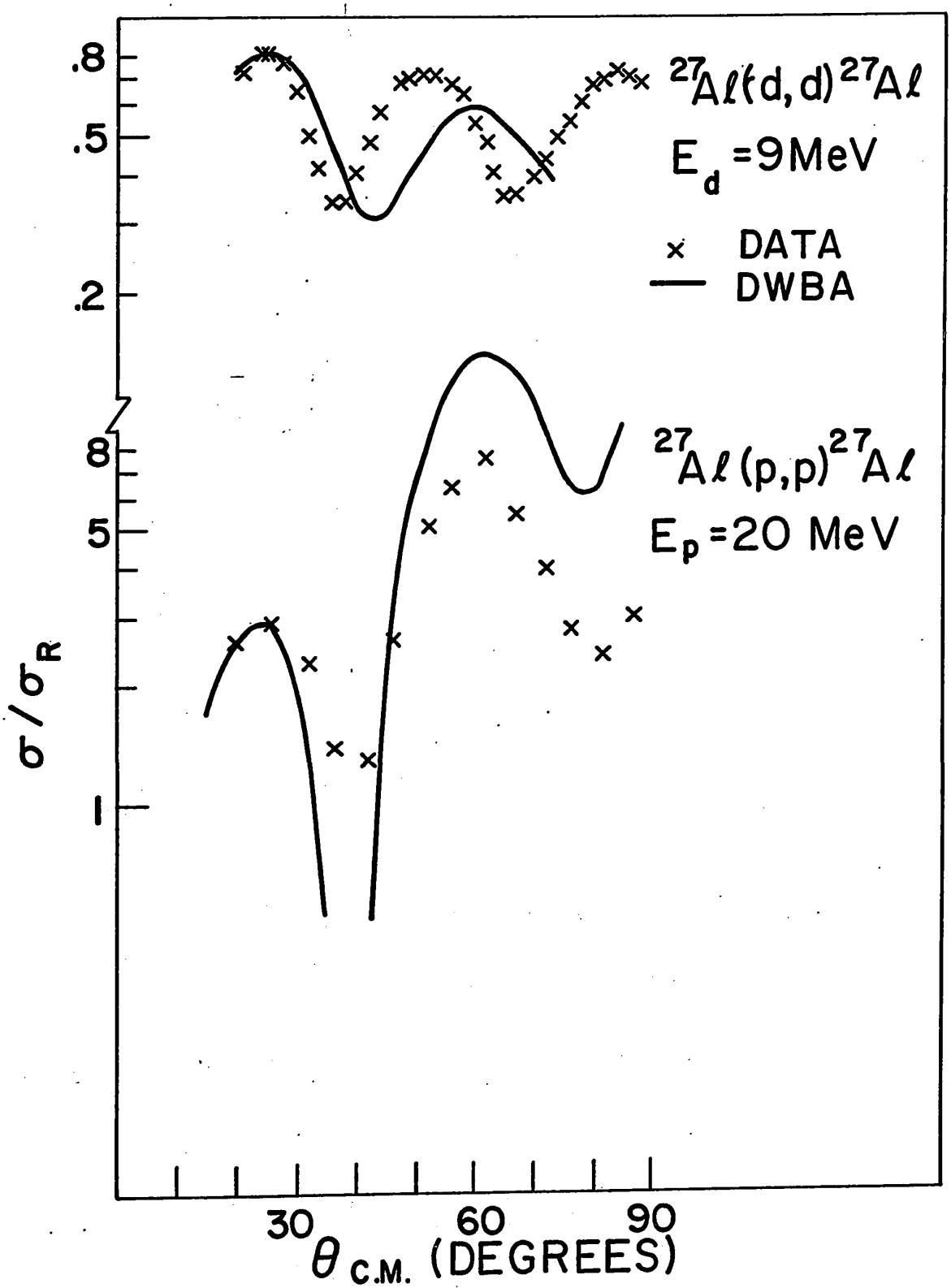
.8
.5
.2
8
5
1
σ/σR
27Al(d,d)27Al
Ed=9MeV
× DATA
— DWBA
27Al(p,p)27Al
Ep=20 MeV
30
60
90
θ c.m. (DEGREES)

Figure 5-3: The $\ell_n = 2$ angular distributions for T = 0 transitions in the reaction $^{27}Al(p, d)^{26}Al$.

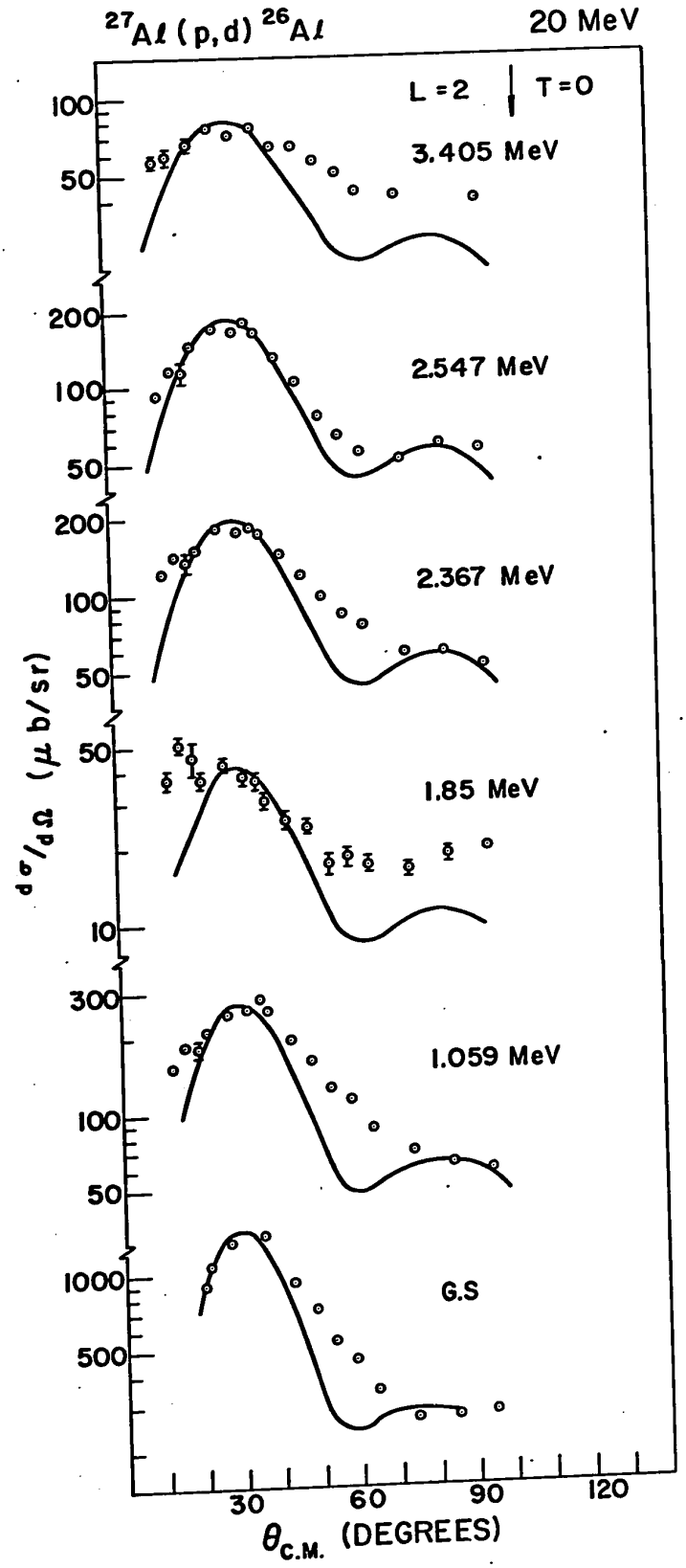
$^{27}Al(p,d)^{26}Al$
20 MeV
L=2
T=0
3.405 MeV
2.547 MeV
2.367 MeV
1.85 MeV
1.059 MeV
G.S
100
50
200
100
50
200
100
50
50
10
300
100
50
1000
500
$d\sigma/d\Omega$ (μb/sr)
30
60
90
120
$\theta_{c.m.}$ (DEGREES)

Figure 5-4: The $\ell_n = 2$ angular distributions for T = 1 transitions in the reaction $^{27}Al(p, d)^{26}Al$.

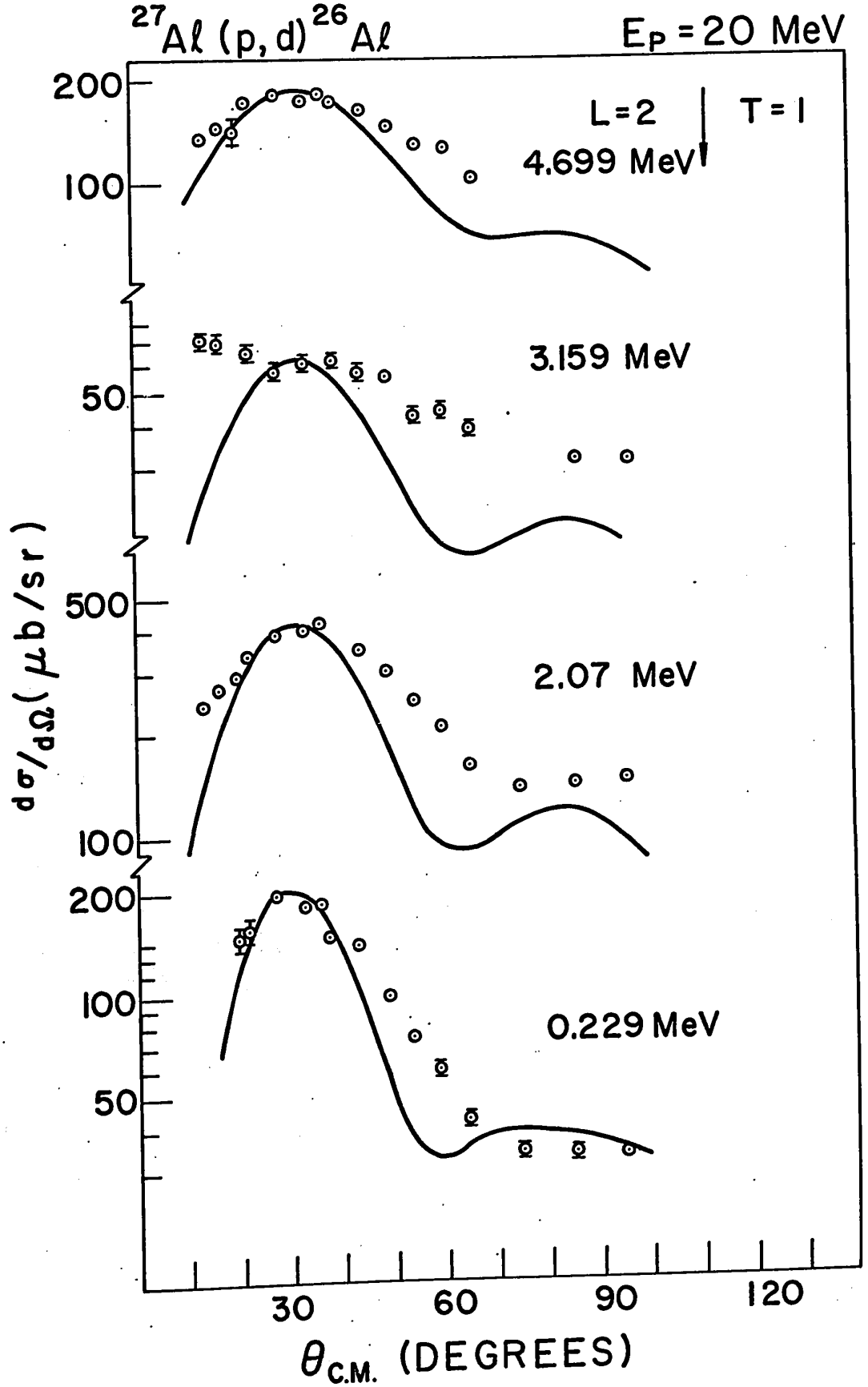
$^{27}Al\,(p,d)\,^{26}Al$
$E_P = 20$ MeV
L=2
T=1
4.699 MeV
3.159 MeV
2.07 MeV
0.229 MeV
200
100
50
500
100
200
100
50
$d\sigma/d\Omega$ (μb/sr)
30
60
90
120
$\theta_{C.M.}$ (DEGREES)

Figure 5-5: The $\ell_n = 0$ angular distribution for T = 0 transition in the reaction $^{27}Al(p, d)^{26}Al$.

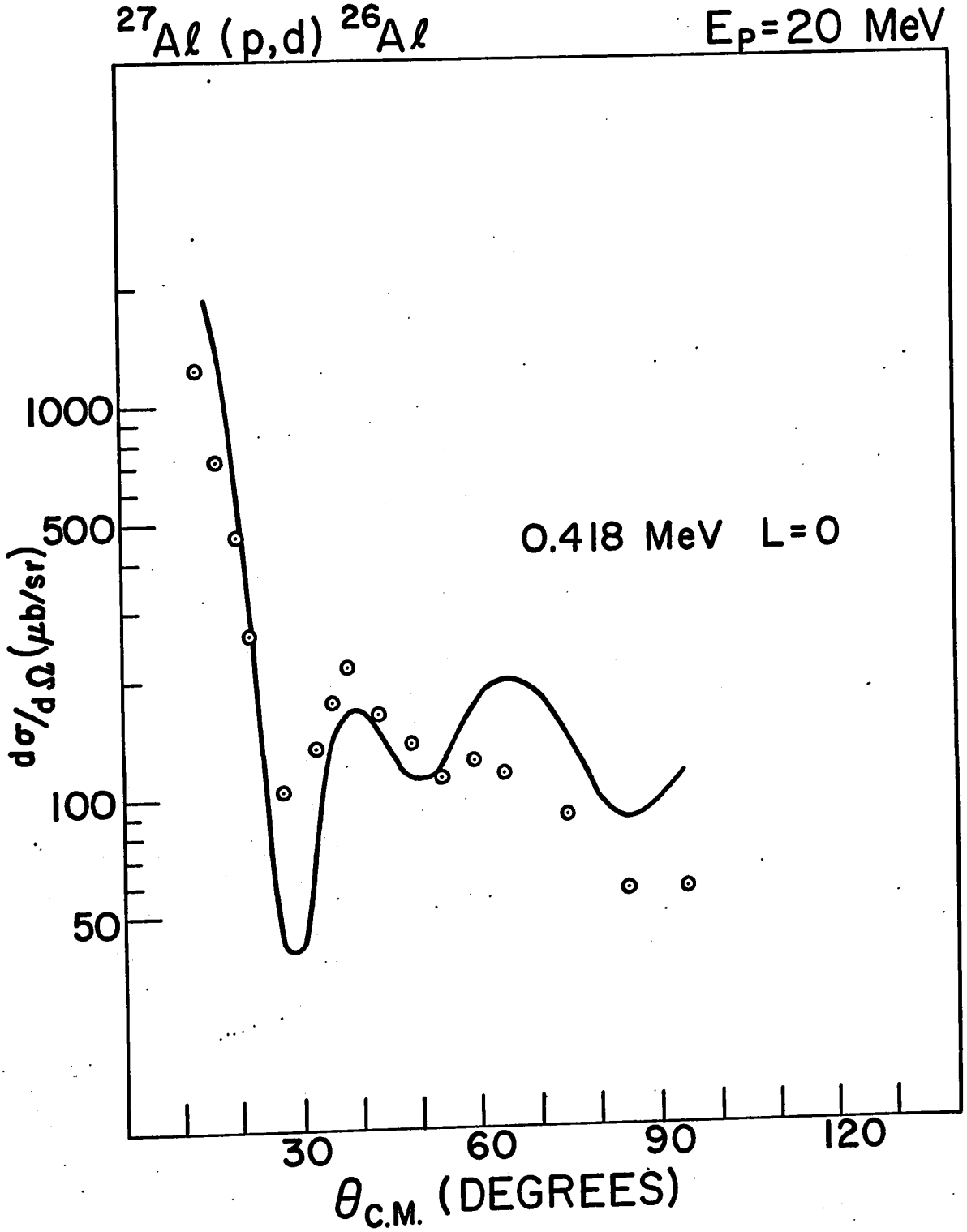
$^{27}Al\ (p,d)\ ^{26}Al$
E_p=20 MeV
0.418 MeV L=0
1000
500
100
50
$d\sigma/d\Omega$ (μb/sr)
30
60
90
120
$\theta_{C.M.}$ (DEGREES)

in order to obtain a complete angular distribution. Moreover some of the angular distributions were quite isotropic, and could not be fitted with DWBA. Also the ^{15}O ground state peak obscured several levels at a large number of angles. These weak transitions are shown in figure 5-6.

5.3 Distorted Wave Analysis

Distorted wave calculations were obtained using the programme written by W. R. Smith. The progamme option to include finite range effects were employed.

A thorough investigation was carried out to determine optical model parameters that would fit the elastic scattering data for the entrance and exit channels. Elastic scattering data have been reported before from the $^{27}Al(d, d)^{27}Al$ reaction at E_d = 11.8 MeV and the $^{28}Si(p, p)^{28}Si$ reaction at E_p = 27.6 MeV. This data was used in the study of the $^{28}Si(p, d)^{27}Si$ reaction (J1) and should be applicable to the present analysis. As a starting point, the optical model parameters used to fit the magnesium angular distributions were considered. Good fits were obtained for the ℓ = 2 transitions, whereas the fit to the ℓ = 0 transition did not agree too well. Subsequently, variations in the geometrical parameters of the potentials, including the neutron boundstate geometrical parameters were considered. Further changes in

Figure 5-6: Angular distributions for weak transitions in the reaction $^{27}Al(p, d)^{26}Al$.

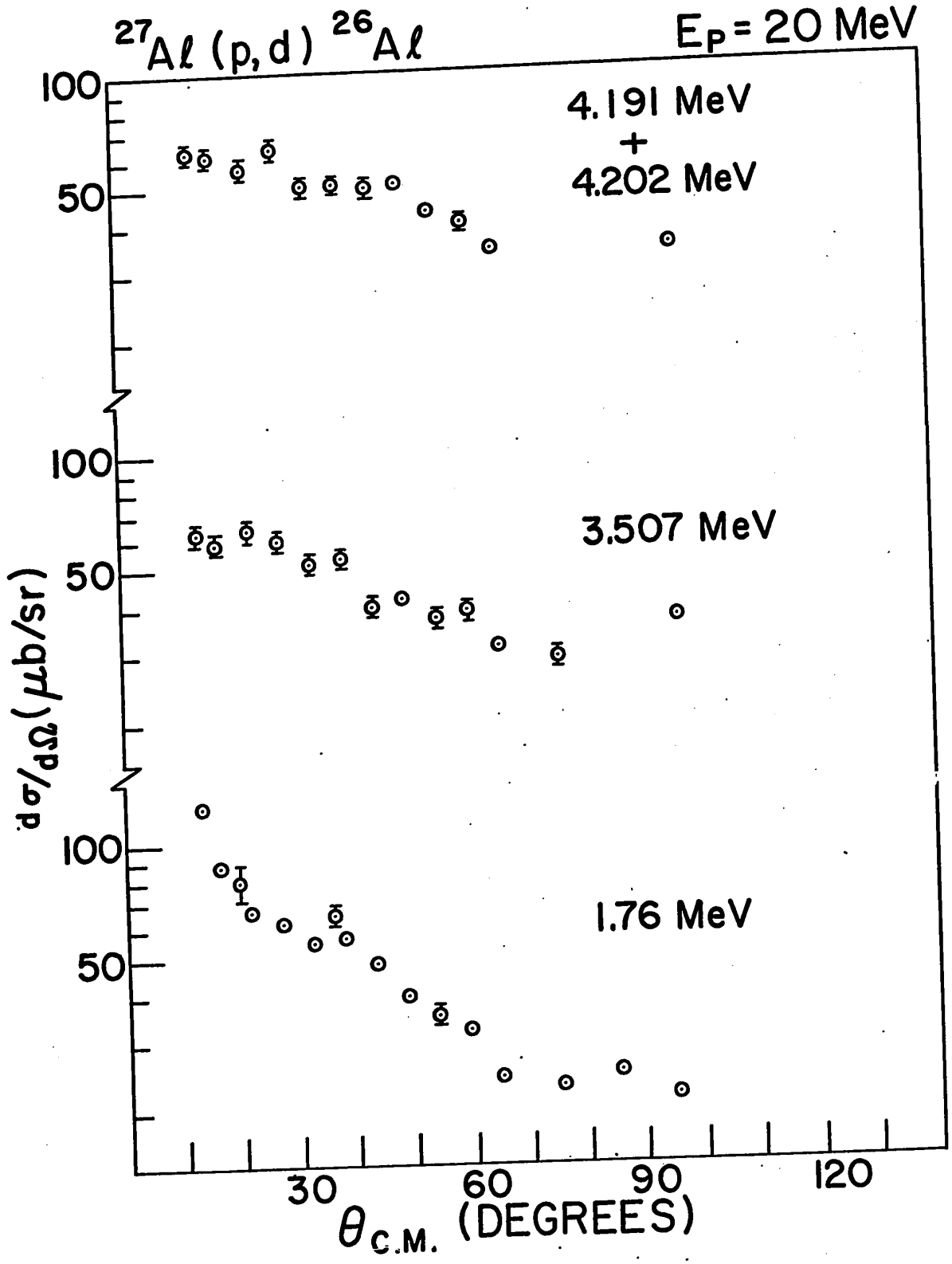
$^{27}Al\,(p,d)\,^{26}Al$
$E_P = 20$ MeV
4.191 MeV
+
4.202 MeV
3.507 MeV
1.76 MeV
100
50
100
50
100
50
$d\sigma/d\Omega$ (μb/sr)
30
60
90
120
$\theta_{C.M.}$ (DEGREES)

the real and imaginary proton potential and a reduction in the deuteron imaginary potential were required to achieve a good fit. The resulting parameters which proved to give the best overall fit to the g.s. and excited states in ^{26}Al are listed in Table 5-1. The fits to the elastic scattering data are compared in figure 5-2. It is noted here that the maxima and minima are correctly located and the forward angle intensities approximately reproduced. Any deviations could be attributed to the lower in-and outgoing particle energies of the present experiment, namely 20.0 MeV for the protons and 9.1 MeV for the deuterons.

In figures 5-3 to 5-5 the measured angular distributions are shown together with the predictions of the DWBA theory. Since the spin of the target nucleus ^{27}Al is unequal to zero, more than one ℓ-value is allowed for most transitions. However, the angular distributions shown are dominated by the $\ell = 2$ transitions. The only transition which could be satisfactorily fitted with a $\ell = 0$ transition is the level at 0.418 MeV. The DWBA calculation is accurately reproduced over the angular range of 13^{o} to 50^{o} for this state. The 0.418 MeV level is thought to be formed by the pick-up of a $2s_{1/2}$ neutron.

Close examination of the $\ell = 2$ angular distributions reveals, as it was the case in the magnesium analysis, that there is a significant difference between the shape of the curve obtained from the DWBA predictions leading to the ground state, and the experimental

Table 5-1: DWBA parameters used in the calculations from which the curves in figures 5-2 to 5-5 were obtained.

Channel	V_s MeV	r_{os} fm	a_s fm	W_s MeV	W_D MeV	r_{oI} fm	a_I fm	r_{oc} fm
Proton	51.8	1.29	0.65	8.6	0	1.29	0.48	1.25
Deuteron	91.08	1.20	0.78	0	24.	1.40	0.60	1.25
bound state		1.3	0.7					1.25

curve (L3). The analysis of Lee and Schiffer (L4) noted that for $\ell = 2$ transitions and deuteron energies between 7 and 10 MeV in nuclei with $16 < A < 44$ and spectroscopic factors greater than 0.1, the experimental $j = 3/2$ transitions exhibit a sharp drop-off and a minimum at $\sim 55^{o}$ whereas the $j = 5/2$ transitions do not.

On this basis the $j = 5/2$ transitions are favored and would indicate pick-up from the $1d_{5/2}$ shell. However in view of the absence of a $j = 3/2$ transition from the data, it is questionable to make a choice based on a j-dependent effect. In addition as noted previously (F2), the j-dependent effects have been explained in terms of Q-value dependence.

5.4 Spectroscopic Analysis

The experimental spectroscopic factors calculated using the expression from section 3.2 are given in Table 5-2 for the states whose angular distributions were compared with DWBA predictions. In addition to the ℓ-values and spectroscopic factors extracted from the present experimental data, a selection of complementary information from the literature is contained in Table 5-2. The experimental absolute spectroscopic factor is reported as C^2S. The isospin coupling coefficient C^2 is equal to 1 for transitions to $T = 0$ levels and 1/3 for transitions

Table 5-2: Level properties of ^{26}Al

E_x [a]	J^π [b]	T [b]	ℓ	Spectroscopic factor $C^2S(\ell)$	
				$C^2S(0)$	$C^2S(2)$
0	5^+		2		1.65
0.229	0^+	1	2		0.24
0.418	3^+		0	0.34	
1.059	1^+		2		0.40
1.760	2^+				
1.852	$(2^+, 3^+), 1^+$		2		0.08
2.0687 } 2.0695	3^+ 2^+	1	2		0.87
2.0715					
2.367	3^+		2		0.47
2.547	$2^+, 3^+$		2		0.47
2.66	$2^+, 3^+$ [c]				
2.74 [d]					
2.915	$2^+, 3^+$				
3.074					
3.159	2^+	1	2		0.21
3.405			2		0.32
3.507					
3.594	$2^+, 3^+$				
3.675	$2^+, 3^+$				
3.719 } 3.746	$2^+, 3^+$				
3.918					
3.962					
4.191 } 4.202	3^+	1			
4.342					
4.424 } 4.477					
4.541					
4.595 } 4.613	2^+	1			
4.699	4^+	1	2		1.66
4.766					
4.935					
5.002					
5.126	2^+ [c]	1 [c]			

a) Excitation energies from ref. (E2)

b) Spin, parity and isospin assignment for the 4.699 MeV state from present experiments, for all other states as in refs. (E2, F1, W4).

c) J^π , T assignments from ref. (F1)

d) Masked by $^{16}O(p, d)^{15}O$

to T = 1 levels.

5.4-1 Comparison with the Nilsson Model

In considering ^{26}Al, we restrict ourselves to the particle configurations in which one nucleon is in Nilsson orbit 5($K^{\pi} = 5/2^{+}$), and the other one is also in the same orbit or in one of the higher orbits. This latter nucleon is then paired off with the additional neutron to form ^{27}Al. The energy levels of the Hamiltonian predicted on the basis of this model description are given by Horvat et al. (H6) and Weidinger et al. (W4).

The spectroscopic factors in the Nilsson model are given by Satchler's formula (S4)

$$S_{\ell j} = \rho^2 \frac{2J_o + 1}{2J + 1} (J_o j K_o \Omega | JK)^2 \langle f|i\rangle^2 C^2_{\ell j \Omega}$$

where $\langle f|i\rangle$ is the core overlap of the initial and final nucleus and is usually set equal to one and $\rho^2 = 2$ if both particles are in the same Nilsson orbit and $\rho^2 = 1$ in the other cases. In the literature the K = 0 case usually is the only one mentioned for $\rho^2 = 2$. All other symbols have been defined previously in section 4.3.

In discussing the levels, the previous interpretation of ^{26}Al by Horvat et al. is followed who assign the band heads of the K = 5 and the two K = 0 bands to the ground state and the first and third excited states, respectively. The configurations $5/2^+(5) \pm 1/2^+(9)$ are proposed for the states at 0.42 MeV and 1.76 MeV. However in the present analysis, the comparison between the measured spectroscopic factors and calculated spectroscopic factors is confined to the $5/2^+(5) \pm 5/2^+(5)$ states. The convention used here denotes a plus-sign as parallel coupling and a minus-sign as anti-parallel coupling.

Within the Nilsson model description for ^{26}Al, no more than two neutron can be in one Nilsson orbit. This simple picture implies an upper limit of $S_{\ell j} = 2.0$. This sum rule was employed in calculating the results of Table 5-3 in the following way,

$$\sum_{\substack{K=5 \\ T=0}} S_{\ell j} + \sum_{\substack{K=0 \\ T=0,1}} S_{\ell j} = 2$$

The calculations tabulated in Table 5-3 were carried out for a deformation parameter of $\eta = 4.3$ and the appropriate isospin coupling coefficient was included.

Table 5-3: Comparison of experimental and theoretical spectroscopic factors for a deformation of $\eta = 4.3$ in ^{26}Al.

^{26}Al	J^{π}, T	ℓ	K	Configuration	C^2S	
					Theoretical	Experimental
0.0	5^+, 0	2	5	$5/2^+(5) + 5/2^+(5)$	1.0	1.65
0.229	0^+, 1	2	0	$5/2^+(5) - 5/2^+(5)$	0.06	0.24
1.059	1^+, 0	2	0	$5/2^+(5) - 5/2^+(5)$	0.36	0.40
2.07	2^+, 1	2	0	$5/2^+(5) - 5/2^+(5)$	0.10	0.87

Table 5-3: Comparison of experimental and theoretical spectroscopic factors for a deformation of $\eta = 4.3$ in ^{26}Al.

^{26}Al	J^{π}, T	ℓ	K	Configuration	C^2S	
					Theoretical	Experimental
0.0	5^+, 0	2	5	$5/2^+(5) + 5/2^+(5)$	1.0	1.65
0.229	0^+, 1	2	0	$5/2^+(5) - 5/2^+(5)$	0.06	0.24
1.059	1^+, 0	2	0	$5/2^+(5) - 5/2^+(5)$	0.36	0.40
2.07	2^+, 1	2	0	$5/2^+(5) - 5/2^+(5)$	0.10	0.87

Table 5-3: Comparison of experimental and theoretical spectroscopic factors for a deformation of $\eta = 4.3$ in ^{26}Al.

^{26}Al	J^{π}, T	ℓ	K	Configuration	C^2S	
					Theoretical	Experimental
0.0	5^+, 0	2	5	$5/2^+(5) + 5/2^+(5)$	1.0	1.65
0.229	0^+, 1	2	0	$5/2^+(5) - 5/2^+(5)$	0.06	0.24
1.059	1^+, 0	2	0	$5/2^+(5) - 5/2^+(5)$	0.36	0.40
2.07	2^+, 1	2	0	$5/2^+(5) - 5/2^+(5)$	0.10	0.87

5.4-2 Comparison with Simple Shell Model Predictions

According to the model (S9), ^{27}Al is considered to be a nucleus composed of a ^{28}Si core and a hole in the $d_{5/2}$ shell, represented usually as $(d_{5/2})^{-1}$. Transitions leading to levels in ^{26}Al could then be represented as $(d_{5/2})^{-2}$ configurations. On this basis, the low lying levels in ^{26}Al can be described by the shell model and jj-coupling for the odd $d_{5/2}$ neutron and proton. The states with J = 0, 2 and 4 should have isospin of T = 1 and the states with J = 1, 3 and 5 an isospin of T = 0. The level at 1.76 MeV appears to be the exception among the lowest levels since it is known to have $(J^{\pi}, T) = (2^{+}, 0)$ (H6). If excitations are considered into $2s_{1/2}$ or $1d_{3/2}$ orbits, the two unpaired nucleons can couple to a total spin of J = 0, 1, 2, 3, or 4 and the proximity of 2^{+} and 3^{+} levels suggests such mixing may be present.

In the simplest case, when configuration mixing is neglected, the spectroscopic factors for the single nucleon pick-up reaction can be calculated using a formula by Macfarlane and French (M2).

$$C^2S = \frac{1}{6} \quad (2J + 1)$$

for all $(d_{5/2})^{-1}$ to $(d_{5/2})^{-2}$ transitions between ^{27}Al and ^{26}Al nuclei.

The spectroscopic factors thus calculated are listed in Table 5-4 and it has been assumed that the total strength of the $(d_{5/2})^{-2}$ wave function for $(J^{\pi}, T) = (3^{+}, 0)$ is in the second excited state at 0.418 MeV. Similarly, the total strength for $(J^{\pi}, T) = (4^{+}, 1)$ has been assigned to the level at 4.699 MeV.

5.5 Isobaric Analog States in ^{26}Al

The analog states of ^{26}Mg in ^{26}Al, i.e. the T = 1 levels, are determined from Coulomb energy differences by comparing our present results with data from the ^{25}Mg(d, p)^{26}Mg reaction (C1, H9, L3). The compilation of energy levels of ^{26}Al by Endt and van der Leun (E1) lists five levels up to 4.595 MeV with isospin T = 1. An updated compilation in 1967 (E2) omits the T = 1 assignment of the 4.595 MeV level, however Fuchs (F1) includes the fifth T = 1 level as belonging to one of the members of the doublet at 4.60 MeV. In our present data the levels at 0.229, 0.207 and 3.159 MeV correspond to analog states in ^{26}Mg at 0, 1.81 and 2.94 MeV respectively. The doublets at 4.2 MeV and 4.6 MeV in ^{26}Al also correspond to T = 1 levels, however in the present analysis these states are not populated with sufficient strength to be considered for further analysis.

Table 5-4: Comparison of experimental and theoretical spectroscopic factors from simple shell model predictions

^{26}Al	J^{π}, T	Theoretical		Experimental	
		ℓ	C^2S	ℓ	C^2S
0	5^+, 0	2	1.833	2	1.65
0.229	0^+, 1	2	0.167	2	0.24
0.418	3^+, 0	2	1.167	0	0.34
1.059	1^+, 0	2	0.500	2	0.40
2.07	2^+, 1	2	0.833	2	0.87
4.699	4^+, 1	2	1.500	2	1.66

Of particular interest is the strong transition to the level at 4.699 MeV, since it is proposed as a candidate to be the sixth T = 1 level in ^{26}Al. Recent results from shell model calculations for ^{26}Mg predict good agreement between spectroscopic factors from the "$d_{5/2}$ - $s_{1/2}$" shell model wave functions for proton pick-up from the $5/2^+$ ground state of ^{27}Al to the five lowest levels of ^{26}Mg. Also the lowest 4^+ model state of ^{26}Mg is predicted to have an $\ell = 2$ spectroscopic factor significantly larger than that for any other state. However, the success of the shell model predictions in ^{26}Mg is somewhat reduced since the probable 4^+ level at 4.34 MeV is part of an unresolved triplet.

The same shell model predictions can be applied to our results, particularly since the analysis of transitions to states in ^{26}Al appears to have the added advantage of not having a triplet state at 4.60 MeV which is the expected position of the analog triplet at 4.3 MeV in ^{26}Mg. In fact, the 4.699 Mev level is the resolved $J^\pi = 4^+$ component from the two nearby levels at 4.60 MeV. The level scheme showing the break-up of the triplet state in ^{26}Mg is presented in figure 5-7. The results of the

Figure 5-7: Energy levels of T = 1 states in the A = 26 system in the region E_x = 4.3 MeV to 4.7 MeV.

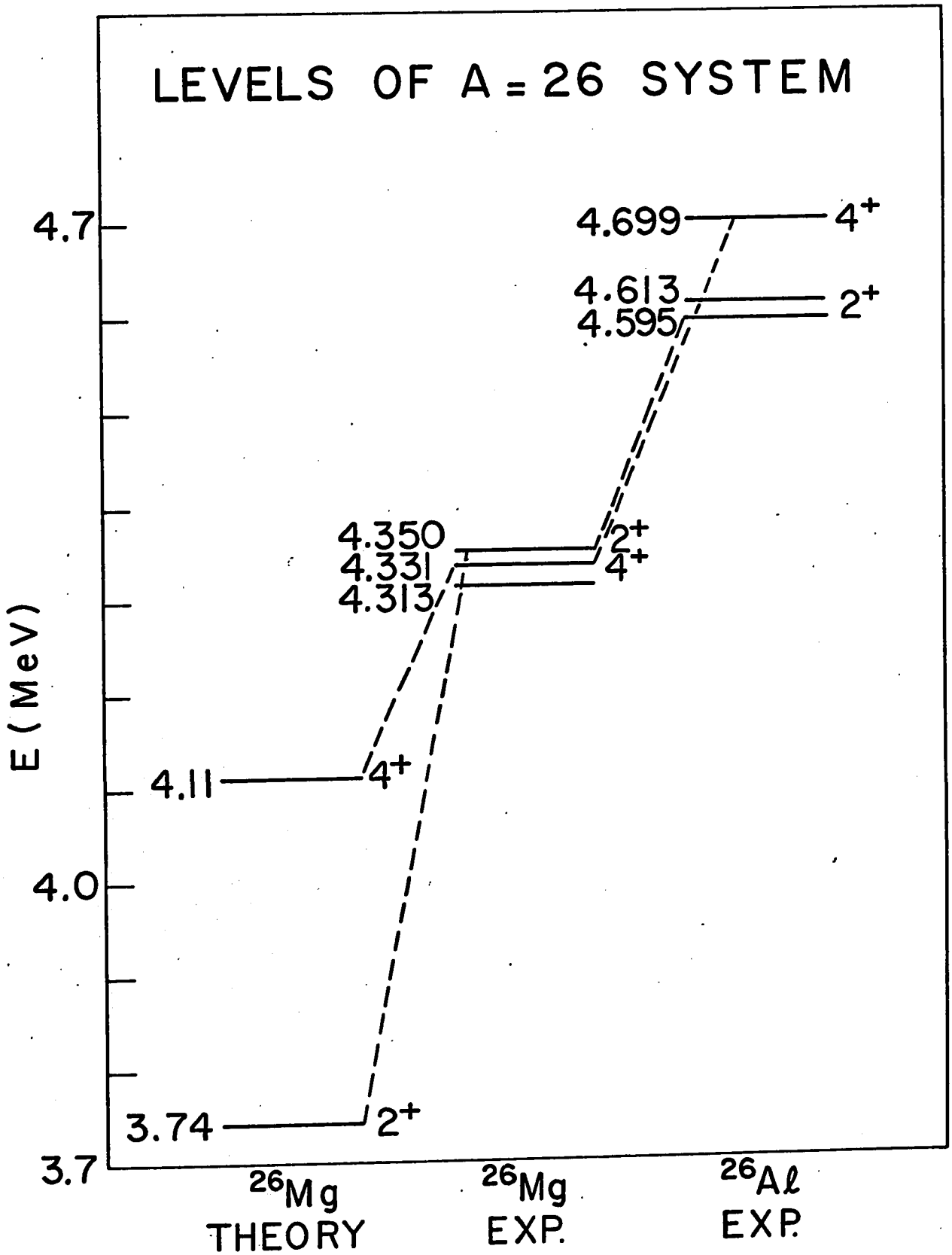
LEVELS OF A = 26 SYSTEM
E (MeV)
4.7
4.0
3.7
4.699
4+
4.613
2+
4.595
4.350
2+
4.331
4+
4.313
4.11
4+
3.74
2+
26Mg THEORY
26Mg EXP.
26Al EXP.

spectroscopic factor comparison are given in Table 5-5. They are presented as relative spectroscopic factors in columns six and seven, thus eliminating the dependence on the isospin coupling coefficient.

5.6 Comparison with other data.

Table 5-6 compares the relative spectroscopic factors of this study with the spectroscopic factors of the $^{27}Al(^{3}He, \alpha)^{26}Al$ (N2) at 10 MeV bombarding energy and the $^{27}Al(p, d)^{26}Al$ (A2) reaction at 16 MeV incident energy. The factors are tabulated as $C^2S_{\ell j}/C^2S_{g.s.}$, since the ($^{3}He$, α) and (p, d) experiments reported only relative values.

Table 5-5: Comparison of spectroscopic factors from present results and $d_{5/2} - s_{1/2}$ wavefunctions leading to T = 1 states in ^{26}Al

Excitation Energy			J^π	ℓ	Relative Spec. factor $S/S_{0.23}$	
$^{26}Al_{expt.}$	$^{26}Mg_{expt.}$	$^{26}Mg_{theor.}$ [a]			Expt.	Theor. [a]
0.229	g.s.	g.s.	0^+	2	1.00	1.00
2.07	1.81	2.34	2^+	2	3.70	2.59
3.159	2.94	3.08	2^+	2	0.87	1.0
4.699	4.331	4.11	4^+	2	7.03	6.21

a) Wildenthal, B. H. and Newman, E., Phys. Rev. 175, 1431 (1968).

Table 5-6: Relative spectroscopic factor comparison with other data.

^{26}Al	J^π, T	(p, d)[a]		(^{3}He, α)[b]		(p, d)[c]	
		ℓ	$C^2S_{\ell j}/C^2S_{g.s.}$	ℓ	$C^2S_{\ell j}/C^2S_{g.s.}$	ℓ	$C^2S_{\ell j}/C^2S_{g.s.}$
0	5^+	2	1.0	2	1.0	2	1.0
0.229	0^+, 1	2	0.14	2	0.23	2	0.13
0.418	3^+	0	0.21	2	0.61	0	0.13
1.059	1^+	2	0.24	2	0.30	2	0.26
1.76	2^+						
1.852	1^+	2	0.05			2	≤0.10
2.0687	3^+						
2.0695	2^+, 1	2	0.53	2	0.59	2	0.23
2.367	3^+	2	0.28			0	0.076
2.547	$2^+,3^+$	2	0.28			0	0.067

a) Present results

b) Ref. N2

c) Ref. A2

5.7 Discussion

For most transitions satisfactory fits were obtained between the theoretical curves predicted from DWBA and the experimental data. In addition, the optical model parameters describe the elastic scattering results closely. In most cases an $\ell = 2$ neutron transfer was found to be consistent with the data. The only $\ell = 0$ transfer was to the 0.418 MeV level. The states at 1.76 MeV and 1.85 MeV were excited weakly and a fit was attempted for the 1.85 MeV level. It has to be concluded that the $\ell = 2$ value assigned in this analysis is ambiguous, since from the shape of the curve it is evident that other ℓ-values could contribute. Recent results from the $^{24}Mg(^{3}He, p\gamma)^{26}Al$ by Bissinger et al. (B4) produced a revised spin assignment of $J = 1^{+}$ to this level. The present results for the 1.76 MeV and the 1.85 MeV states do not make detailed analysis worthwhile due to their small cross-sections. The fits to the levels at 3.159 MeV and 3.405 MeV are not adequately reproduced with an $\ell = 2$ neutron transfer but further analysis seems fruitless due to their small transition strength.

The absolute experimental spectroscopic factors as listed in Table 5-2 show several strong spectroscopic strengths. In particular the observed spectroscopic factor for the state at 4.699 MeV is very large with a spectroscopic strength comparable to the ground state

spectroscopic factor and twice as large as any other observed T = 1 transition.

In Table 5-3 the measured spectroscopic factors are compared with predictions of the Nilsson model. Agreement was obtained for the 1.059 MeV state only. In fact the results are not encouraging enough to consider more complicated configurations. Also it is noted that this particular Nilsson calculation is independent of the degree of deformation since the expansion coefficient $C_{2,\ 5/2,\ 5}$ is equal to 1. In conclusion, the present results confirm the inapplicability of the Nilsson model description for ^{26}Al.

The agreement obtained between the experimental spectroscopic factors and the spectroscopic factors predicted from the simple shell model calculations is quite surprising as shown in Table 5-4. The disagreement obtained for the 0.418 MeV level suggests that the assumption made to attribute the total strength of the $(d_{5/2})^{-2}$ wavefunction for $(J^{\pi},\ T) = (3^{+},\ 0)$ to this state is incorrect. This is contrary to the conclusion reached by Nurzynski et al., who reported an $\ell = 2$ transition to this level and found good agreement. The converse situation seems to exist for the 0.229 MeV state, since the present results obtain good agreement whereas the $(^{3}He, \alpha)$ results report a considerable discrepancy.

In general, the model description in which ^{27}Al and ^{26}Al are considered to consist of $(d_{5/2})^{-1}$ and $(d_{5/2})^{-2}$ configurations only, has creditability and determines the spin of the 4.699 MeV level to be 4^+. In addition the sum-rule predictions compare favorably:

$$\sum_{T = 0,1} C^2 S_{\ell j} = 6 \quad \text{Theory}$$

$$\sum_{T = 0,1} C^2 S_{\ell j} = 5.3 \quad \text{Exp.}$$

Table 5-5 shows the good agreement obtained between relative spectroscopic factors from the "$d_{5/2}$ - $S_{1/2}$" shell-model wave functions and the experimental results. In particular, the large $\ell = 2$ spectroscopic factor predicted by the shell model calculations for the state at 4.33 MeV in ^{26}Mg is observed in the present results and is concentrated in the 4.699 MeV level. On the basis of this striking agreement the spin for this state is selected to be $J^\pi = 4^+$. This then confirms the success of the model since it accounts for energy levels and spectroscopic factors in accordance with experiment.

The comparison of relative spectroscopic factors in Table 5-6 indicates good agreement between our results and the (^3He, α) results

for all levels except the 0.418 MeV state. The (^{3}He, α) reaction prefers to proceed via the higher ℓ-value when ℓ = 0 or 2 are possible. The (p, d) results at 16 MeV are lower especially the spectroscopic factors at 2.07 MeV and 0.418 MeV which are reduced by a factor of two. This could point to a Q-value dependence of the reaction cross-section.

CHAPTER 6

THE $^{37}Cl(p, d)^{36}Cl$ REACTION

6.1 Introduction

The earlier studies of the doubly odd ^{36}Cl nucleus are reviewed in the 1967 compilation by Endt and van der Leun (E2). Most of the experimental information listed in this review originated from (n, γ) reactions on ^{35}Cl and in particular the ^{35}Cl (d, p)^{36}Cl reaction (H10) which established 70 levels in ^{36}Cl below 7 MeV. More recently, several additional (n, γ) reactions have been reported (F3, K3, H11) in order to resolve ambiguities in γ-ray intensities and to determine some spin values of excited levels.

Spectroscopic factor information has become available from the $^{37}Cl(^{3}He, \alpha)^{36}Cl$ reaction (L5) and the $^{35}Cl(d, p)^{36}Cl$ reaction (D6).

The study of the $^{37}Cl(p, d)^{36}Cl$ reaction was undertaken to measure ℓ_n values and spectroscopic factors. The spectroscopic information extracted is most relevant to test the detailed many-

particle shell model calculations of the s-d shell nuclei (G2, G3, G4, W6, D7). Furthermore, the (p, d) reaction populates the lowest energy $0^+(T = 2)$ state in ^{36}Cl for which an accurate excitation energy is calculated.

6.2 Experimental Results

The $^{37}Cl(p, d)^{36}Cl$ reaction has been studied at an incident energy of 19 MeV. The target material NaCl enriched to 96.52% in ^{37}Cl, was obtained from Oak Ridge. The targets were then produced by evaporation onto a carbon backing. Targets had a thickness of 50 $\mu g/cm^2$ as determined by weighing.

Emergent deuterons were detected in a counter telescope, a detailed description of which has been given in chapter 2. Only one change was made in the telescope, namely the 300μ E counter was substituted with a 500μ counter in order to accommodate higher energy deuterons due to the less negative Q-value of this reaction with respect to the previous reactions.

The 20^o energy spectrum is shown in figure 6-1, where due to the composition of the target, levels of ^{36}Cl and ^{22}Na are indicated. The ^{22}Na states will be discussed further in chapter 7. The con-

Figure 6-1: Energy spectrum of the $^{37}Cl(p, d)^{36}Cl$ reaction.

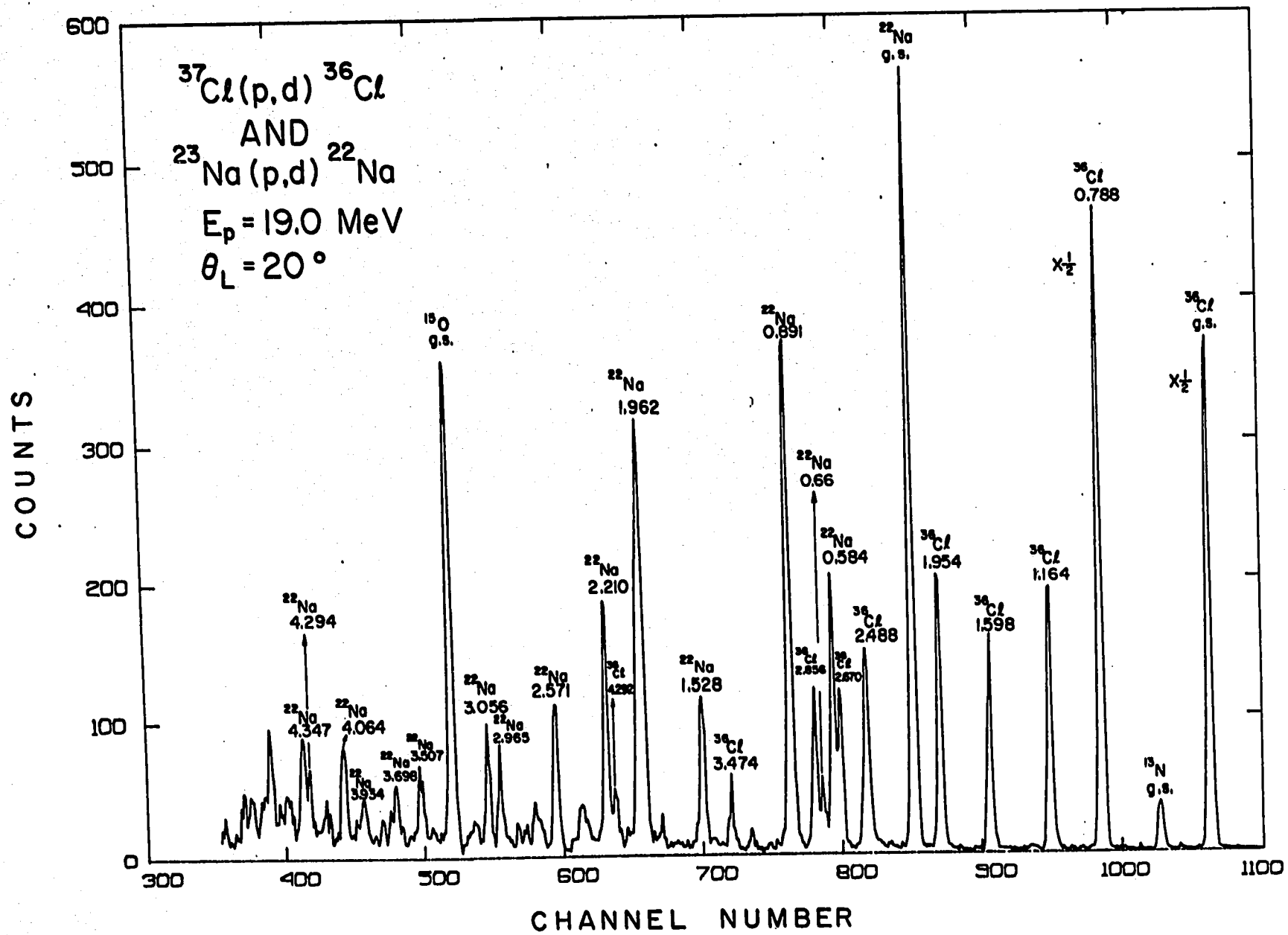
$^{37}Cl(p,d)\,^{36}Cl$
AND
$^{23}Na(p,d)\,^{22}Na$
$E_p = 19.0$ MeV
$\theta_L = 20°$
COUNTS
CHANNEL NUMBER
0
100
200
300
400
500
600
300
400
500
600
700
800
900
1000
1100
^{22}Na g.s.
^{36}Cl 0.788
$X\frac{1}{2}$
^{36}Cl g.s.
$X\frac{1}{2}$
^{15}O g.s.
^{22}Na 0.891
^{22}Na 1.962
^{22}Na 0.66
^{22}Na 0.584
^{36}Cl 1.954
^{36}Cl 1.164
^{36}Cl 1.598
^{36}Cl 2.488
^{22}Na 2.210
^{36}Cl 2.856
^{36}Cl 2.670
^{36}Cl 4.292
^{22}Na 1.528
^{36}Cl 3.474
^{22}Na 4.294
^{22}Na 4.347
^{22}Na 4.064
^{22}Na 3.934
^{22}Na 3.698
^{22}Na 3.307
^{22}Na 3.056
^{22}Na 2.965
^{22}Na 2.571
^{13}N g.s.

taminants are from nitrogen and oxygen and are labelled with the residual nucleus symbol. The excitation energies of the observed states were determined by analyzing the data with the computer program Lorna (L1), as described in section 2.3. The calibration curve was provided by the $^{36}Cl_{g.s.}$ and the known levels at 0.788, 1.164 and 1.598 MeV. The measured excitation energies and their associated errors (± 20 keV) are within the quoted errors of the $^{37}Cl(^{3}He, \alpha)^{36}Cl$ reaction (L5). The doublet at 1.949 MeV, which is separated by only 8 keV, and triplet at 2.469 MeV were not resolved in this experiment. Of particular interest is the state at 4.292 MeV, which is the 0^{+} analog to the ground state of ^{36}S (T = 2).

Angular distributions have been extracted for the above mentioned transitions in ^{36}Cl over the angular range of 15^{o} to 70^{o} at 5^{o} intervals, except for the level at 4.292 MeV which was masked by the 1.96 MeV state in ^{22}Na at angles greater than 40^{o}. No angular distribution was obtained for the 2.856 MeV excited state, since at most angles it was obscured by ^{22}Na levels.

6.3 The DWBA Analysis

The experimental angular distributions were compared with DWBA calculations from the Smith code, using the finite range option. In the absence of proton and deuteron elastic scattering data from ^{37}Cl, two sets of parameters for the potentials were considered. The first set was taken from the DWBA analysis of the $^{37}Cl(d, p)^{38}Cl$ reaction (R2) at 7.5 MeV incident energy, and the second set was obtained from the study of the $^{36}Ar(p, d)^{35}Ar$ reaction at a bombarding energy of 27.5 MeV. For both reactions the optical parameters were obtained by fitting with a Perey program (P1). An improved fit to the data was obtained using the latter set and the parameters are listed in Table 6-1.

The results of the DWBA calculations are presented in figures 6-2 to 6-4 as solid lines. The transition to the 1.164 MeV level contains a 20% $\ell = 0$ admixture and the level at 1.598 MeV includes a 50% $\ell = 2$ admixture. The spectroscopic factors were derived using the expression from section 3.2.

Table 6-1: Optical model parameters used in the DWBA calculation

Channel	V_s MeV	r_{os} fm	a_s fm	W_s MeV	W_D MeV	r_{oI} fm	a_I fm	r_{oc} fm
Proton	48.85	1.18	0.7935	2.0	8.2	1.3428	0.4697	1.25
Deuteron	95.94	1.15	0.7325	0	16.13	1.34	0.6542	1.30
Bound State		1.3	0.7					1.25

Figure 6-2: The $\ell_n = 2$ angular distributions for the reaction $^{37}Cl(p, d)^{36}Cl$.

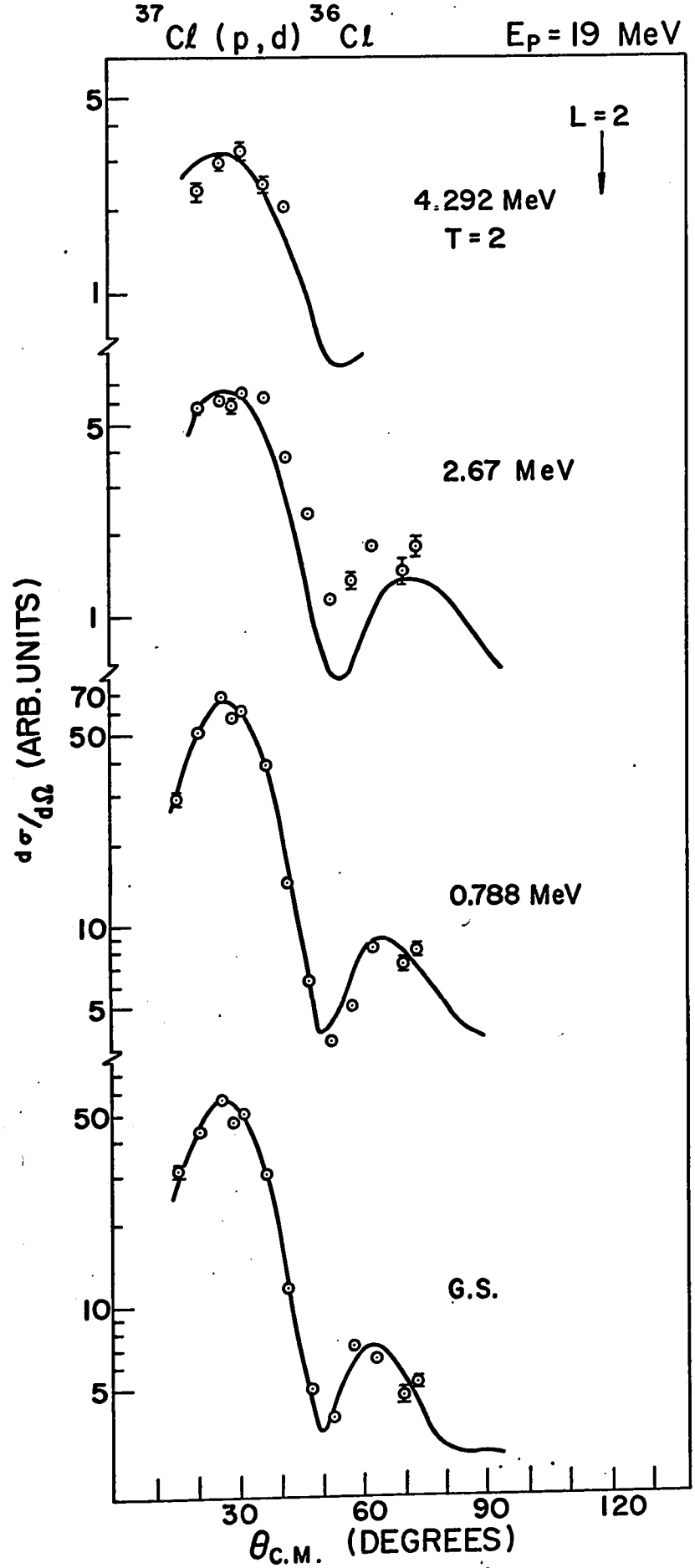
$^{37}Cl\ (p,d)\ ^{36}Cl$
$E_P = 19$ MeV
L = 2
4.292 MeV
T = 2
2.67 MeV
0.788 MeV
G.S.
$d\sigma/d\Omega$ (ARB. UNITS)
$\theta_{C.M.}$ (DEGREES)
5
1
5
1
70
50
10
5
50
10
5
30
60
90
120

Figure 6-3: The $\ell_n = 0$ angular distributions for the reaction $^{37}Cl(p, d)^{36}Cl$.

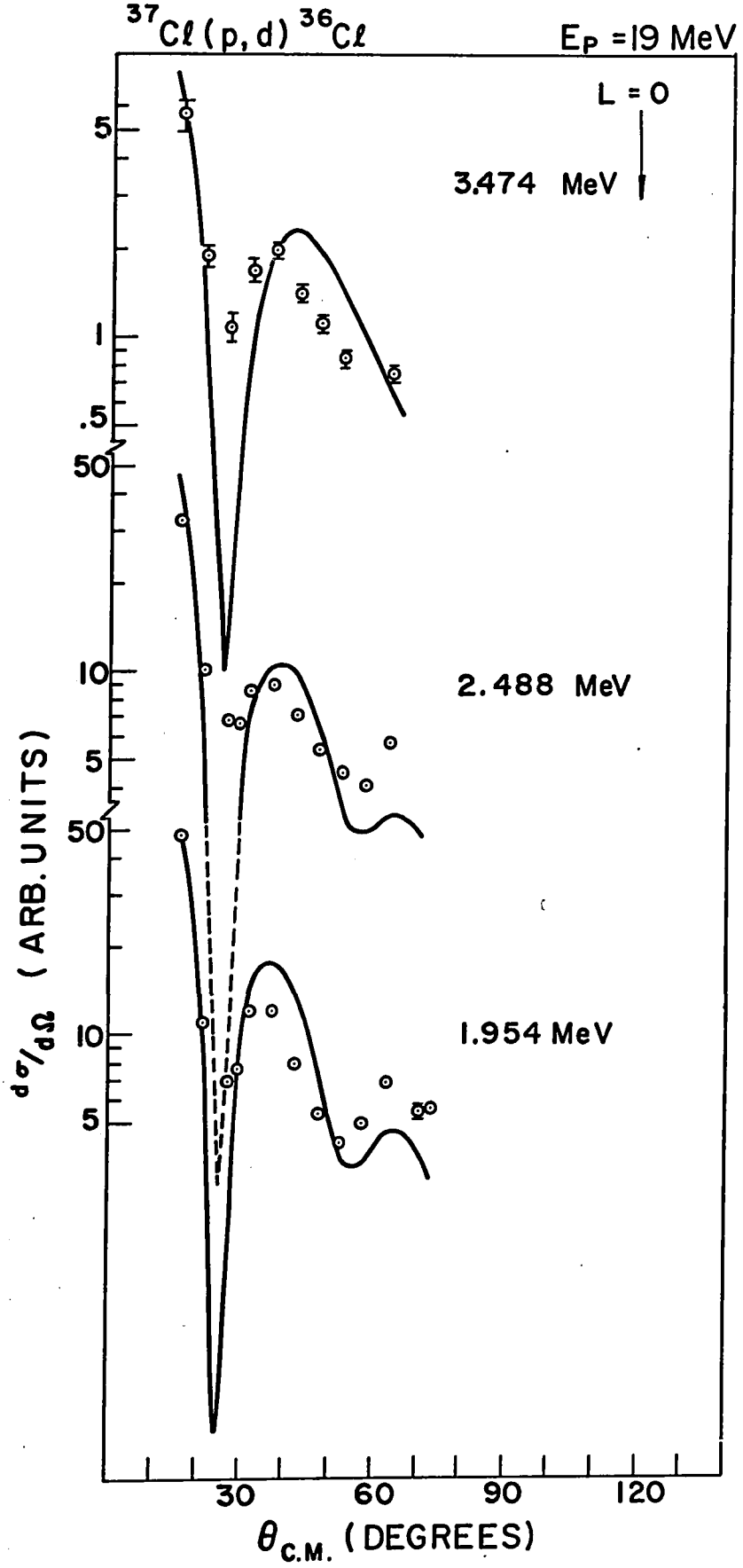
$^{37}Cl(p,d)^{36}Cl$
E_P = 19 MeV
L = 0
3.474 MeV
2.488 MeV
1.954 MeV
5
1
.5
50
10
5
50
10
5
$d\sigma/d\Omega$ (ARB. UNITS)
30
60
90
120
$\theta_{C.M.}$ (DEGREES)

Figure 6-4: The ℓ_n = 0 + 2 angular distributions for the reaction $^{37}Cl(p, d)^{36}Cl$.

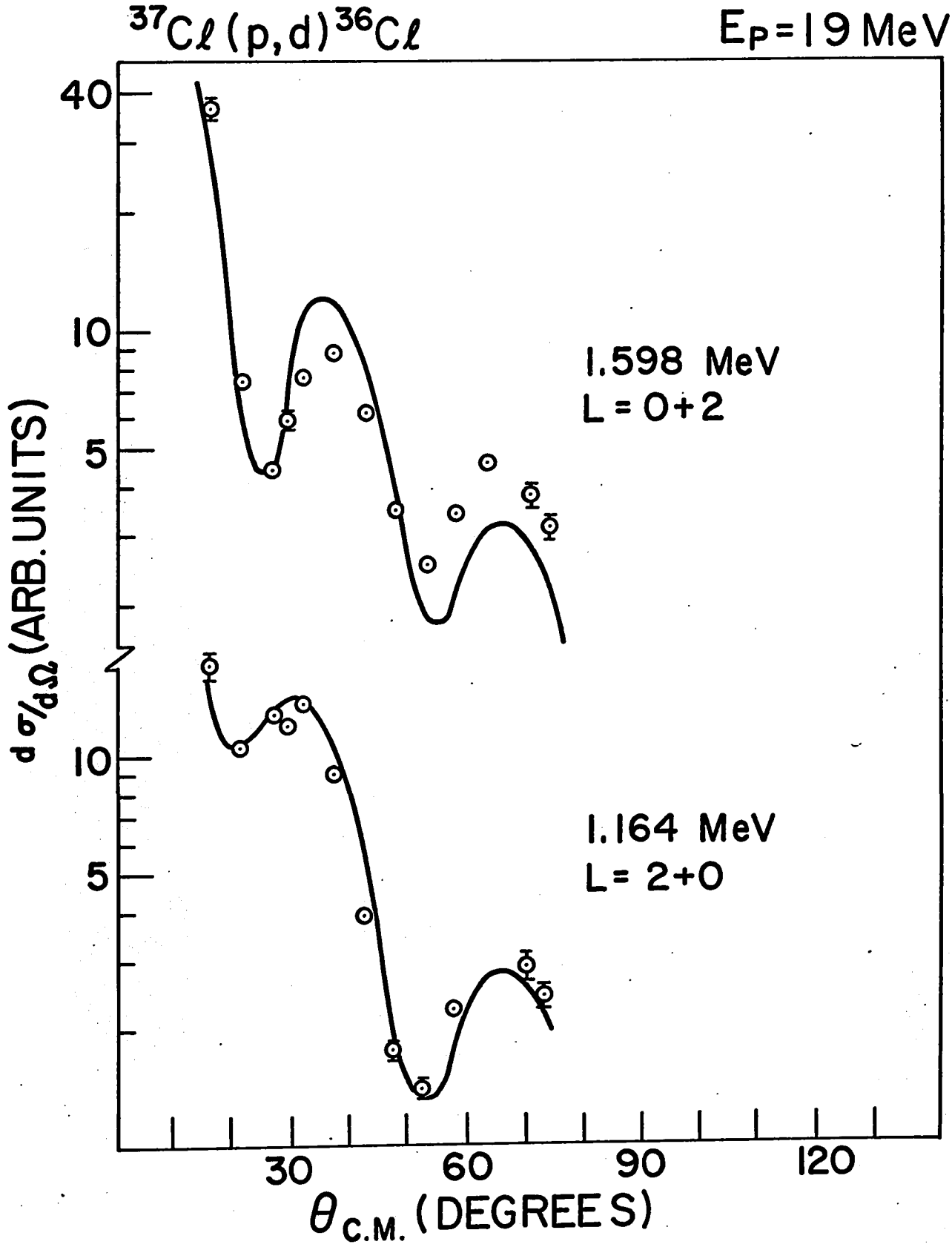
$^{37}Cl(p,d)^{36}Cl$
E_P=19 MeV
40
10
5
10
5
1.598 MeV
L = 0+2
1.164 MeV
L= 2+0
$d\sigma/d\Omega$ (ARB. UNITS)
30
60
90
120
$\theta_{C.M.}$ (DEGREES)

6.4 Results from Shell-Model Calculations

Wavefunctions of ^{37}Cl and ^{36}Cl have been calculated in two different configuration spaces. Model I is based on a shell-model calculation as described by Glaudemans et al. (G2, G3, G4) and further extended by Davies et al. (D7) in the analysis of the ^{31}P(t, p)^{33}P reaction. The model assumes ^{28}Si to be an inert core and considers the additional active nucleons to be in the $2s_{1/2}$ and $1d_{3/2}$ shells. The residual interactions between these active nucleons can be expressed as a sum of two-particle interactions (D8). With this assumption the internucleon interactions between the many possible configuration can be specified by 15 two-body matrix elements and 2 single-particle binding energies.

There are several ways for determining the values of these 17 parameters. Glaudemans et al. calculated the matrix elements by adjusting them so as to obtain a least-square fit to the binding energies of 50 selected levels in nuclei between ^{28}Si and ^{40}Ca. The energy levels and spectroscopic factors for the present study of the ^{37}Cl(p, d)^{36}Cl reaction were generated using matrix elements set IV and V as reported in the (t, p) paper by Davies et al. Set IV matrix elements were calculated as before, except that in this case 35

excitation energies (relative to the various ground states) rather than the binding energies were considered. In set V a particular form of the nucleon-nucleon interaction was assumed. The interaction potential was represented by the surface delta interaction (G4), which reduced the number of free parameters from 17 to 3.

In model II, the space of model I has been extended. The inert core is assumed to be ^{16}O and active nucleons are considered to be in the $2s_{1/2}$, $1d_{3/2}$ and $1d_{5/2}$ orbitals (W6, W7). The two-body interaction potential was derived from the Hamada-Johnston* nucleon-nucleon scattering potential (H13). The energy levels and spectroscopic factors from two different interactions were calculated. The first Hamiltonian, 11.0 h + a SPE, will be referred to as HAM 1, where the harmonic oscillator term was taken to be $\hbar\omega$ = 11.0 MeV and the single particle energies were adjusted (a SPE) so as to give a least square fit to 23 measured excitation energies in the mass region A = 35 - 39. The second interaction, 12.5p + ^{17}O, referred to as HAM 2 uses a harmonic oscillator parameter of $\hbar\omega$ = 12.5 MeV. The single particle energies were taken directly from the observed spectrum of ^{17}O. With the assumption of the Hamada-Johnston potential, the 63 matrix elements of the full s-d configuration space are specified by only four parameters. Together with the three single-particle energies, this leads to a total of seven parameters to specify the complete Hamiltonian.

* see Errata.

The energy levels as generated by model I are shown in figure 6-5 and the relative spectroscopic factors are listed in table 6-2. The relative spectroscopic factors and energy levels relevant to our study based on model II are also tabulated in table 6-2, for each of the Hamiltonians used. They are designated as HAM 1 and HAM 2. The relative spectroscopic factor C^2S_{rel} is equal to $C^2S_{\ell j}/C^2S_{g.s.}$. The isospin coupling coefficient C^2 is 1 for transitions to T = 1 levels and 1/5 for transitions to T = 2 levels in ^{36}Cl.

6.5 Spectroscopic Factor comparison with other data

Table 6-3 summarizes the excitation energies, ℓ_n and relative experimental spectroscopic factors from the (p, d) reaction and the $^{37}Cl(^3He, \alpha)^{36}Cl$ reaction (L5) which was initiated by a 15 MeV ^3He beam. The factors are reported as $C^2S_{rel.}$, as defined in section 6.4.

Figure 6-5: Experimental and calculated energy level scheme for ^{36}Cl based on model I.

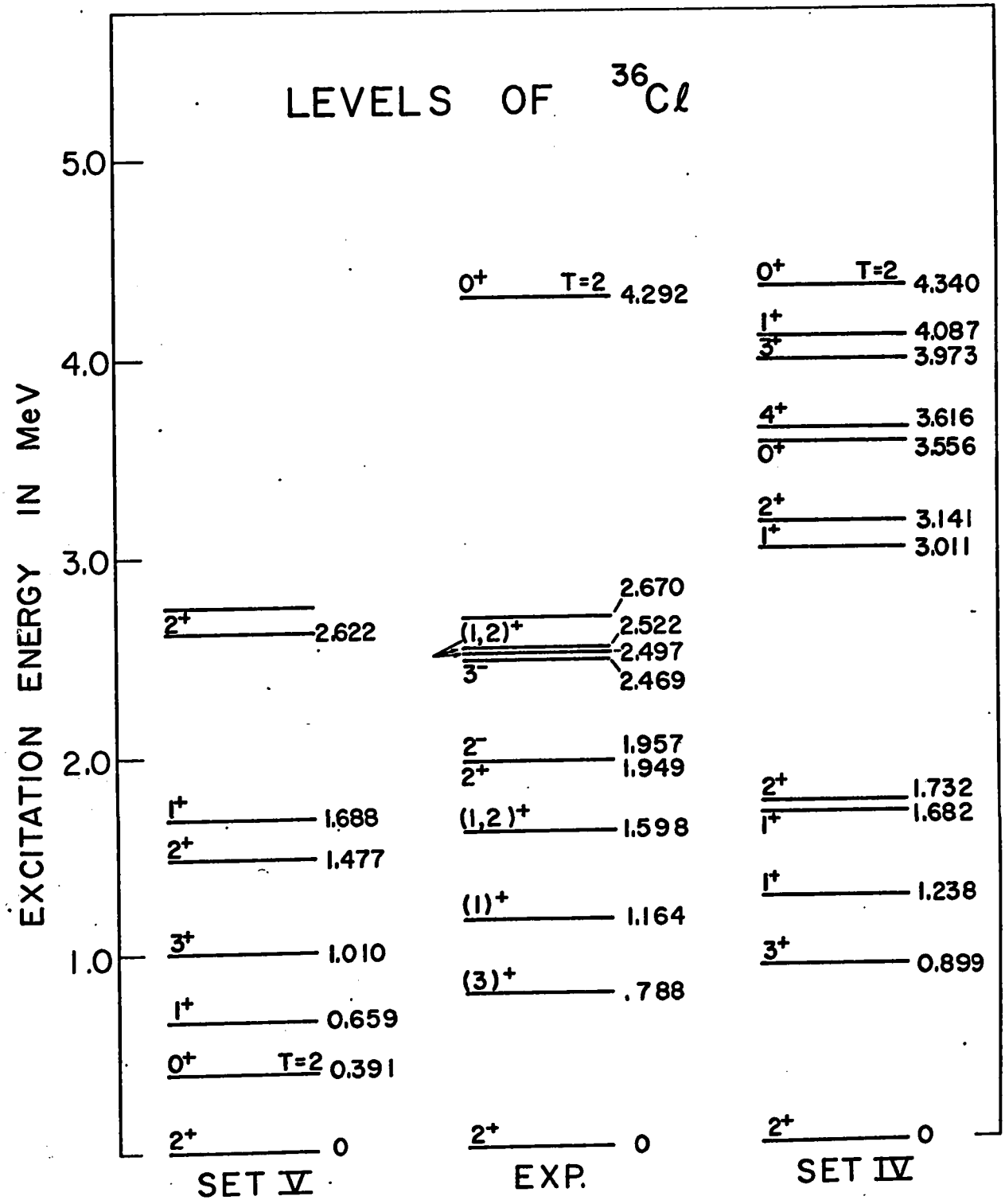
LEVELS OF ^{36}Cl
EXCITATION ENERGY IN MeV
5.0
4.0
3.0
2.0
1.0
2+ 2.622
1+ 1.688
2+ 1.477
3+ 1.010
1+ 0.659
0+ T=2 0.391
2+ 0
SET V
0+ T=2 4.292
2.670
(1,2)+ 2.522
2.497
3- 2.469
2- 1.957
2+ 1.949
(1,2)+ 1.598
(1)+ 1.164
(3)+ .788
2+ 0
EXP.
0+ T=2 4.340
1+ 4.087
3+ 3.973
4+ 3.616
0+ 3.556
2+ 3.141
1+ 3.011
2+ 1.732
1+ 1.682
1+ 1.238
3+ 0.899
2+ 0
SET IV

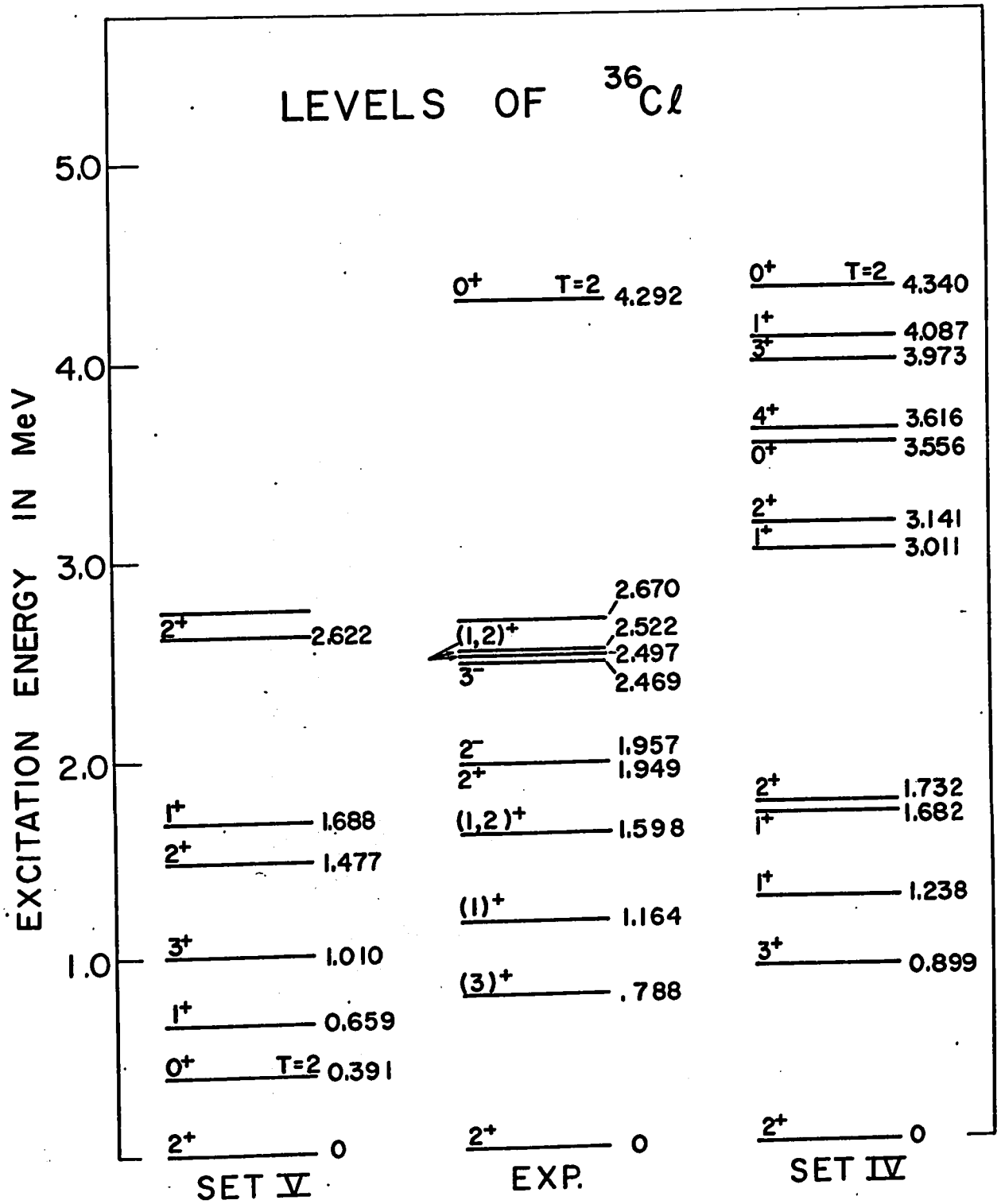
LEVELS OF ^{36}Cl
EXCITATION ENERGY IN MeV
5.0
4.0
3.0
2.0
1.0
2^+ 2.622
1^+ 1.688
2^+ 1.477
3^+ 1.010
1^+ 0.659
0^+ T=2 0.391
2^+ 0
SET V
0^+ T=2 4.292
2.670
$(1,2)^+$ 2.522
2.497
3^- 2.469
2^- 1.957
2^+ 1.949
$(1,2)^+$ 1.598
$(1)^+$ 1.164
$(3)^+$ .788
2^+ 0
EXP.
0^+ T=2 4.340
1^+ 4.087
3^+ 3.973
4^+ 3.616
0^+ 3.556
2^+ 3.141
1^+ 3.011
2^+ 1.732
1^+ 1.682
1^+ 1.238
3^+ 0.899
2^+ 0
SET IV

Table 6-2: Excitation energies and relative spectroscopic factors for states of ^{36}Cl from shell-model calculations.

EXPERIMENT			MODEL I								MODEL II							
			SET IV				SET V				HAM 1				HAM 2			
E_x [a]	J^π [b]	T	$E_{calc.}$	J^π, T	$C^2S_{rel.}$		$E_{calc.}$	J^π, T	$C^2S_{rel.}$		$E_{calc.}$	J^π, T	$C^2S_{rel.}$		$E_{calc.}$	J^π, T	$C^2S_{rel.}$	
					ℓ=0	ℓ=2			ℓ=0	ℓ=2			ℓ=0	ℓ=2			ℓ=0	ℓ=2
0	2^+	1	0	2^+, 1	0.008	1.0	0	2^+, 1	0.005	1.0	0	2^+, 1		1.0	0	2^+, 1		1.0
0.788	3^+	1	0.899	3^+, 1		1.45	1.010	3^+, 1		1.42	0.98	3^+, 1		1.41	0.83	3^+, 1		1.41
1.164	$(1)^+$	1	1.238	1^+, 1	0.13	0.39	0.659	1^+, 1	0.07	0.49	0.84	1^+, 1	0.03	0.23	1.15	1^+, 1	0.05	0.41
1.598	$(1,2)^+$	1	1.682	1^+, 1	0.09	0.01	1.688	1^+, 1	0.02	0.003	1.84	1^+, 1	0.12	0.13	2.18	1^+, 1	0.05	0.04
1.954 [c]	2^+, 2^-	1	1.732	2^+, 1	0.13	0.002	1.477	2^+, 1	0.05	.001	1.59	2^+, 1	0.05	0.05	1.71	2^+, 1	0.26	0.33
2.488 [d]	3^-, $(1, 2)^+$	1	3.141	2^+, 1	0.49	0.01	2.622	2^+, 1	0.69	0.01	2.18	2^+, 1	0.38	0.14	2.26	2^+, 1	0.05	0.02
2.670		1	3.011	1^+, 1	0.20	0.18					2.50	1^+, 1		0.13	2.69	1^+, 1	0.01	0.03
4.292		2	4.340	0^+, 2		0.19	0.391	0^+, 2		0.19	4.35	0^+, 2		0.20	4.55	0^+, 2		0.21

a) as determined from present experiments

b) ref. E2

c) doublet state, ref. E2

d) triplet state, ref. E2

$S_{abs.}$ for g.s. are 1.186, 1.179, 1.11 and 1.08 for SET IV, V and HAM 1, 2 respectively.

Table 6-3: Experimental relative spectroscopic factor (C^2S) comparison for transitions to states in ^{36}Cl.

E_x (MeV)	J^π	T	$^{37}Cl(p, d)^{36}Cl$				E_x [a]	$^{37}Cl(^3He, \alpha)^{36}Cl$	
			$C^2S_{rel.}$		$C^2S_{norm.}$			C^2S_{rel}	
			$\ell = 0$	$\ell = 2$	$\ell = 0$	$\ell = 2$		$\ell = 0$	$\ell = 2$
0	2^+	1		1.0		1.29	0		1.0
0.788	3^+	1		1.50		1.94	0.793		1.47
1.164	$(1)^+$	1	0.06	0.32	0.08	0.41	1.165		0.34
1.598	$(1,2)^+$	1	0.20	<.10	0.26	<.13	1.608	0.17	
1.954	$2^+,2^-$	1	0.43		0.55		1.970	0.39	
2.488	3^- $(1,2)^+$	1	0.31		0.40		2.497	0.35	
2.670		1		0.31		0.40	2.682		0.34
3.474		1	0.10		0.13		3.492	0.14	
4.292		2		0.28		0.36	4.333		0.27

a) ref. L5

6.6 Discussion

The choice of optical model parameters made for the present analysis produced satisfactory DWBA fits, not only to the g.s. but also to the excited states. The quality of the fits obtained are illustrated in figures 6-2 to 6-4. In particular, the 20% $\ell = 0$ admixture to the 1.164 MeV transition improves the fit remarkably, indicative of a $2s_{1/2}$ configuration admixture in the wavefunction for this level. The 50% $\ell = 2$ admixture to the 1.598 MeV transition, has the effect of filling in the first mimima of the $\ell = 0$ DWBA angular distribution without affecting seriously the shape or magnitude of the points at less than $20^{o}_{C.M.}$. Since the experimental spectroscopic factor for a $\ell = 0$ angular distribution is usually extracted at angles less than $20^{o}_{C.M.}$, no further attempt was made to include $\ell = 0$ admixtures to levels at 1.954 MeV and 2.488 MeV. The DWBA fit to the 4.292 MeV, T = 2 excited state would be of greater value if more data points had been obtained. However, an unambiguous $\ell = 2$ assignment can be made on the basis of the available results.

The real significance of the shell-model calculations can be assessed, if each model prediction is compared to the relevant experimentally observed excitation energies and spectroscopic factors. The energy level diagram of figure 6-5, based on set IV and V of Model I,

shows that each produces an acceptable fit to the level spacings, although set IV appears to give the best overall agreement, in that it predicts the correct sequence for the lower excited states. In addition, the lowest T = 2 state is predicted accurately by set IV at 4.34 MeV, whereas set V predicts a T = 2 level at 0.391 MeV. The set V prediction is not meaningful since it does not calculate normalized binding energies for T = 2 levels. Furthermore, it should be noted, in order to make the results more realizable, that the levels originally used in the matrix element determination for set IV consisted of the g.s. and the first two excited states of ^{36}Cl.

The level predictions based on Model II, which are indicated in columns 12 and 16 of table 6-2, also show good agreement. HAM 2 in this instance achieves the best overall agreement. Both HAM 1 and HAM 2 accurately predict the T = 2 level in ^{36}Cl.

In summation, both models correctly reproduce basic features of the energy level data.

It will now be of interest to investigate in more detail the validity of the calculated wavefunctions, and for this purpose we will examine and compare the predicted spectroscopic factors with the corresponding experimental values. The measured spectroscopic factors

from the (p, d) reaction are listed in column 4 and 5 of table 6-3.

According to the shell-model, the neutron shell is closed at ^{37}Cl. The total number of $d_{3/2}$ neutrons available for pick up in this case is four, with only one proton in the same shell. Consequently, a simple model description for ^{36}Cl could be considered by coupling a $d_{3/2}$ neutron hole to a $d_{3/2}$ proton. This gives rise to four states of spin 3^+, 2^+, 1^+ and 0^+. From the experimental and shell model results, these states can unambiguously be identified based on the foregoing assumption, since these transitions should have an appreciable $\ell = 2$ pick up strength with no $\ell = 0$ component. On this basis the g.s. (2^+), 0.788 (3^+), 1.164 (1^+) and 4.292 (0^+) are chosen to be representative of this coupling model description. The possible admixtures of configurations with a $s_{1/2}$ neutron hole coupled to a $d_{3/2}$ proton should be apparent in other 1^+ and 2^+ states in ^{36}Cl.

Support for the aforementioned coupling model description is obtained from the HAM 2 model wave function (W7), for the g.s., the first excited state and the T = 2 level at 4.292 MeV. The dominant configuration for all three levels is $(d_{5/2})^{12}$ $(s_{1/2})^4$ $(d_{3/2})^4$, with an intensity of 71%, 75% and 87% respectively. In this representation the $d_{5/2}$ and $s_{1/2}$ shells are filled and the $d_{3/2}$ shell consists of 3 neutrons and 1 proton. In addition, both models calculate $\ell = 2$

spectroscopic factors in excellent agreement with the experimentally determined $C^2S_{rel.}$ values for the states at 0, 0.788, 1.164 and 4.292 MeV. The $\ell = 2$ pick up spectroscopic factor for the first excited state is observed to have a magnitude 1.5 times that to the ground state.

The only departure from this simple coupling model description is the strong $\ell = 0$ component of the 1.164 MeV state. The dominant configuration for this level is again $(d_{5/2})^{12}\ (s_{1/2})^4\ (d_{3/2})^4$, however, the intensity is reduced to 43%. The configuration indicative of $2s_{1/2}$ pick up, ie., $(d_{5/2})^{12}\ (s_{1/2})^3\ (d_{3/2})^5$, now accounts for about 17% of the total intensity. This represents an eight-fold increase in comparison with the strength of this configuration for the g.s., 0.788 MeV and 4.292 MeV state. Experimentally, the $\ell = 0$ admixture in the wavefunction is estimated to be 20% of the $\ell = 2$ spectroscopic factor strength. The shell model results predict the $\ell = 0$ contribution to be as low as 10% and as high as 30%.

If one considers the $2s_{1/2}$ admixture in the wavefunction of the 1.164 MeV state to be a minor deviation from this coupling model description, then there seems justification to normalize the sum of the $\ell = 2$ spectroscopic factors for these four states to four. The corrected results are tabulated in column 6 of table 6-3, and consequently some measure of the absolute spectroscopic strength for all transitions has been obtained.

spectroscopic factors in excellent agreement with the experimentally determined $C^2S_{rel.}$ values for the states at 0, 0.788, 1.164 and 4.292 MeV. The $\ell = 2$ pick up spectroscopic factor for the first excited state is observed to have a magnitude 1.5 times that to the ground state.

The only departure from this simple coupling model description is the strong $\ell = 0$ component of the 1.164 MeV state. The dominant configuration for this level is again $(d_{5/2})^{12}\ (s_{1/2})^4\ (d_{3/2})^4$, however, the intensity is reduced to 43%. The configuration indicative of $2s_{1/2}$ pick up, ie., $(d_{5/2})^{12}\ (s_{1/2})^3\ (d_{3/2})^5$, now accounts for about 17% of the total intensity. This represents an eight-fold increase in comparison with the strength of this configuration for the g.s., 0.788 MeV and 4.292 MeV state. Experimentally, the $\ell = 0$ admixture in the wavefunction is estimated to be 20% of the $\ell = 2$ spectroscopic factor strength. The shell model results predict the $\ell = 0$ contribution to be as low as 10% and as high as 30%.

If one considers the $2s_{1/2}$ admixture in the wavefunction of the 1.164 MeV state to be a minor deviation from this coupling model description, then there seems justification to normalize the sum of the $\ell = 2$ spectroscopic factors for these four states to four. The corrected results are tabulated in column 6 of table 6-3, and consequently some measure of the absolute spectroscopic strength for all transitions has been obtained.

Beyond the second excited state, the calculated spectroscopic factors are sensitive to the choice among our models. The set IV model spectrum suggests that the next two levels in the experimental spectrum are 1^+ and 2^+. This spin sequence is contradicted by set V, HAM 1 and HAM 2. However recent results from the $^{35}Cl(p, d)^{36}Cl$ reaction (D6), assign a 2^+ spin to the higher level of the doublet at 1.954 MeV.

The third excited state (1.598 MeV) is therefore assigned 1^+, and is observed to have a strong $\ell = 0$ pick up spectroscopic factor, indicating excitations from the $2s_{1/2}$ shell. The $\ell = 2$ admixture contained in the DWBA fit to this transition can only place an upper limit to the strength of this component and is reported in table 6-3 to be < 0.10. The theoretical-experimental agreement is only satisfactory when set IV and HAM 1 results are used. The calculated $\ell = 2$ pick up spectroscopic factor for the model II results is due to $d_{3/2}$ pick up.

Next, sufficient attention should be directed to the intercomparison of calculated spectroscopic factors from Model I and II, since significant admixtures of configurations representing holes in the $1d_{5/2}$ shell occur beyond 1.6 MeV. In fact, all of the $\ell = 2$ spectroscopic strength for the levels at 1.59 MeV, 1.71 MeV, 2.18 MeV and 2.26 MeV is due to $d_{5/2}$ pick up. Model I wavefunctions are somewhat inferior in this respect since excitations from the $1d_{5/2}$ shell are not included.

However, if only $\ell = 0$ calculated spectroscopic factors are compared with experimental values for the levels at 1.954 MeV and 2.488 MeV, it is observed that set IV achieves the best agreement, although the HAM 1 results corresponding to the state at 2.488 MeV are reasonable. The level at 2.67 MeV is compared to levels in the model spectrum that have a spin of 1^+. It is to be noted here, that the Model II results calculate a $\ell = 2$ spectroscopic factor due to pick up from the $d_{3/2}$ shell. It appears that HAM 1 gives the best agreement.

Other states with spin values of $J^\pi = 0^+$, 3^+ are predicted between 2 and 3 MeV excitation. One of these, $J^\pi = 3^+$, is noteworthy since it contains a large part of the $1d_{5/2}$ spectroscopic strength. HAM 1 and HAM 2 placed this 3^+ state at 2.71 MeV and 2.18 MeV with a $\ell = 2$ spectroscopic factor of 0.46 and 0.75 respectively.

All the ℓ-assignments are in good agreement with the results of Lars Broman et al. (L5), as shown in table 6-3, and with the results from the $^{35}Cl(d, p)^{36}Cl$ reaction (D6) except for the 2.67 Mev state. The ℓ-assignment from the (p, d) and (^3He, α) experiments indicate positive parity, whereas the (d, p) results exhibit an $\ell = 1$ pattern or negative parity. In conclusion, it is seen in table 6-3, that the measured spectroscopic factors from both reactions are in excellent agreement.

CHAPTER 7

THE $^{23}Na(p, d)^{22}Na$ REACTION

7.1 Introduction

In choosing NaCl as a target material for the study of properties of some nuclear states of ^{36}Cl, a large number of ^{22}Na levels were populated from the $^{23}Na(p, d)^{22}Na$ reaction that deserve further attention. A total of 16 transitions were observed, one of which provides confirmation of a previously unreported level (01, G5) at an excitation energy of 4.294 MeV.

Previous studies of ^{22}Na have provided spin assignments for 15 of the first 16 excited states (01) below 4.1 MeV. This has provided sufficient information to permit identification of several rotational bands based on the Nilsson model, where the odd proton and odd neutron are placed in the lowest available Nilsson orbit, $K^{\pi} = 3/2^{+}$. A negative parity band has also been suggested by placing the odd neutron in Nilsson orbit number 4, $K^{\pi} = 1/2^{-}$.

Single nucleon transfer reactions such as the $^{23}Na(^{3}He, \alpha)^{22}Na$ reaction (H14, G6), $^{23}Na(p, d)^{22}Na$ reaction (A2, H15), and the $^{23}Na(d, t)^{22}Na$ reaction (W8) have also yielded information on levels of ^{22}Na. In particular, the $(^{3}He, \alpha)$ reaction (G6) and the (p, d) reaction (H15) have provided spectroscopic information, which is useful for the purpose of comparison with the present (p, d) reaction. Although not a great deal of new information is extracted from the present results, an attempt is made to resolve some of the uncertainties that have been outlined in the literature. The first of these is the positive parity assignment of the state of 2.571 MeV via the $^{19}F(\alpha, n\gamma)^{22}Na$ reaction (B5). In all cases, the single nucleon transfer reactions have suggested negative parity due to pick up from the $p_{1/2}$ shell, Nilsson orbit number 4. Secondly, it was observed in comparing negative parity spectroscopic factors from the $(^{3}He, \alpha)$ reaction (G6) and the (p, d) reaction (H15), that the (p, d) factors were consistently larger than the $(^{3}He, \alpha)$ results.

The present study provides experimental information relevant to the abovementioned problems.

7.2 Summary of results and conclusions

The spectrum of deuterons leading to states in ^{22}Na is shown in figure 6-1. Altogether 16 levels were resolved with an energy resolution of 35 keV. The excitation energies were calculated using the Lorna program, which computed a calibration curve based on known levels at 0, 0.891, 1.528 and 2.21 MeV. All level energies are consistent within ±15 keV with the results from Olness et al. (O1). This reaction then confirms the identification of a new level at 4.294 excitation energy. The peak broadening at 1.962 MeV is expected since this level represents a triplet state. The level at 4.347 MeV is a doublet.

Experimental angular distributions of the deuteron groups leading to six bound states of ^{22}Na are shown in figures 7-1 to 7-3. DWBA predictions are shown as solid curves in figures 7-1 and 7-2.

The analysis of the angular distributions was performed using the Smith code, including finite range effects. The optical model parameters used are listed in table 7-1, which were determined from elastic scattering fits by Perey (P1, P2).

Figure 7-1: The ℓ_n = 2 angular distributions for the reaction $^{23}Na(p, d)^{22}Na$.

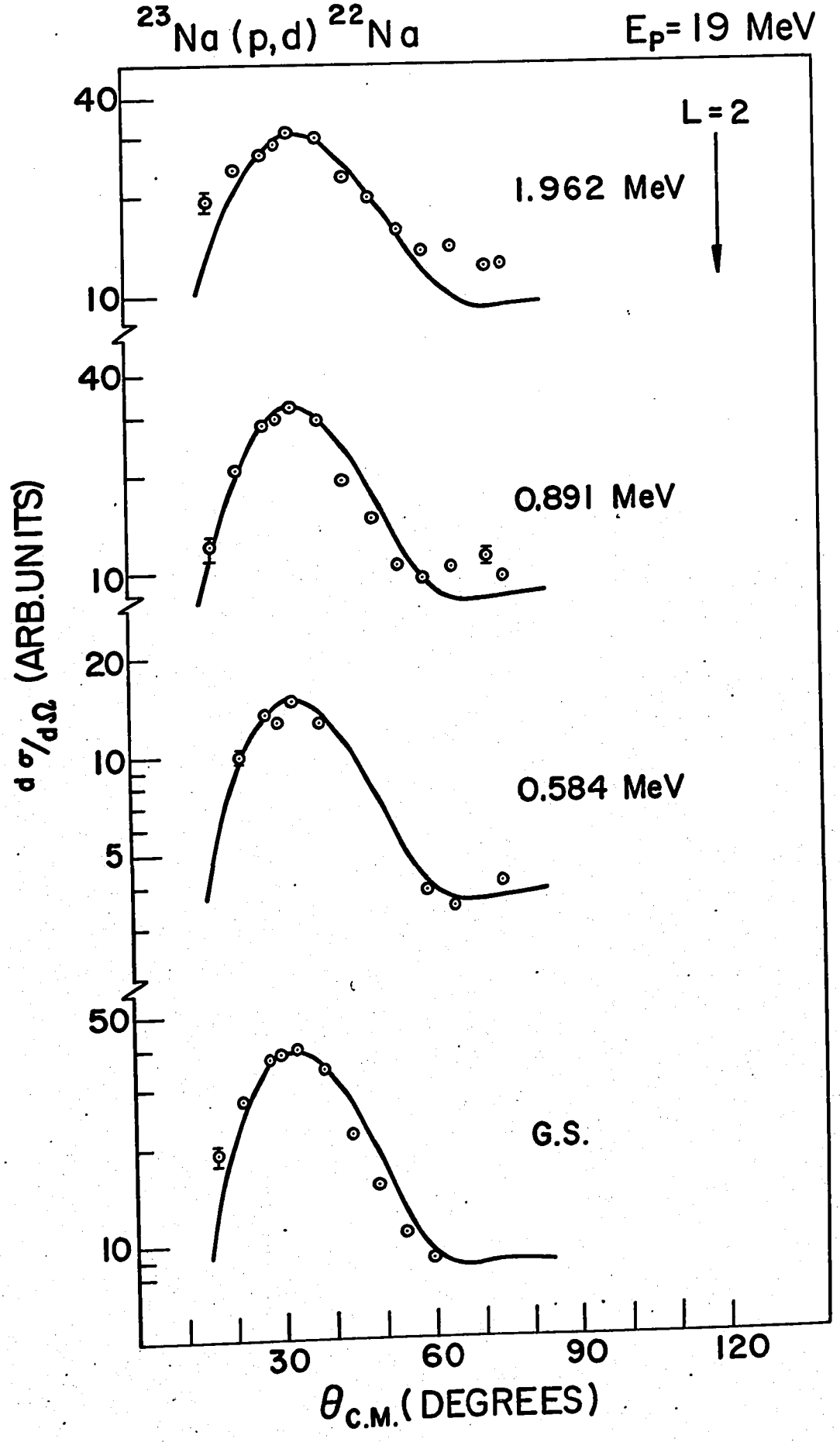
^{23}Na (p,d) ^{22}Na
E_p= 19 MeV
L=2
1.962 MeV
0.891 MeV
0.584 MeV
G.S.
40
10
40
10
20
10
5
50
10
30
60
90
120
$d\sigma/d\Omega$ (ARB.UNITS)
$\theta_{C.M.}$ (DEGREES)

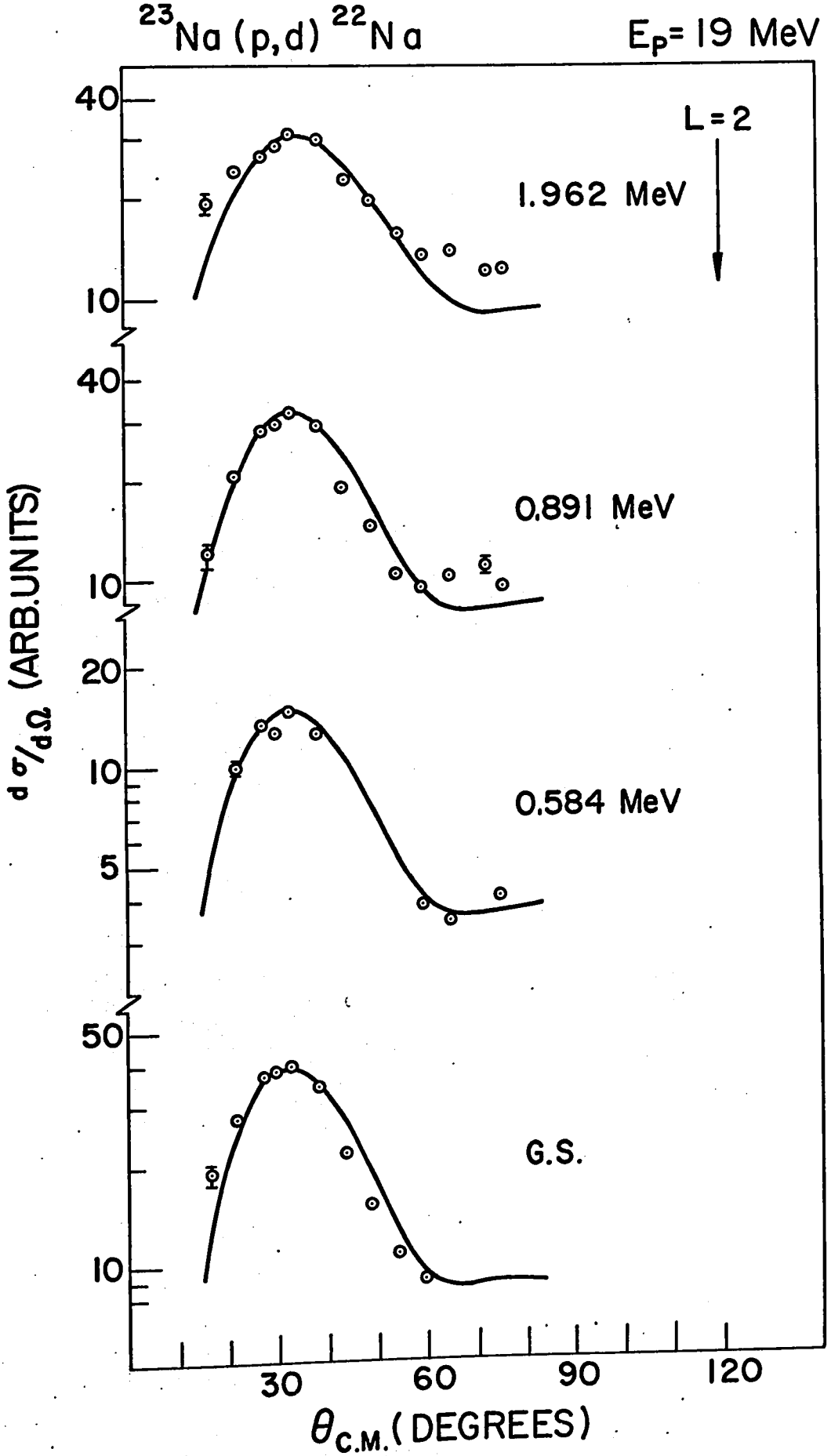
^{23}Na (p,d) ^{22}Na
E_p= 19 MeV
L=2
1.962 MeV
0.891 MeV
0.584 MeV
G.S.
40
10
40
10
20
10
5
50
10
30
60
90
120
$d\sigma/d\Omega$ (ARB.UNITS)
$\theta_{C.M.}$ (DEGREES)

Figure 7-2: The $\ell_n = 1$ angular distributions for the reaction $^{23}Na(p, d)^{22}Na$.

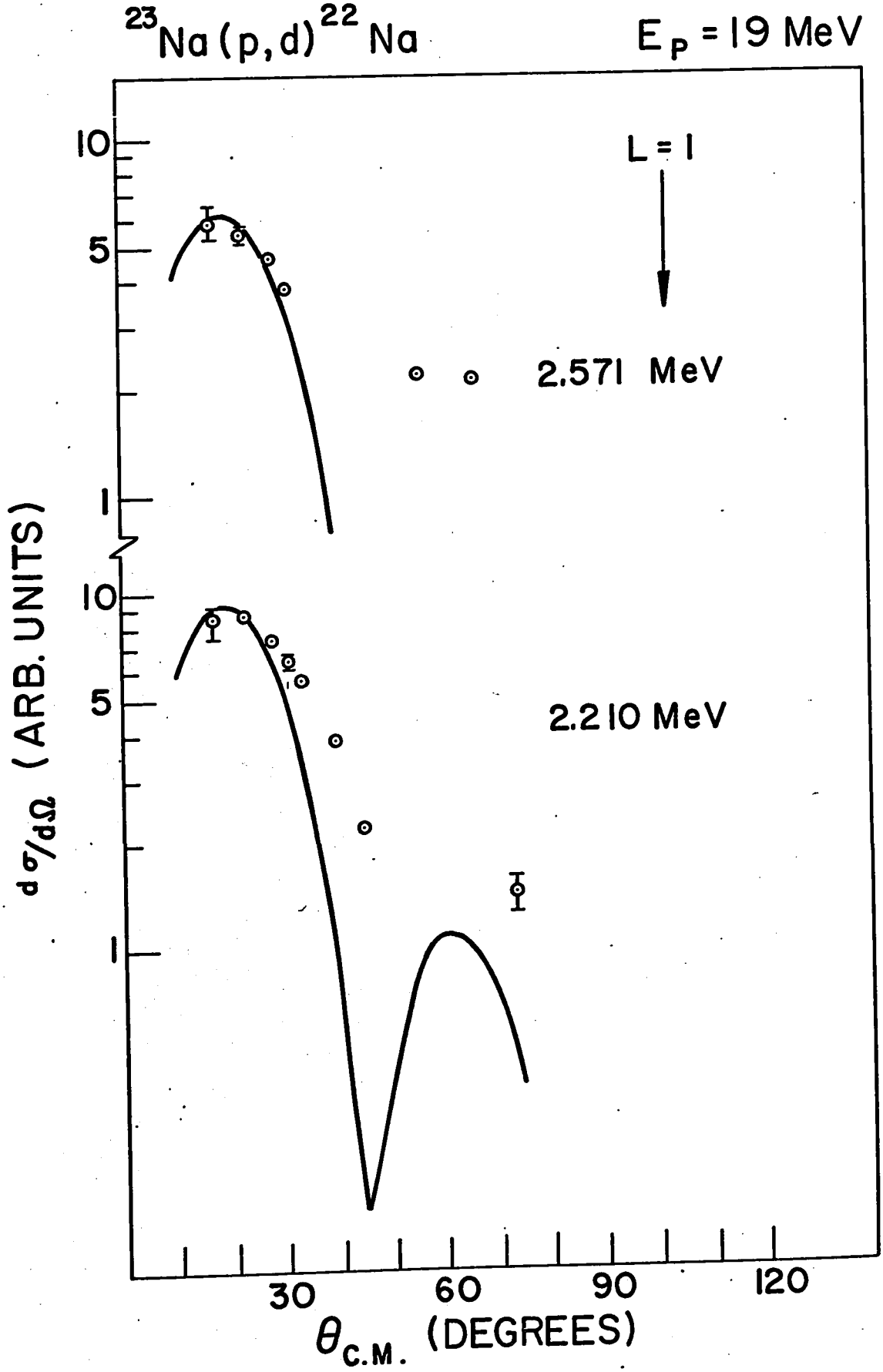
$^{23}Na(p,d)^{22}Na$
$E_p = 19$ MeV
L = 1
2.571 MeV
2.210 MeV
10
5
1
10
5
1
$d\sigma/d\Omega$ (ARB. UNITS)
30
60
90
120
$\theta_{C.M.}$ (DEGREES)

Figure 7-3: Angular distributions for transitions exhibiting no stripping pattern in the reaction $^{23}Na(p, d)^{22}Na$.

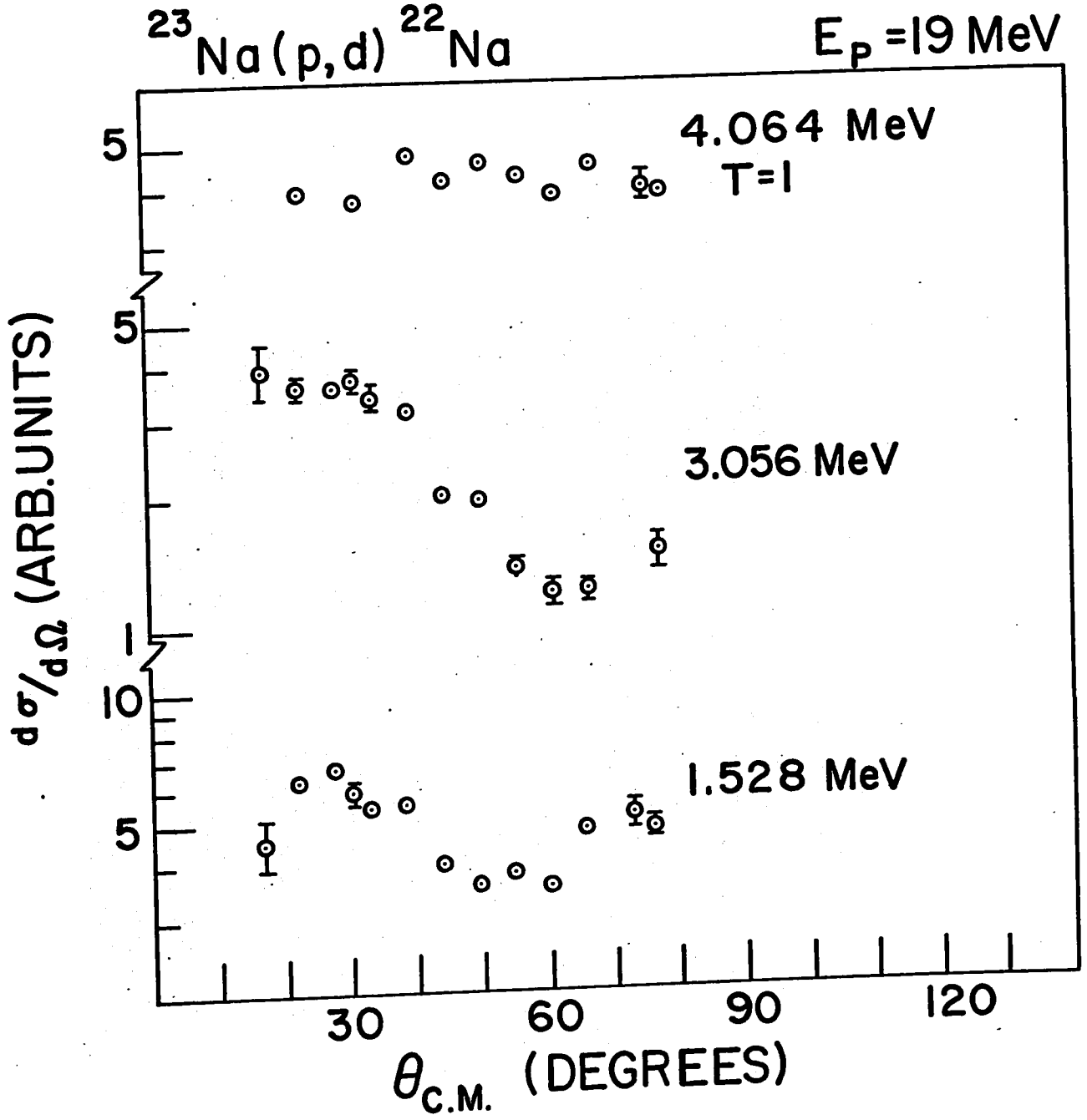
^{23}Na(p,d)^{22}Na
E_p =19 MeV
4.064 MeV
T=1
3.056 MeV
1.528 MeV
5
5
1
10
5
30
60
90
120
$d\sigma/d\Omega$ (ARB.UNITS)
$\theta_{c.m.}$ (DEGREES)

Table 7-1: Optical model parameters used in the DWBA calculation

Channel	V_s MeV	r_{os} fm	a_s fm	W_s MeV	W_D MeV	r_{oI} fm	a_I fm	r_{oc} fm
Proton	45.5	1.25	0.65		7.5	1.25	0.47	1.25
Deuteron	88.0	1.35	0.81		11.25	1.34	0.68	1.35
Bound State		1.3	0.7					1.25

Extracted spectroscopic factors are compared with those calculated using Satchler's formula (see subsection 5.4-1) and from the (^{3}He, α) and (p, d) reaction. The results are presented in table 7-2.

The angular distributions shown in figure 7-3 are weak transitions, that do not exhibit stripping like structure. Other observed levels at 0.66, 2.965, 3.507, 3.934 and 3.698 MeV were still weaker and a complete angular distribution was not attainable. The state at 1.528 MeV was the strongest transition among the weak ones, comparable in strength to about 1/5 times the strength leading to the g.s. This state is known to have $J^{\pi} = 5^+$ and cannot be populated by pick-up from the 1d-2s shell. This level would be a candidate to be explained via a two-step process.

In table 7-2 it is observed that the Nilsson calculation was performed to include both j_n's and that the tabulated spectroscopic factor (C^2S_{exp}) is for the j_n that has the larger calculated spectroscopic factor. This then indicates that all $\ell = 2$ neutron pick up is from the $1d_{5/2}$ shell. If two j's contribute, the sum of $C^2S_{th.}$ should be compared with C^2S_{exp}. The $C^2S_{th.}$ for the T = 1 state at 1.952 MeV includes the isospin coupling coefficient of 1/3.

Table 7-2: Comparison of measured and predicted spectroscopic factors leading to states of ^{22}Na.

E_x [a] (MeV)	J^π, T	ℓ_n	Nilsson Calculation [b]				C^2S_{exp}		
			Configuration	K	j_n	$C^2S_{th.}$	(p, d)[c]	(^{3}He,α)[d]	(p,d)[e]
g.s.	3^+, 0	2	$(3/2\ [\#7])^2$	3	5/2	0.33	0.52	0.52	0.52
					3/2	0.12			
0.583	1^+, 0	2	$(3/2\ [\#7])^2$	0	5/2	0.18	0.22	0.21	0.20
					3/2	0.05			
0.891	4^+, 0	2	$(3/2\ [\#7])^2$	3	5/2	0.55	0.48	0.49	0.56
1.937 / 1.952	2^+, 1	2	$(3/2\ [\#7])^2$	0	5/2	0.38	0.59	0.49	0.70 ±.20
					3/2	0.03			
1.984	3^+, 0	2	$(3/2\ [\#7])^2$	0	5/2	0.26		0.25	
					3/2	<0.01			
2.211	1^-, 0	1	$(3/2\ [\#7],\ 1/2^-[\#4])$	1	3/2	0.04	0.31	0.23	0.31
					1/2	0.28			
2.572	2^-, 0	1	$(3/2\ [\#7],\ 1/2^-[\#4])$	1	3/2	0.06	0.24	0.18	0.28
					1/2	0.09			

a) from ref. 01

b) calculated for a deformation parameter $\delta = 0.525$, Nilsson coefficients from ref. G6

c) present work, normalized to S(g.s.) = 0.52

d) ref. G6

e) ref. H15, normalized to S(g.s.) = 0.52

The comparison between theoretical spectroscopic factors based on Nilsson configuration $(3/2^{+}[\ \#7])^2$ and the experimental spectroscopic factors is excellent. The results also show that the present (p, d) spectroscopic factors are larger than the corresponding (^{3}He, α) values for the negative parity states. The excitation from the $1p_{1/2}$ shell for the state at 2.211 MeV is well supported on the basis of the excellent agreement between measured (p, d) and calculated pick-up factors. The situation for the state at 2.572 MeV is less convincing. However the unsatisfactory $\ell = 1$ fit as shown in figure 7-2 could be improved if a $\ell = 3$ admixture is included.

In summary, the dominant configuration for the 2.211 and 2.572 MeV states is most likely to be identified with a negative parity K = 1 rotational band, based on a hole in Nilsson orbit 4.

CHAPTER 8

CONCLUSIONS

It was found that the extension to the Nilsson model in the form of the Coriolis band mixing calculation provided for an improved agreement between the calculated and measured spectroscopic factors. The V_α filling coefficients can then be used to formulate the wavefunction of the ground state of ^{26}Mg,

$$\psi(^{26}Mg) = 0.78\ (5/2^+, \#5)^2 + 0.57\ (1/2^+, \#9)^2 + 0.30\ (1/2^+, \#11)^2$$

The Nilsson model is not successful in its description of the low-lying levels of ^{26}Al. The excellent agreement with the "$d_{5/2} - s_{1/2}$" shell model wave functions represents a striking success for the model. It was also found that the ^{27}Al ground state configuration has predominantly a $d_{5/2}$ component.

Good agreement was obtained in general for the spectroscopic factor comparison between experimental values and shell model results for ^{36}Cl, for both models. In particular, a high degree of confidence can be placed in set IV. The ground state configuration of ^{37}Cl consists

of two components mainly. An estimate of approximately 75% can be placed upon the amount of the $1d_{3/2}$ component and 25% on the $2s_{1/2}$ component.

The Nilsson model describes successfully the low-lying states of ^{22}Na.

APPENDIX 1

APPLICATION OF RUTHERFORD SCATTERING TO TARGET THICKNESS MEASUREMENTS

A1.1 Introduction

For the determination of absolute experimental spectroscopic factors in nuclear structure studies, it is necessary to measure the absolute values of cross sections. In measuring absolute cross-sections, it is often the thickness of the target that accounts for the largest inaccuracy. In this experiment the target thickness was determined by means of an independent measurement of the Rutherford scattering of a 6 MeV ^{4}He-beam using a single silicon counter set at 20^o, 40^o and 60^o respectively. It was possible in this way to resolve the target constituents. The same geometry for the beam, the target and the counter slits was used as in the pick-up measurements, so that no additional cross-systematic errors were introduced in the absolute differential cross-section calculation.

A1.2 Formalism of Rutherford Scattering

The differential cross-section for the Rutherford scattering of a charged particle by a nucleus is, in the centre of mass system (G8):

$$\sigma_R = \frac{d\sigma}{d\Omega} = \left(\frac{Zze^2}{4E}\right)^2 \sin^{-4}\left(\frac{\theta}{2}\right)$$ where

z is the charge of the incident particle,

Z is the charge of the nucleus,

E is the energy of the incident particle in the C.M.

θ is the angle of deflection of the incident particle in the C.M.

If the number of incident particles is N, and the number scattered into a solid angle ($d\Omega$) subtended by the detector is N_{det} then the expression for the target thickness is given by,

$$T = \frac{N_{det}\ A\ J}{N\ N_A\ \sigma_R\ (d\Omega)}$$ where

A is the atomic weight of the scatterer,

T is the target thickness in $\mu g/cm^2$,

N_A is Avogadro's number.

J is the factor for conversion from laboratory to C.M. coordinates.

References

A1 Ascuitto, R. J. and Glendenning, N. K., Phys. Rev. 181 1396(1969).

A2 Anderson, A. S. and Bevington, P. R., Bull. Am. Phys. Soc. 11, 908(1966).

A3 Anderson, A. S., Ph.D. Thesis, Stanford University, 1968 (unpublished).

B1 Bishop, G. R., Nucl. Phys. 14 376(1959/60).

B2 Bassichis, W. H. and Wilets, L., Phys. Rev. Lett 22, 799(1969).

B3 Bouten, M. C., Elliott, Y. P. and Pullen, J. A. Nucl. Phys. A97, 113(1967).

B4 Bissinger, G. A., Quin, P. A. and Chagnon, P. R., Nucl. Phys. A115, 33(1968).

B5 Baxter, A. M., Gillespie, B. W. J. and Kuehner, J. A., Can. J. Phys. 48 2434(1970).

B6 Bassel, R. H., Drisko, R. M. and Satchler, G. R., "The Distorted Wave Theory of Direct Nuclear Reactions" ORNL-3240.

B7 Buttle, P. J. A. and Goldfarb, L. J., Proc. Phys. Soc. 83 701(1964).

C1 Cujec, B., Phys. Rev. 136, B1305(1964).

C2 Cohen, B. L. and Price, R. E., Phys. Rev. 121, 1441(1961).

C3 Crawley, G. M. and Garvey, G. T., Phys. Rev. 167, 1070(1968).

C4 Crawley, G. M. and Garvey, G. T., Phys. Rev. 160, 981(1967).

D1 Davidson, J. P., Rev. Mod. Phys. 37, 105(1965).

D2 Dehnard, D. and Yntema, J. L., Phys. Rev. 160, 964(1967).

D3 Daniels, T., Calver, J. M. and Adams, A., Nucl. Phys., A110, 339(1968).

D4 Davidson, J. P., "Collective Models of the Nucleus", Academic Press, N.Y.(1968).

D5 Dehnard, D. and Yntema, J. L., Phys. Rev. 155, 1261(1967).

D6 Decowski, P., Nucl. Phys. A169, 513(1971).

D7 Davies, W. G., Hardy, J. C. and Darcey, W., Nucl. Phys. A128, 465(1969).

D8 de-Shalit, A. and Talmi, I., Nuclear Shell Theory (Academic Press, New York, 1963).

E1 Endt, P. M. and Van der Leun, C., Nucl. Phys. 34, 1(1962).

E2 Endt, P. M. and Van der Leun, C., Nucl. Phys. A105, 1(1967).

F1 Fuchs, H., Grabisch, K., Kraaz, P. and Roschert, G., Nucl. Phys. A110, 65(1968).

F2 Forster, J. S. et al., Nucl. Phys. A101, 113(1967).

F3 Fubini, A., Popa, M., Prosperi, D. and Terrasi, F., IL Nuovo Cimento, 2A, 109(1971).

F4 Fortune, H. T., Betts, R. R., Neogy P. and Pullen, D. J., Phys. Letts. 36B, 215(1971).

G1 Goulding, F. S., Landis, D. A., Cerny, J. and Pehl, R. H., Nucl. Instr. and Meth. 31, 1(1964).

G2 Glaudemans, P., Wiechers, G. and Brussaard, P., Nucl. Phys. 56, 529(1964).

G3 Glaudemans, P., Wiechers, G. and Brussaard, P., Nucl. Phys. 56, 548(1964).

G4 Glaudemans, P., Wildenthal, B. H. and McGrory, J. B., Phys. Letts. 21, 427(1966).

G5 Garrett, J. D., Middleton, R. and Fortune, H. T., Phys. Rev. C.4, 165(1971).

G6 Garrett, J. D., Ph.D. Thesis, University of Pennsylvania, 1970 (unpublished).

G7 Glendenning, N. K., Ann. Rev. Nucl. Sci. 13, 191(1963).

G8 Goldstein, H., Classical Mechanics (Addison-Wesley).

H1 Hird, B., Ollerhead, R. W., Nucl. Inst. and Meth. 71, 231(1969).

H2 Hinds, S., Marchant, H. and Middleton, R., Proc. Phys. Soc. 78, 473(1961).

H3 Hamburger, E. W. and Blair, A. G., Phys. Rev. 119, 777(1960).

H4 Hinterberger, F., Mairle, G. Schmidt-Rohr, H., Wagner, G. J. and Turek, P., Nucl. Phys. A111, 265(1968).

H5 Hodgson, P. E., "The Optical Model of Elastic Scattering", Oxford University Press, 1963.

H6 Horvat, P., Kump, P. and Povh, B., Nucl. Phys. 45 341(1963).

H7 Hutcheon, D. A., Olsen, W. C., Sykes, D. H. and Vermette, C. W., to be published.

H8 Hausser, O. and Anyas-Weiss, N., Can. J. Phys. 46 2809(1968).

H9 Hinds, S.,Marchant, H. and Middleton, R. Nucl. Phys. 67 257(1965).

H10 Hoogenboom, A. M., Kashy, E. and Buechner, W., Phys. Rev. 128, 305(1962).

H11 Honzatko, J., Kajfosz, J. and Konecny, K. Czech. J. Phys. B20, 1059(1970).

H12 Hardy, J. C., Brunnader, H. and Cerny, J., Phys. Rev. C 1, 561(1970).

H13 Hamada, T. and Johnston, I. D., Nucl. Phys. 34, 382(1962).

H14 Hinds, S., Marchant, H. and Middleton, R., Nucl. Phys. 51, 427(1964).

H15 Haight, R. C., Ph.D. Thesis, Princeton University, 1969 (unpublished).

I1 Iano, P. J., Penny, S. K. and Drisko, R. M., Nucl. Phys. A127, 47(1969).

J1 Jones, G. D., Johnson, R. R. and Griffiths, R. J., Nucl. Phys. A107, 659(1968).

K1 Kerman, A. K., Kgl. Danske Videnskab. Selskab. Mat. Fys. Medd. 30, no. 15(1956).

K2 Kokame et al., Proc. Int. Conf. on Nuclear Structure, Tokyo, 351(1967).

K3 Kopecky, J. and Warming, E., Nucl. Phys. A127, 385(1969).

L1 Program written by C. Maples, Jr., Lawrence Radiation Lab., Berkeley, California.

L2 Litherland, A. E., McManus, H., Paul, E. B., Bromley, D. A. and Gove, H. E., Can. J. Phys. 36, 378(1958).

L3 Lutz, H. F. and Eccles, S. F., Nucl. Phys. 88, 513(1966).

L4 Lee, Jr., L. L. and Schiffer, J. P., Phys. Rev. 136, B405(1964).

L5 Lars Broman, Fou, C. M. and Baruch Rosner, Nucl. Phys. A112, 195(1968).

M1 Mottelson, B. R. and Nilsson, S. G., Kgl. Danske Videnskab. Selskab, Mat. Fys. Skrifter Medd. 1, No. 8(1959)

M2 Macfarlane, M. H. and French, J. B., Rev. Mod. Phys. 32, 567(1960).

N1 Nilsson, S. G., Kgl. Danske Videnskab. Selskab. Mat. Fys. Medd. 29, No. 16(1955).

N2 Nurzynski, J., Bray, K. H. and Robson, B. A., Nucl. Phys. A107, 581(1968).

O1 Olness, J. W., Harris, W. R., Paul, P. and Warburton, E. K., Phys. Rev. C. 1 , 958(1970).

P1 Perey, F. G., Phys. Rev. 131, 745(1963).

P2 Perey, F. G. and Perey, C. M., Phys. Rev. 132, 755(1963).

P3 Perey, C. M. and Perey, F. G., Phys. Rev. 134, B353(1964).

R1 Reynolds, G. M., Ph.D. Thesis, University of Minnesota 1966 (unpublished).

R2 Rapaport, J. and Buechner, W. W., Nucl. Phys. 83 80(1966).

S1 Standing, K. G., Phys. Rev. 94, 731(1954).

S2 Stokes, R. H., Northrop, J. A. and Boyer, K., Rev. Sci. Intr. 29, 61(1958).

S3 Sheline, R. K. and Harlan, R. A., Nucl. Phys. 29 177(1962).

S4 Satchler, G. R., Ann. of Phys. 3, 275(1957).

S5 Sharpey-Schafer, J. F., Ollerhead, R. W., Ferguson, A. J. and Litherland, A. E.; Can. J. Phys. 46, 2039(1968).

S6 Smith, W. R., DWBA deuteron stripping programme, ORNL-TM-1151, (unpublished).

S7 Schulz, H., Wiebicke, H. J., Fulle, R., Netzband, D. and Schlott, K., Nucl. Phys. A159, 324(1970).

S8 Smith, W. R. and Ivash, E. V., Phys. Rev. 131, 304(1963).

S9 de-Shalit, A., Phys. Rev. 122, 1530(1961).

S10 Satchler, G. R., Nucl. Phys. 55, 1(1964).

T1 Tepel, J. W., Nucl. Intr. and Meth. 40, 100(1966).

W1 Williamson, C., Boujot, J. P. and Picard, J., Rapport no. CEA-R3042 (Saclay, 1966).

W2 Wasielewski, P. and Malik, F. B., Nucl. Phys. A160, 113(1971).

W3 Wildenthal, B.H., McGrory, J. B., Halbert, E. C. and Glaudemans, P. W. M., Phys. Letters 26B, 692(1966).

W4 Weidinger, A., Siemssen, R. H., Morrison, G. C. and Zeidman, B., Nucl. Phys. A108, 547(1968).

W5 Wildenthal, B. H. and Newman, E., Phys. Rev., 175, 1431(1968).

W6 Wildenthal, B., Halbert, E. C., McGrory, J. B. and Kuo, T. T. S., Phys. Letters, 32B, 339(1970).

W7 Wildenthal, B., Halbert, E. C., McGrory, J. B. and Kuo, T. T. S., (to be published).

W8 Wei, T., Bull. Am. Phys. Soc., 12, 85(1968).

Y1 Yoshida, S., Phys. Rev. 123, 2122(1961).